

**INFLUENCE OF ANNEALING TEMPERATURE ON  
MAGNETIZATION AND INITIAL PERMEABILITY OF Fe-  
Ni BASED AMORPHOUS RIBBONS**

**By**

**Nitish Chandra Mollik**

**Roll No: 1055503**

**Session: Jan-2010**

**A THESIS SUBMITTED TO THE DEPARTMENT OF PHYSICS,  
KHULNA UNIVERSITY OF ENGINEERING & TECHNOLOGY IN  
PARTIAL FULFILMENT OF THE REQUIRMENT FOR THE DEGREE  
OF MASTER OF PHILOSOPHY**



**DEPARTMENT OF PHYSICS  
KHULNA UNIVERSITY OF ENGINEERING & TECHNOLOGY  
KHULNA - 9203, BANGLADESH  
OCTOBER- 2014**



## DECLARATION

This is to certify that the thesis work entitled as “**Influence of Annealing Temperature on Magnetization and Initial Permeability of Fe-Ni Based Amorphous Ribbons**” has been carried out in partial fulfilment of the requirement for M. Phil. degree in the Department of Physics, Khulna University of Engineering & Technology, Khulna-9203, Bangladesh. The above research work or any part of this work has not been submitted to anywhere for the award of any degree or diploma. No other person’s work has been used without due acknowledgement.

1. Supervisor



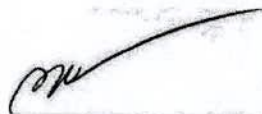
.....  
Prof. Dr. Shibendra Shekher Sikder

Candidate



.....  
Nitish Chandra Mollik

2. Joint-supervisor



.....  
Prof. Dr. Md. Abu Hashan Bhuiyan

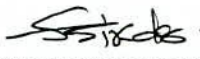




**KHULNA UNIVERSITY OF ENGINEERING & TECHNOLOGY  
DEPARTMENT OF PHYSICS**

**Approval**

This is to certify that the thesis work submitted by Nitish Chandra Mollik entitled "Influence of Annealing Temperature on Magnetization and Initial Permeability of Fe-Ni Based Amorphous Ribbons" has been accepted by the Board of Examiners for the partial fulfillment of the requirements for the degree of *Master of Philosophy* in the Department of *Physics*, Khulna University of Engineering & Technology (KUET), Khulna, Bangladesh on 18 October 2014.

**Board of Examiners**

**Sl. No. Name, Designation & Address**

- |    |   |   |
|----|---|---|
| 1. | Prof. Dr. Shibendra Shekher Sikder<br>Department of Physics<br>Khulna University of Engineering & Technology                  | <br>.....<br>Supervisor & Chairman       |
| 2. | Prof. Dr. Md. Abu Hashan Bhuiyan<br>Department of Physics<br>Bangladesh University of Engineering & Technology<br>Dhaka -1000 | <br>.....<br>Joint-Supervisor & Member |
| 3. | Prof. Dr. Jolly Sultana<br>Head<br>Department of Physics<br>Khulna University of Engineering & Technology<br>Khulna 9203      | <br>.....<br>Member                    |
| 4. | Prof. Dr. Md. Abdullah Elias Akhter<br>Department of Physics<br>Khulna University of Engineering & Technology<br>Khulna 9203  | <br>.....<br>Member                    |
| 5. | Prof. Dr. Syed Jamal Ahmed<br>Department of Physics<br>Dhaka University of Engineering & Technology<br>Gazipur                | <br>.....<br>Member (External)         |

**TO**

**MY PARENTS**



## Acknowledgements

I express, with due respect, my deep sense of sincere gratitude and indebtedness to my Supervisor Prof. Dr. Shibendra Shekher Sikder, Department of Physics, Khulna University of Engineering & Technology (KUET) for introducing the present research topic and his indispensable guidance, keen interest, constructive suggestions, fruitful discussion and constant inspiration throughout the research work. The critical reading of the script and subsequent corrections are much appreciated. Any mistakes that remain are of course mine.

I want to acknowledge the memorable guidance of my Joint-Supervisor Prof. Dr. Md. Abu Hashan Bhuiyan, Department of Physics, Bangladesh University of Engineering and Technology (BUET), Dhaka, for his inspiring guidance and valuable suggestions throughout the research work. He has also consistent support and necessary motivation to progress my experimental works.

I am indebted to Prof. Dr. Jolly Sultana, Head, Department of Physics, KUET, for giving me a strong support in various ways during the entire period of my study in this Department.

I am also grateful to Prof. Dr. Afia Begum, Head, Department of Physics, BUET, Dhaka, for providing me with the necessary experimental facilities, kind co-operation and inspiration.

I am grateful to Mrs. Shireen Akhter, Head & Chief Scientific Officer (CSO), Materials Science Division (MSD), Atomic Energy Centre, Dhaka (AECD) for providing kind opportunity to work her laboratory for experimental work.

I am also also grateful to Dr. Dilip Kumar Saha, CSO, MSD, AECD of his generous help in doing measurements and analysis magnetization results. My thanks are also to Mr. H. N. Das and Mr. M. A. Mamun, Scientific Officer, MSD, AECD, for providing me with technical assistance during my research work.

I am mostly indebted forever to Dr. Md. Zakir Hossain Khan, Assistant Professor, Fultala M. M. College, Khulna and Mr. Sujit Kumer Shil, Assistant Professor Department of Physics, KUET, Khulna. I realize it was not possible to complete my thesis work except their cordial help with generous thinking, expert skillful suggestions and perfect instructions.

I gratefully acknowledge the helpful co-operation of Prof. Dr. Md. Mahbub Alam and Prof Dr. Abdullah Elias Akther, Department of Physics, KUET, Khulna, for their co-operation in my thesis work. My thanks are also to Mr. Md. Kamrul Hasan Reza, Assistant Professor and Mr. Md. Alamgir, Lecturer, Department of Physics, KUET.

My thanks are also to Mr. Ratan Krishna Howlader, Ph.D. Student and Mr. Zashed Iqbal, M. Phil student for their useful suggestion and help to carry out my research work. I am very much grateful to Samapti Mistri and Principal Mr. Gopal Chandra Ghosh for releasing me from my duties to complete thesis work.

My thanks are due to the Director, Atomic Energy Centre, Dhaka for her kind permission to use the Laboratory of MSD, AECD.

I am thankful to Ms. Alhamra Parveen and Ms. Anjuman Ara Begum of MSD, AECD, for their co-operation during the experiments and heartfelt help during the entire period of my research work at the laboratory of AECD.

My special thanks for Mrs. Nandita Saha wife of Prof. Dr. S. S. Sikder, who inspired me a lot during the period of my research work. I express my gratitude to my Father, Mother, Brother, Sister and my wife Nibadita Mondal, who delivered a great family support to fulfill my thesis work. My daughter and son also helped me by giving inspiration.

I also wish to thank the authority of KUET, for providing me with the necessary permission and financial assistance for conducting this thesis work.

Nitish Chandra Mollik



## ABSTRACT

Iron-Nickel-Boron (Fe-Ni-B) amorphous ribbons with composition  $\text{Fe}_x\text{Ni}_{80-x}\text{B}_{20}$  have been prepared by the melt spinning technique where Ni has been substituted by Fe at constant metalloïd Boron. The complex permeability of amorphous ribbon with composition  $\text{Fe}_x\text{Ni}_{80-x}\text{B}_{20}$  [ $x = 20, 30, 40 \text{ \& } 50$ ] are measured as a function of frequency in the range 1 kHz to 13 MHz. The annealing temperature effect on real part of the initial permeability, imaginary part of complex permeability and relative quality factor have been measured for different annealing temperature in the range of room temperature to Curie temperature ( $T_c$ ). The real part of the initial permeability ( $\mu'$ ) of all the samples affected by annealing temperature at constant annealing time, is measured at low frequency (1 kHz) and at very low field ( $H=0.11 \text{ A/m}$ ). The  $\mu'$  increases monotonously with increasing annealing temperature. These effects of annealing lead to the ordering of magnetic atomic pairs, which decreases anisotropy and increase permeability. These effects contribute to an increase of  $\mu'$  but at the same time the imaginary component is also influenced, particularly due to eddy currents effects. The magnetic ordering of Fe-Ni-B amorphous ribbons is studied by temperature dependence of initial part of complex permeability at constant frequency. The temperature dependence of ac permeability has been measured by using induction method. The  $T_c$  corresponds to temperature at which the sharp fall of permeability occurs. It is notable that addition of Fe has significant effects on enhancement of  $T_c$ .  $T_c$  of the residual amorphous phase gradually decreases with increase of annealing temperature. A vibrating sample magnetometer (VSM) has been used for measuring magnetization of Fe-Ni-B ribbons of different compositions at room temperature to study for the composition dependence of magnetization. The effect of annealing temperature on magnetization has also been measured using a VSM and observed that saturation magnetization slightly increased in saturation state. The best choice of these parameters depends on the desired characteristics of the material in respect of permeability below than  $T_c$  and annealing effects on these properties.

## List of Symbols

$a_0$	=	Lattice parameter
$B$	=	Magnetic induction
$D_g$	=	Grain size
DTA	=	Differential Thermal Analysis
DSC	=	Differential Scanning Calorimetry
$d$	=	Average diameter
FWHM	=	Full Width at Half Maximum
$H$	=	Magnetic field
$H_c$	=	Coercivity
$H_a$	=	Applied magnetic field
[hkl]	=	Miller Indices
$k$	=	Magnetic hardness parameter
$K_{eff}$	=	Effective magnetic anisotropy constant
$L$	=	Self inductance of the sample core
$L_o$	=	Inductance of the winding coil without sample
$L_{ex}$	=	Ferromagnetic exchange length
$M$	=	Magnetization
$M_s$	=	Saturation magnetization
nm	=	nano meter
NM	=	Nobel metal
RAM	=	Random anisotropy model
TTT	=	Temperature, time & transformation
$T_a$	=	Annealing temperature
$T_c$	=	Curie temperature
$T_g$	=	Glass transition temperature
$T_x$	=	Crystallization temperature
$T_m$	=	Melting point
$T_{x_1}$	=	Primary crystallization temperature
$T_{x_2}$	=	Secondary crystallization temperature
$T_{p_1}$	=	Primary crystallization peak temperature

$T_{p_2}$	=	Secondary crystallization peak temperature
$\tan\delta$	=	Loss factor or loss tangent
VSM	=	Vibrating Sample Magnetometer
XRD	=	X-ray diffraction
$\mu$	=	Permeability
$\mu_i$	=	Initial permeability
$\mu'$	=	Real part of the complex permeability
$\mu''$	=	Imaginary part of the complex permeability
$\mu_m$	=	Maximum permeability
$\mu_0$	=	Vacuum magnetic permeability
$\lambda$	=	Wave length
$\theta$	=	Scattering angle
$t_0$	=	Time constant
$\beta$	=	Heating rate
$\rho$	=	Electric Resistivity
$\omega$	=	Frequency
$\sigma$	=	Effective stress
Q	=	1/ $\tan\delta$ (quality factor)
$\mu'^*Q$	=	Relative quality factor
$\langle K \rangle$	=	Average anisotropy
$T_c^{am}$	=	Curie temperature of residual amorphous matrix
$ Y $	=	Absolute value of admittance
$ Z $	=	Absolute value of impedance
$\Delta H$	=	Enthalpy of crystallization



# Contents

	Page No.
Title Page	
Declaration Page	i
Acknowledgement	iii
Abstract	v
List of Symbols	vi
Contents	viii
List of figures	xi
List of tables	xv
<b>CHAPTER-I INTRODUCTION</b>	
1.1 Introduction	01
1.2 The Aim and Objectives of the Present Work	03
1.3 Reason for Choosing this Research Work	04
1.4 Application of Amorphous Ribbons	05
1.5 Review of research Work	06
1.6 Outline of the Thesis	08
<b>CHAPTER-II PREPARATION OF AMORPHOUS RIBBONS</b>	
2.1 Introduction	10
2.2 The Structure of an Amorphous Alloy	11
2.3 Conditions for Forming Amorphous Material	15
2.4 Conditions Necessary for Preparing Amorphous Materials	17
2.5 Preparation Technique of Amorphous Ribbon	17
2.5.1 The Atomic Deposition Methods	17
2.5.2 The fast cooling of the Melt	18
2.5.3 Master alloy Preparation	19
2.5.4 Rapid Quenching Method	20
2.6 Experimental details of the Preparation of Amorphous Ribbon	21
2.6.1 Important Factors to Control the Thickness of Ribbons	22
2.7 Factors Contributing to Glass Formation	22
2.8 Examining the Amorphous Ribbon	24

### **CHAPTER-III THEORETICAL ASPECTS**

3.1	Amorphous Alloy or Metallic Glass	26
3.1.1	Nature and Formation of Amorphous Alloys	26
3.2	Factors Contributing to Glass Formation and Stability	28
3.2.1	Structure and Microstructure of Amorphous and Nanocrystalline alloys	30
3.3	Stability of the Amorphous Nanocrystalline Materials	32
3.3.1	Annealing Effects if Amorphous Alloy	33
3.4	Initial Permeability of Amorphous Ribbons	34
3.4.1	Theories of Permeability	35
3.4.2	Measurement of Initial Permeability	37
3.4.3	Relative permeability	37
3.4.4	High Frequency Behavior and Losses	38
3.4.5	Losses	39
3.5	Magnetic Dipole Moments and Magnetization	40
3.5.1	Magnetization of the Amorphous Ribbons	42
3.5.2	Ferromagnetic Ordering (Curie) Temperatures	43

### **CHAPTER-IV EXPERIMENTAL DETAILS**

4.1	Thermal Treatment of the Amorphous Ribbon	46
4.2	Annealing	46
4.2.1	Stages	47
4.2.2	Set up and Equipment	47
4.3	Impedance Analyzer	47
4.3.1	Preparation of the Samples for Complex Permeability Measurement	50
4.3.2	Components of Complex Permeability Measurements	50
4.3.3	Real and Imaginary Components of Complex Permeability	51
4.4	Curie Temperature	52
4.4.1	Inductance Analyzer	53
4.4.2	Curie Temperature determination from temperature dependence of ac Permeability	53
4.5	Magnetization Measurement Techniques	56
4.5.1	Vibrating Sample Magnetometer	56
4.5.2	Principle of Vibrating Sample Magnetometer	56

4.5.3	Electronic Circuits of the VSM	58
4.5.3.1	Sensitivity limits	59
4.5.3.2	Stability Tests Differential Measurements	59
4.5.3.3	Vibration Amplitude	60
4.5.3.4	Image Effects	60
4.5.3.5	Vibration Frequency	60
4.5.3.6	Vibration problems	60

## **CHAPTER-V          RESULTS AND DISCUSSION**

5.1	Dynamic Magnetic Properties of Fe -Ni Based Amorphous Ribbons	61
5.1.1	Initial permeability of as-cast Fe-Ni-B Amorphous Ribbons	62
5.1.2	Complex Permeability of the Fe-Ni-B Amorphous Ribbons	66
5.1.3	Frequency Dependence of the Real part of the Complex Permeability Fe-Ni-B Amorphous Ribbons with Different Annealing Temperatures	69
5.1.4	Frequency Dependence of Imaginary Part of the Complex Permeability of Fe-Ni-B Amorphous Ribbons with Different Annealing Temperature	75
5.1.5	Relative Quality Factor of Fe-Ni- B Amorphous Ribbons with Different Annealing Temperatures	78
5.2	Curie Temperature Measurements of Amorphous Fe-Ni-B Ribbons	82
5.2.1	Annealing Temperature Effects on Curie Temperature Measurements of Fe-Ni-B Amorphous Ribbons	84
5.3	Specific Magnetization Measurements of Fe-Ni-B Amorphous Ribbons	88
5.3.1	Effect of Annealing Temperature on Specific Magnetization of Fe-Ni-B Amorphous Ribbons at Room Temperature	90

## **CHAPTER-VI          CONCLUSIONS**

6.1	Conclusions	95
6.2	Suggestions for further work	97

<b>REFERENCES</b>	98
-------------------	----

<b>CONFERENCE PAPER</b>	105
-------------------------	-----



## List of Figures

### CHAPTER II

	Page No.
Fig. 2.1 Short range order as a function of radial distance	12
Fig. 2.2 Free energy versus temperature curves	13
Fig. 2.3 Glass formation as a function of reduced glass transition temperature	14
Fig. 2.4 Viscosity versus Temperature curve	14
Fig. 2.5 Compositional dependence of melting point	16
Fig. 2.6 Experimental values of critical velocity versus reduced glass transition temperature	16
Fig. 2.7 Vacuum arc Melting Machine	19
Fig. 2.8 Thin layer of molten alloy intimate contact with the outer surface of metallic rotor is quenched in to amorphous	20
Fig. 2.9 Temperature dependence of enthalpy $H$ , $G$ and $G'$ corresponds to the transition to the crystalline state	23
Fig. 10 Examining the Amorphous Ribbon	25

### CHAPTER III

Fig. 3.1 Schematic TTT diagram for the onset of crystallization	28
Fig. 3.2 Typical pair correlation function for (a) a completely disordered, (b) a crystalline completely ordered and (c) an amorphous short-range ordered material	31
Fig. 3.3 Low core losses and Fe-based amorphous alloy at high frequency	39

### CHAPTER IV

Fig.4.1 Impedance Analyzer Model-Hewlett-Packard 4192A	49
Fig.4.2 Schematic diagram for the experimental setup for determination of Curie temperature	55

Fig.4.3	Vibrating sample magnetometer	57
Fig-4.4	Schematic diagram of the electronic system of the VSM	58

## CHAPTER- V

Fig. 5.1	Permeability versus ac magnetic field of amorphous ribbon with composition $Fe_xNi_{80-x}B_{20}$	62
Fig. 5.2	Variation of Initial permeability with the change in the Fe-content in $Fe_xNi_{80-x}B_{20}$ at $H = 0.11A/m$	63
Fig. 5.3	Frequency dependence of the real part of initial permeability of amorphous ribbon for different field with composition $Fe_xNi_{80-x}B_{20}$ at constant annealing time 1 hour (a) $x=20$ , (b) $x=30$ , (c) $x=40$ & (d) $x=50$	65
Fig. 5.4	Frequency dependence of the real part of complex permeability of amorphous ribbons with composition $Fe_xNi_{80-x}B_{20}$	67
Fig. 5.5	Frequency dependence of the imaginary part of initial permeability of amorphous ribbons with compositions $Fe_xNi_{80-x}B_{20}$	68
Fig. 5.6	Frequency dependence of relative quality factor of amorphous ribbons with compositions $Fe_xNi_{80-x}B_{20}$	69
Fig.5.7	Frequency dependence of the real part of initial permeability of amorphous ribbon for different annealing temperature with composition $Fe_{50}Ni_{30}B_{20}$ at constant 1hr annealing time	69
Fig.5.8	Frequency dependence of the real part of initial permeability of amorphous ribbon for different annealing temperature with composition $Fe_{40}Ni_{40}B_{20}$ at constant 1hr annealing time	70
Fig.5.9	Frequency dependence of the real part of initial permeability of amorphous ribbon for different annealing temperature with composition $Fe_{30}Ni_{50}B_{20}$ at constant 1hr annealing time	71
Fig.5.10	Frequency dependence of the real part of initial permeability of amorphous ribbon for different annealing temperature with composition $Fe_{20}Ni_{60}B_{20}$ at constant 1hr annealing time	71
Fig.5.11	Real part of permeability versus annealing temperature of	72



- amorphous ribbons with composition  $\text{Fe}_x\text{Ni}_{180-x}\text{B}_{20}$  at applied frequency 1 kHz and applied low field 0.11A/m
- Fig.5.12 Frequency dependence of the imaginary part of the initial permeability of amorphous ribbons for different annealing temperature with composition  $\text{Fe}_{50}\text{Ni}_{30}\text{B}_{20}$  at constant 1 hr annealing time 75
- Fig.5.13 Frequency dependence of the imaginary part of the initial permeability of amorphous ribbons for different annealing temperature with composition  $\text{Fe}_{40}\text{Ni}_{40}\text{B}_{20}$  at constant 1 hr annealing time 76
- Fig.5.14 Frequency dependence of the imaginary part of the initial permeability of amorphous ribbons for different annealing temperature with composition  $\text{Fe}_{30}\text{Ni}_{50}\text{B}_{20}$  at constant 1 hr annealing time 77
- Fig.- 5.15 Frequency dependence of the imaginary part of the initial permeability of amorphous ribbons for different annealing temperature with composition  $\text{Fe}_{20}\text{Ni}_{60}\text{B}_{20}$  at constant 1 hr annealing time 77
- Fig.- 5.16 Frequency dependence of the relative quality factor of  $\text{Fe}_{50}\text{Ni}_{30}\text{B}_{20}$  amorphous ribbon for different temperature at constant annealing time 1hr ( $H = 0.11 \text{ A/m}$ ) 79
- Fig.5.17 Frequency dependence of the relative quality factor of  $\text{Fe}_{40}\text{Ni}_{40}\text{B}_{20}$  amorphous ribbon for different annealing temperature at constant annealing time 1hr ( $H = 0.11 \text{ A/m}$ ) 79
- Fig.5.18 Frequency dependence of the relative quality factor of  $\text{Fe}_{30}\text{Ni}_{50}\text{B}_{20}$  amorphous ribbon for different annealing temperature at constant annealing time 1hr ( $H = 0.11 \text{ A/m}$ ) 80
- Fig.5.19 Frequency dependence of the relative quality factor of  $\text{Fe}_{20}\text{Ni}_{60}\text{B}_{20}$  amorphous ribbon for different annealing temperature at constant annealing time 1hr ( $H = 0.11 \text{ A/m}$ ) 80
- Fig.5.20  $T_C$  determination from temperature dependence of real part of 83

	complex initial permeability of amorphous ribbons with composition $Fe_xNi_{80-x}B_{20}$ at constant frequency 10kHz and heating rate $10^0C/min$	
Fig.5.21	Variation of $T_C$ due to change in the Ni-content in $Fe_xNi_{80-x}B_{20}$ amorphous ribbons	84
Fig.5.22	Temperature dependence real part of complex initial permeability of $Fe_{50}Ni_{30}B_{20}$ ribbon at different annealing temperature for constant annealing time 1hr	85
Fig.5.23	Temperature dependence real part of complex initial permeability of $Fe_{40}Ni_{40}B_{20}$ ribbon at different annealing temperature for constant annealing time 1hr	86
Fig.5.24	Temperature dependence real part of complex initial permeability of $Fe_{30}Ni_{50}B_{20}$ ribbon at different annealing temperature for constant annealing time 1hr	86
Fig.5.25	Temperature dependence real part of complex initial permeability of $Fe_{20}Ni_{60}B_{20}$ ribbon at different annealing temperature for constant annealing time 1 hr	87
Fig.5.26	Specific magnetization versus magnetic field of amorphous ribbons with composition $Fe_xNi_{80-x}B_{20}$	89
Fig.5.27	Variation of Specific magnetization due to change in the Ni-content in $Fe_xNi_{80-x}B_{20}$ amorphous ribbons	90
Fig.5.28	Specific Magnetization versus magnetic field of $Fe_{50}Ni_{30}B_{20}$ ribbon at different annealing temperature for constant annealing time 1hr	91
Fig.5.29	Specific Magnetization versus magnetic field of $Fe_{40}Ni_{40}B_{20}$ ribbons at different annealing temperature for constant annealing time 1hr	93
Fig.5.30	Specific Magnetization versus magnetic field of $Fe_{30}Ni_{50}B_{20}$ ribbons at different annealing temperature for constant annealing time 1hr	93
Fig.5.31	Specific Magnetization versus magnetic field of $Fe_{20}Ni_{60}B_{20}$ ribbon at different annealing temperature for constant annealing time 1hr	94



## List of Tables

	Page No.
Table 2.1 Thickness of Ni-based samples	24
Table 3.1 Spontaneous and room temperature magnetizations, magnetic dipole moments and curie temperatures for elemental ferromagnets	41
Table 5.1 The initial permeability in the vanishing field region of the amorphous ribbon with composition $Fe_xNi_{80-x}B_{20}$	63
Table 5.2 The real part of initial permeability of the amorphous magnetic ribbon $Fe_xNi_{80-x}B_{20}$ at different annealing temperature at a constant low field of $H=0.11$ A/m and constant 1 hr annealing time for 1kHz	73
Table 5.3 The real part of initial permeability of the amorphous magnetic ribbon $Fe_xNi_{80-x}B_{20}$ at different annealing temperature at a constant low field of $H=0.11$ A/m and constant 1 hr annealing time for 100kHz	73
Table 5.4 The real part of initial permeability of the amorphous magnetic ribbon $Fe_xNi_{80-x}B_{20}$ at different annealing temperature at a constant low field of $H=0.11$ A/m and constant 1 hr annealing time for 1MH	74
Table 5.5 Curie temperature of Fe-Ni-B ribbons for as cast condition	82
Table 5.6 Curie temperature of $Fe_xNi_{80-x}B_{20}$ amorphous ribbons for as cast and different annealing temperature at constant 1hr annealing time	87
Table 5.7 Specific magnetization of $Fe_xNi_{80-x}B_{20}$ at room temperature	88
Table 5.8 Saturation magnetization of $Fe_xNi_{80-x}B_{20}$ amorphous ribbons for as cast and different annealing temperature for 1hr	92

**CHAPTER I**  
**INTRODUCTION**

# INTRODUCTION

## 1.1 Introduction

In the Past few years there has been literary explosion of both theoretical and experimental results on amorphous magnetic alloys. Amorphous Fe-Ni-B alloys are of great interest as soft magnetic materials and the magnetic properties of amorphous alloys are currently the focus of considerable attention. Amorphous and nano crystalline alloys continue to have significant potential for application and are already deployed specially in transformers. Fe, Co & Ni-based metallic glasses have received a great deal of attention in recent years owing to a very attractive combination of magnetic applications. Fe, Co & Ni with metalloids such as B, Si or C produce amorphous alloys with excellent soft magnetic properties.

Amorphous alloys as a new magnetic materials being studied all over the world for their technical uses and for theoretical interest [1.1-1.4]. The terms amorphous solid and glass have on precise meaning. These terms are generally accepted to mean "non crystalline on any significant scale". Simple amorphous solids have random structures but with differing degrees of short range order depending on the nature of their atomic bonding. Thus amorphous metals in which nearest neighbor central forces dominate, for structures similar to the random packing of hard spheres. The principal order present is imposed by roughly constant separation of nearest neighbors. Other types of order may also be present for example directional ordering due to magnetic or stress annealing. However, not all disordered materials are amorphous since there are disordered crystalline alloys where different atoms regular occupy sites of a regular crystal lattice.

However, in 1960 A. L. Gubanov [1.5] predicted on the basis of theoretical analysis, that amorphous solids would be ferromagnetic. The first reports of an amorphous metallic alloy appear to have been made by A. Bernner et. al. [1.6]. The present interest of amorphous metals research stems from reports by P. R. Duwez [1.7] on the preparation technique of amorphous metallic alloys. Precisely this is why the current interest in metallic ribbon is born. The subject is of interest to physicists, material scientists, electrical and electronic engineers.



To physicists the attraction lies to look at how the absence of crystal structure modifies collective magnetic phenomena, which are mainly governed by short range interactions. Material scientist are interested in the spectrum of new material produced by this method capable of yielding microscopically homogenous alloys of compositions unattainable in crystals, and the new possibilities of tailoring the magnetic properties as desired. Electronic and electrical engineers are interested to find possible uses they can make of metallic ribbon in electronic and power applications.

Amorphous state for pure metals like Fe, Co, Ni etc are obtained only at extremely low temperature, where as this disorder in the amorphous state is more complex than that in the crystalline alloys. The disorder can be classified into two types – one is structural disorder which is lack of periodicity in the atomic arrangements and the other is chemical disorder in which the chemical composition losses its periodicity. The macroscopic quantities which are the averages of properties in the atomic scale are more perturbed by structural disorder .But looking in more detail it is apparent that the chemical and structural disorders interfere with each other and the effects of each kind on physical properties are different to isolate.

The studies of the effects of magnetic annealing on stability and magnetic properties have lead to the prediction and preparation of alloy compositions possessing greatly improved stability; by suitably annealing amorphous alloys, a verity of compositions have been demonstrated to have dynamic losses, permeability's and magnetization which make them competitive in quality to existing commercial amorphous ribbons. There is no theory develop to explain the thermal irreversible behavior of magnetization in amorphous magnetic alloys. The magnetic and structural stability has been evaluated at higher temperatures and are found to be adequate for most foreseeable applications.

The optimal soft magnetic properties of amorphous ribbon can be developed through a variety of thermal treatments. These properties along with the effect of thin geometrical shape controlled by the preparation process make amorphous ribbons very convenient for various magnetic applications. Since the formation of amorphous ribbons is not constrained by phase transformations alloys with continuous range of compositions can be formed in amorphous state. Magnetic moments, complex permeability, loss factor, relative quality factor, initial permeability, coercivity, Curie temperature, magnetic anisotropy and magnetostriction, which determine the characteristics needed for technological uses of soft magnetic materials can

conveniently be tailored in amorphous magnetic ribbons. The questions of the magnetic properties of amorphous Fe-Ni rich amorphous ribbon has received much attention since it was realized that fluctuating positive and negative exchange interaction could possibly lead to a spin glass state or other complex non-collinear spin structures [1.8].

Various annealing techniques have been employed to improve the magnetic properties of ferromagnetic metallic glasses. The behavior of the complex permeability in as quenched and annealed ribbons is discussed in terms of domain wall pinning as affected by the preparation process and annealing [1.9]. A large number of magnetic characteristics such as saturation magnetization and it needed to be studied for the understanding of this magnetic system. As known as controlled annealing of amorphous ribbons leads to the new materials with a polycrystalline structure which have excellent soft magnetic properties for example an enhanced permeability and very low power losses. There are only few reports with the frequency dependent behavior of this quantity for amorphous ribbons [1.10- 1.13]. Increased attention is being given to the production of wide ribbons and the preparation of amorphous ribbons for particular application and for understanding the origin of extrinsic and intrinsic properties. These are important for practical applications of magnetic materials and for evaluating and understanding the long terms stability of this amorphous ribbons.

Study involves of thesis work is to compare the magnetization process and frequency dependence of initial permeability of amorphous Fe-Ni based ribbons with compositions  $Fe_xNi_{80-x}B_{20}$  [ $x = 20, 30, 40 \& 50$  ] are as cast and annealed condition. Research in the development and application of amorphous ribbon can thus be profitable, specially at its present new phase. In the conclusions we would like to emphasis the fact that large gaps between theoretical and experimental results themselves exist which demand more careful experiments in this fields specially with more varied composition and annealing temperature variation.

## **1.2 The Aim and Objectives of the Present Work**

The main objective of the present work is to study the evaluation of the effect of annealing temperature on magnetization process and initial permeability of  $Fe_xNi_{80-x}B_{20}$  [ $x = 20, 30, 40 \& 50$ ] amorphous alloys.



The objectives of the research works are as follows:

- Synthesis of the  $\text{Fe}_x\text{Ni}_{80-x}\text{B}_{20}$  alloys in the form of the ribbon with varying amount of Fe and Ni in the amorphous state by rapid solidification technique.
- Growth of crystalline phase of amorphous material by thermal treatment.
- Optimization of annealing temperature corresponding to the soft magnetic properties.
- Initial permeability measurement as a function of frequency has been evaluated for their dependence on annealing to see the effect of heat treatment on the domain structure affecting permeability.
- Curie temperature measurement of temperature dependence initial permeability and to see annealing effect. Specific magnetization process as a function of magnetic field and annealing effect to see. This provides information about the nature of residual strains in as prepared melt spun ribbons and their effects on domain wall pinning.

### **1.3 Reason for Choosing this Research Work**

Amorphous Fe-Ni-B alloys are of great interest as soft magnetic materials and the magnetic properties of amorphous alloys are currently the focus of considerable attention. The dynamic measurements on the amorphous Fe-Ni-B has been carried out to determine the frequency dependence of complex permeability, loss factor, relative quality factor and initial permeability and its annealing temperature effect and field effect. The dynamic measurement of the eddy current losses which occurs due to irreversible domain wall movements that are frequency dependent is very important. The measurement of complex permeability gives us valuable information about the domain walls. Theoretical models have been suggested for the describing the motion of  $180^\circ$  Bloch walls. As known controlled annealing of amorphous ribbon leads to the new materials with polycrystalline structure, which have excellent soft magnetic properties, for example an enhanced permeability and very low power losses. There are only a few papers dealing this quantity for amorphous ribbons [1.14-1.17]. Amorphous ribbons are made by melt spinning technique, which is very efficient and give the final product in the form thin ribbons. These materials can be tailored by choosing different composition, cooling rates during the preparation and by controlling the annealing process to be used for high frequency transformation, magnetically soft ribbons can also be used for

magnetic shielding and in delay lines. Research in the development and application of amorphous ribbons can thus be profitable, especially at its present new phase.

#### **1.4 Application of Amorphous Ribbons**

The class of amorphous TM-M alloys with TM = Fe, Co or Ni and M = B, P, C, Al or Si have received much attention with respect to their favorable properties concerning various commercial applications such as power supplies, transformers, magnetic heads and magnetic shielding. The amorphous ribbons materials parameters are generally significant for a variety of applications. Possible applications of material may be determined either by its static or dc properties, or by its dynamic or ac properties. In addition to the magnetic properties required, the temperature co-efficient of properties, the stability of properties and cost of materials must be considered. The properties available in the amorphous ribbons cover a wide range by changing alloy composition and heat treatment, and has been presented generally amorphous ribbons are characterized by a high electrical resistivity, high mechanical strength, good corrosion resistance the absence of the crystalline state.

Amorphous ribbons with high  $\frac{B_r}{B_s}$  are practically suited to devices such as switch cores, high gain magnetic amplifiers and low frequency inverters or transformers where minimum losses are important. The high electrical resistivity and the small thickness of the melt-quenched ribbons lead to low eddy current losses. The low hysteresis losses, results in very low core losses which is of interest for power electronics at high frequencies. For application is small electronic devices, the amorphous ribbons have somewhat poorer losses and permeability than the Fe-Ni-B ribbon but better than the Fe-Co-B-Si and Fe-B-Si ribbons. The design optimization requires the lower cost of the amorphous ribbons. The higher induction compared to the Fe-Ni-B ribbons.

Research in the development and application of amorphous ribbon can thus be profitable. Specially at its present new phase of local electrochemical potential difference. Thus by a recently developed technique called LASER glazing, surfaces of extensive metallic equipment are made amorphous to avoid corrosion.



## 1.5 Review of research Work

The low field behavior corresponds to the reversible initial permeability of domain walls which are pinned due to inhomogeneities of the sample reported by E. Amano et.al [1.18] and J. T. S. Irvine [1.19]. The measurement of complex permeability gives us valuable information about the domain wall movements. Theoretical models have been proposed for describing the motion of  $180^\circ$  Bloch walls [1.20-1.23]. Earlier complex permeability measurements by G. Ban et.al [1.24] performed on polycrystalline permealloy and permalloy materials could be fitted as developed K. M. Polivanov et. al. [1.20]. The real and imaginary components of the complex permeability in an ac condition have been measured as a function of the instantaneous value of a sine wave core current density by means of an adapted ac bridge method as described by G. Buttino et. al. [1.25]. Actually under ac condition the number of domain walls increases and more deeply pinned walls begin to move as the frequency is increased as explained by S. D. Washko et.al. [1.26].

In the present work attempts are made to describe the unusual character of the thermodynamic parameters in amorphous ribbons using a theoretical model developed by B. T. Cong [1.27] for disordered localized Ising spin lattice. Recently soft magnetic amorphous alloys have been developed by T. K. Miyaki et.al.[1.28] and O. Komoto et.al. [1.29] and they are used for the magnetic cores of switched mode power supplies, magnetic recording heads and other devices. Most of the amorphous ribbons are reported by applications manufactured from Co-based amorphous ribbons are reported with zero magnetostriction [1.30]. Studies on Fe- based amorphous are excellent in the higher saturation flux density [1.31-1.32], but they are inferior in the soft magnetic properties in composition with Co-based amorphous ribbons [1.33-1.34].

The amorphous ribbon specimens of ring shaped cores with  $\frac{\text{outside}}{\text{inside}}$  diameter =  $\frac{34}{30}$  were made from the as cast ribbons. At room temperature the frequency dependence of the complex permeability  $\mu = \mu' - i\mu''$  and the core loss of the tape wound core were measured by impedance bridge up to the MHz range and by a core loss measuring equipment for sine wave induction in the frequency range  $f = (1-300)$  kHz [1.35-1.36]. The magnetic permeability relaxation is of great importance to practical applications. The experiments have shown that the total permeability decay of  $\text{Fe}_{82}\text{B}_{18-x}\text{C}_x$  and  $\text{Fe}_{82}\text{B}_{18-x}\text{Si}_x$  metallic glasses occurs [1.37-1.39]. The measurements of permeability with increasing field were used for this purpose by



T. Mizoguch et. al.[1.40]. The permeability which gradually decreases with time after demagnetization undergoes a sudden drop with a certain time period which depends on the applied field amplitude and frequency as well as temperature as measured by T. Jagielinski et. al. [1.41].

Magnetization is the most common parameter of a magnetic material. Measurements are usually expressed as average moment in unit  $\text{Am}^2/\text{kg}$ . A brief discussion of amorphous alloys is reported by Alben et. al. [1.42], which follows from ideas of local chemical bonding. In atomic states high spin have low electron - electron coulomb repulsion energies. The behavior of the amorphous Fe-based ribbon is very different from Co-based ribbons. Apparently a small amount of impurity is necessary to stabilize the strong ferromagnetism in the amorphous Fe-Si as reported by W. Felsch [1.43] but this is not confirmed by the result of Y. Shimada and H. Kojima [1.44]. J. G. Wright [1.45] has recently reviewed the status of the information available on 'pure' amorphous elements. In all cases it appears that the saturation moment is the same or less than its value in the crystalline state, which shows that no effective electron transfer occurs from the magnetic atoms of matrix.

Becker et. al. [1.46] showed that rigid band model as above is somewhat more satisfying to the data as obtained by using individual moments varying with composition. This is described by Kouvel [1.47] in his analysis of crystalline alloys. The individual atomic moments of Fe and Ni are then given by

$$\mu_{Fe} = 2.20 + 0.80(1 - x) \text{ and}$$

$$\mu_{Ni} = 0.57 + 0.20x \text{ in } \text{Fe}_x\text{Ni}_{1-x}$$

Becker studied the moment and Curie temperature of amorphous ribbon of  $(\text{Fe-Ni})_{80}(\text{P-B})_{20}$ . The room temperatures saturation magnetizations are of more practical importance. The effect of additions of the transition metal to amorphous ribbon is observed by Fujimori et. al. [1.48]. The number of electrons denoted can be listed as  $-\text{P}_{13}\text{C}_7>-\text{Si}_{15}\text{B}_{10}>-\text{P}_{16}\text{B}_6\text{Al}_3>-\text{P}_{14}\text{B}_6>-\text{Si}_9\text{B}_{13}>-\text{B}_{20}$  based on the relative magnitude of  $4\pi M_s$ . The reduction in moment is greatest for  $-\text{P}_{14}\text{B}_6$  and less for  $\text{P}_{13}\text{B}_8$  and least for  $-\text{B}_{20}$  alloys. The results for  $(\text{Fe}_x\text{Ni}_{1-x})_{79}\text{P}_{13}\text{B}_8$  reported by J. Durand [1.49] show a pronounced change in slope.

The Barkhausen jumps occurring during the magnetization of amorphous Fe-Ni-B-Si alloys have been studied by the measurement of the derivative of magnetization with respect to time  $(\frac{dM}{dt})$ . The peak in  $\frac{dM}{dt}$  vs applied field (H) reproducible averaging over some fifty

cycles of magnetization as observed by J. Horvat et. al. [1.50]. The derivative of magnetization with time  $\frac{dM}{dt}$  in respect to  $M_m$  can provide a more direct justification of the use of the model for the explanation of the process of magnetization in soft magnetic materials as suggested by J. Horvat. et. al [1.51].

The study Curie temperature ( $T_c$ ) at which thermal excitation of structural relaxations and stress relief take place. The relaxation of local atomic configurations perturb both the magnetic and chemical environment and as much, the moment distribution change as observed by J. W. Cable [1.52] Consequently, as temperatures is raised towards  $T_c$ , substantial irreversible changes in moment distribution and reordering of paramagnetic inclusion is expected. Thus although the samples can preserve the amorphous state, they are structurally different on a local scale as compared to the as-quenched system.  $T_c$  has to be considered as the spin order disorder transition temperature of a relaxed system that preserved the amorphous state as explained by E. Figueroa et. al. [1.53] and R. Malmhall et. al. [1.54]. The aim of the thesis work is to report the latest technique of investigating the temperature dependence initial permeability as well as the possible effect of annealing on the crystallization process. The effect of annealing magnetization measurement technique seems to be a quite effective method for studying isothermal kinetics of grain growth on Fe-Ni-B amorphous magnetic ribbon in amorphous matrix.

## 1.6 Outline of the Thesis

Organization of this thesis is divided into six chapters.

Chapter-I gives general introduction followed by a review of earlier research work, the aim and objectives of present work. Reasons for choosing this Research work and applications of amorphous magnetic materials.

The preparation procedures are described in Chapter-II. The theories of permeability and magnetization are discussed in Chapter-III.

Chapter-IV contains the experimental details including Impedance Analyzer,  $T_c$  measurements and Vibrating Sample Magnetometer (VSM).

Chapter-V describes the results and discussion about the optimization of  $Fe_xNi_{80-x}B_{20}$  amorphous ribbons. Experimental results of field dependence specific magnetization and its annealed effect. Experimental results of temperature dependence initial permeability and its



annealed effect. It also contain on the suitably of the specimen studies in respect of relative quality factor, loss factor and annealed effects on frequency spectrum in which materials can be used.

Chapter-VI contains conclusion, achievement of works and further suggestion of this work. Finally a complete list of reference has been given towards the end of the Chapter.



**CHAPTER II**  
**PREPARATION OF AMORPHOUS RIBBONS**

## PREPARATION OF AMORPHOUS RIBBONS

### 2.1 Introduction

Amorphous alloys are of interest because they do not have any long range atomic order. The study of metallic glasses dates back to the pioneering work of Pol Duwez et.al at Caltech in 1950. P. Duwez employed atomization [2.1] and gun techniques [2.2] prior to splat quenching [2.3 - 2.4]. Ferromagnetic amorphous alloys were first reported by S. Mader and A. S. Nowik [2.5]. Since the discovery of metallic glass in 1960 by Pol. Duwez et. al. [2.6], in the same year A. L. Gobonov [2.7] predicted the possible existence of ferromagnetic ordering in non crystalline solids on the basis of theoretical analysis. The interest in amorphous materials is increasing steadily for technological interest developed after Pond and Maddine in 1969 [2.8] reported preparation of continuous ribbons of amorphous alloys. Soon after, C. C. Tsuei and P. Duwez [2.9] reported splat quenched amorphous ferromagnets with interesting soft magnetic properties.

Amorphous states of pure metals like Fe, Co, Ni etc can be obtained only at a very low temperature. Alloys of these metals with glass forming materials can be obtained in the amorphous state by cooling the melt at a relatively lower rate of million degrees per second which can remain in the metastable state over an extended range of Temperature. Two important classes of amorphous magnetic materials are being studied in recent time. They are the transition metal metalloid (TM - M) glass and the rare earth transition metal glass (RE - TM) reported by T. Mizoguchi [2.10], R. Alben et. al. [2.11], E. M. Gyorgy [2.12] and G. S. Cargill [2.13]. TM - M glasses are suitable for composition around 75 - 80% of TM (Fe, Co, Ni etc or in their combinations). Typical composition for RE - TM glass is  $RE_{33}TM_{67}$ , where RE is one of the behavior rare earth metals like Gd, Tb, Dy, Y etc and TM is one of the 3d transition metals like Fe, Co or Ni. Recently the metalloids in TM - M glass are prepared by non-magnetic metals like Zr, Hf. etc by T. Masumoto et. al. [1.14]. The new amorphous and metastable alloys prepared by such techniques were used in the early works to explore the many possibilities opened up by these new rapid quenching techniques.

## 2.2 The Structure of an Amorphous Alloy

The structure of amorphous ribbons has been given by G. S. Cargill [2.15] and also a detail discussion is given by M. A. Asgar [2.16]. An amorphous ribbon material has no long range order and the co-relations that exist must be of short range order in the sense that certain values of the interatomic distance are more common than others. Structure can be discussed on many levels. For example, in terms of the external size and shape of the solid; in terms of cracks, voids, inclusions, compositions gradients and other heterogeneities resolvable by optical microscopy or other technique. However, the more recently, attention is being given to larger scale structural effects which may strongly influence the technical and normally extrinsic magnetic properties such as coercive force, losses and permeability. The stability increases with the number of components in an amorphous ribbon. The disorder can be classified into two types following Alben et al. [2.17].

- (i) Structural disorder –lack of periodicity in atomic arrangement and
- (ii) Chemical disorder –lack of periodicity in chemical environment.

The chemical species and relative positions of the nearest neighbor of an atom are thus randomly altered in chemically disordered solids. Since the most important magnetic integrations are dependent on what happens at quite short range, then the atomic scale properties such as magnetic moments are controlled by chemical disorder. The structural arrangement of the atoms in amorphous solids can be given in terms of a radial distribution function. The radial distribution function (RDF).  $F(r)$  is defined as the number of atoms lying between  $r$  and  $(r + dr)$  of the centre of any given atoms

$$F(r) = 4\pi r^2 \rho(r) \quad (2.1)$$

Where  $\rho(r)$  is the atomic pair co relation function

$$\rho(r) = 0 \text{ for } r < \text{nearest neighbor separation}$$

$$\rho(r) = \rho_0 \text{ average density at larger.}$$

Radial distribution functions are defined for systems at different atoms as weighted average.

The distribution functions are sometimes presented in slightly different forms as

$$G(r) = 4\pi r [\rho(r) - \rho_0] \quad (2.2)$$

If we consider the density  $\rho_0$  is constant than  $F(r) = 4\pi\rho_0 r^2$ . Since the density is constant so  $F(r)$  follows the parabolic distribution



$$W(r) = \frac{f(r)}{4\pi r^2 \rho_0} = \frac{4\pi r^2 \rho(r)}{4\pi r^2 \rho_0}$$

$$W(r) = \frac{\rho(r)}{\rho_0} \quad (2.3)$$

Often called the “reduced radial distribution function” and the “pair correlation function” respectively, where  $\rho_0$  is the average atomic density. Theoretical curve of the radial distribution function as a function of  $r$  is shown in Fig. 2.1

Amorphous solids can be considered as a super cooled liquid. A metallic glass is distinct from a liquid or a solid, because of its deviation from thermodynamic equilibrium, while both a melt and its corresponding crystalline phase have minimum free energy, an amorphous material because of its non equilibrium state is at a higher value of free energy. Free energy as a function of temperature for a crystalline solid, an amorphous solid and a liquid is shown in Fig. 2.2.

Fig. 2.3 shows the reduced glass transition temperature  $\tau = \frac{T_g}{T_m}$  for amorphous solids compared to crystalline solids. It is to be noted that for higher values of  $\tau$  only glass formation is possible.

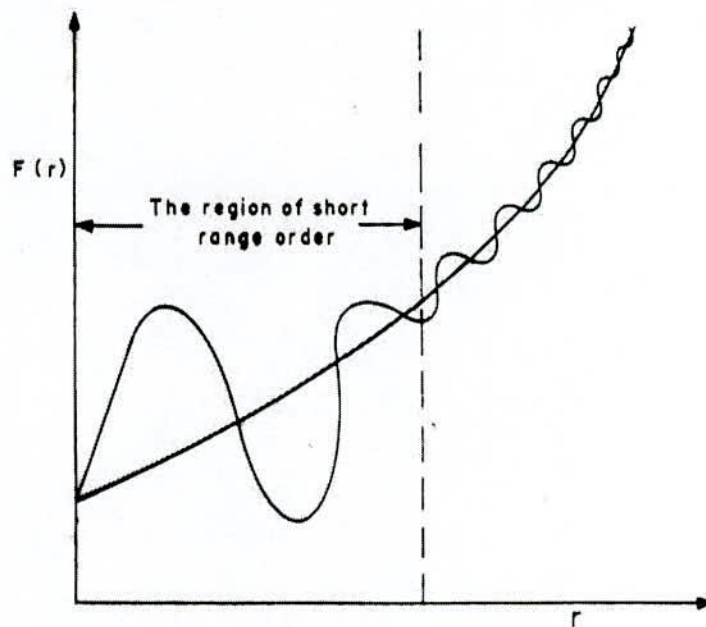


Fig. 2.1 Short range order as a function of radial distance

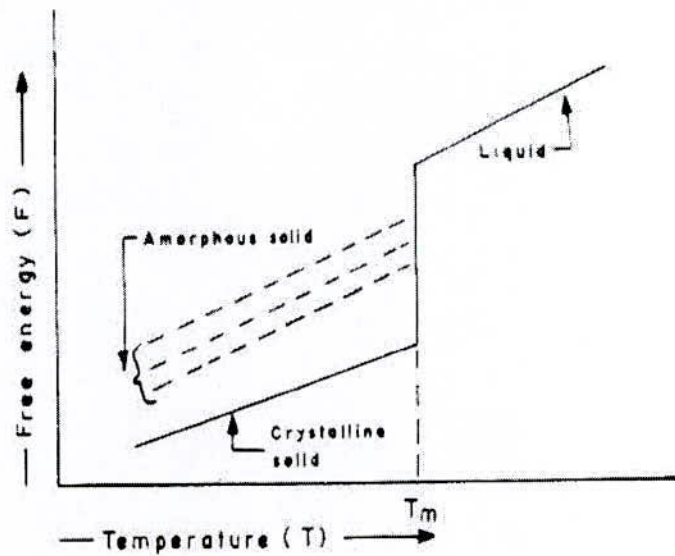


Fig. 2.2 Free energy versus temperature curves

When a melt is cooled too rapidly, its viscosity and relaxation time increase to the point where the internal equilibrium can no longer be maintained and the equilibrium configuration become inaccessible.

Two ways of solidification

- (i) Crystallization process and
- (ii) By increasing viscosity.

Mechanical hardness of the condensed mater is dependent on the viscosity such that although amorphous materials structurally resemble a liquid state, their viscosity become comparable to that of a solid and this determines the stability of amorphous materials. Fig. 2.4 represents the variation of viscosity of amorphous materials with temperature.

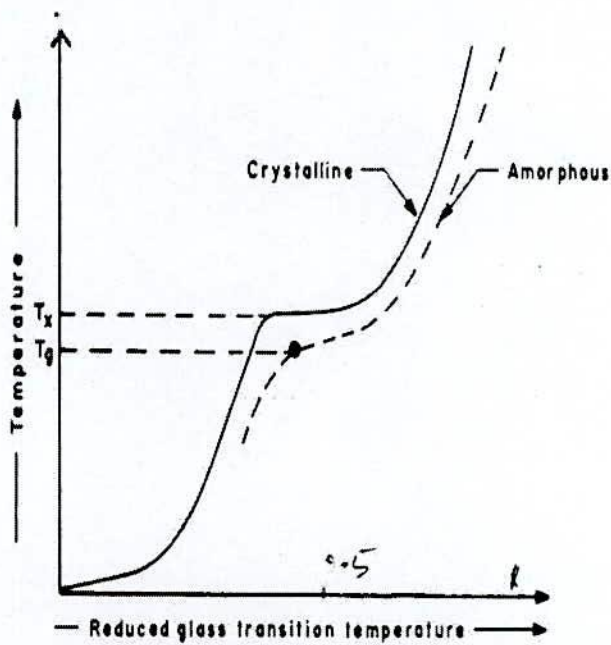


Fig. 2.3 Glass formation as a function of reduced glass transition temperature

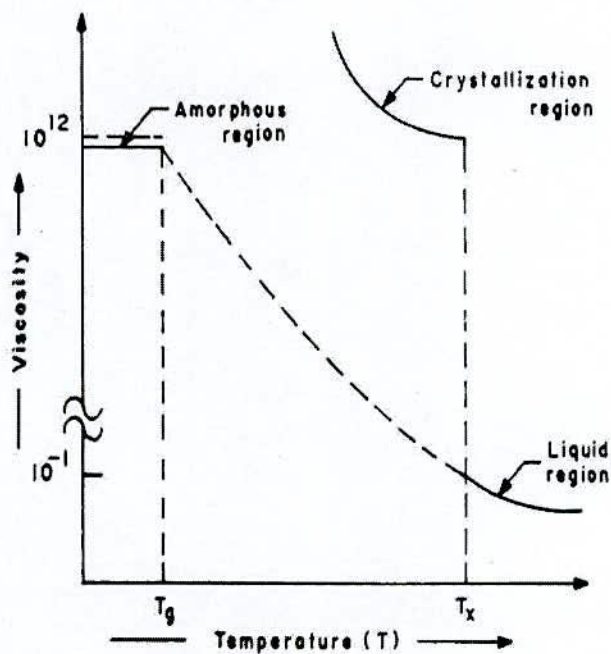


Fig. 2.4 Viscosity versus Temperature curve



### 2.3 Conditions for Forming Amorphous Material

It is very difficult to get pure metals in the amorphous state. It is necessary to add glass-forming materials to pure metals or alloys to get the amorphous state and to bring to the cooling rate within a reasonable rate. Usually around 20% of glass forming materials like B, Si, P, C etc, which have atomic radii relatively small compare to these of metallic atoms and the glass forming atoms occupy the voids left between the bigger atoms of metals when they are closely packed. It can be showed that when there is random close packing of hard spheres there is about 20% voids created between these atoms. The glass forming materials also reduces the melting point of the alloys and there by the separation between the glass forming temperature and the crystallization temperature is reduced. In fact  $\frac{T_g}{T_m}$ , which is called the reduced glass transition temperature is an important parameter determining the glass forming tendency of an alloy.

The more complex an alloy us greater is the possibility of forming the amorphous state. This is because the arrangement of the atoms in the crystalline form of complex system takes more time, which means a greater relaxation time. The presence of glass forming materials contributes to this complexity and thereby increases the relaxation time. The stability of a metallic glass is also increased due to the presence of the glass forming material. Since a metallic glass is in a met stable state, the stability with respect to temperature is determined by the local potential barrier produced by the disordered state of the amorphous material. When  $\frac{T_g}{T_m}$  is large the cooling rates needed for glass formation may be reduced, this mean that critical velocity of the copper disk can be reduced. The dependence of reduced glass transition temperature and the phase diagram indicating the dependence of melting point on composition of the malt us shown is Fig. 2.5

To increase the stability it is necessary to introduce some atoms of B, Si, or P (i.e. atoms with smaller radius) in the matrix. From statistics we know that the amorphous material has a porosity of 20% on the average therefore  $TM_{80}M_{20}$  [M = B, P, Si, C etc = 20% at atomic) is generally introduces to form a good amorphous marital. From Fig. 2.6 it is

observed that the minimum linear velocity of the drum is around 10m/min for preparation of an amorphous ribbon by melt spinning technique.

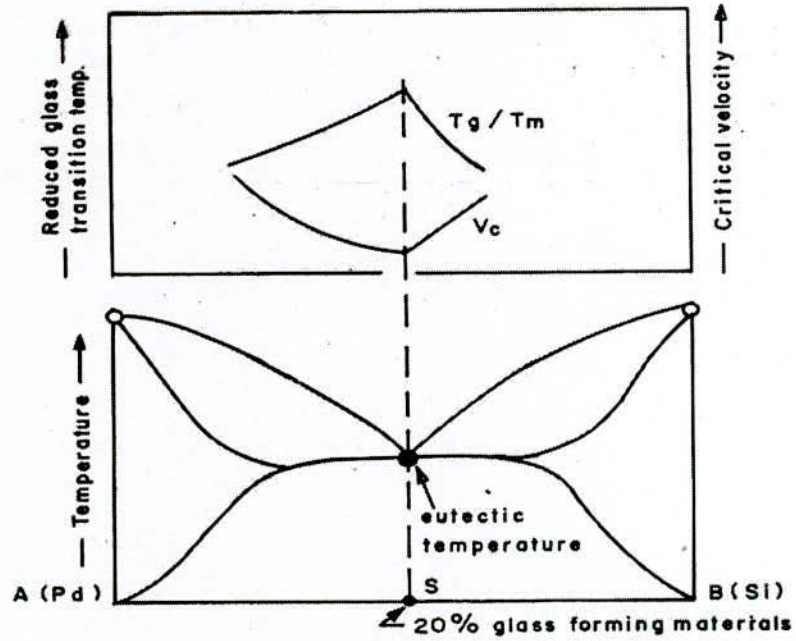


Fig. 2.5 Compositional dependence of melting point

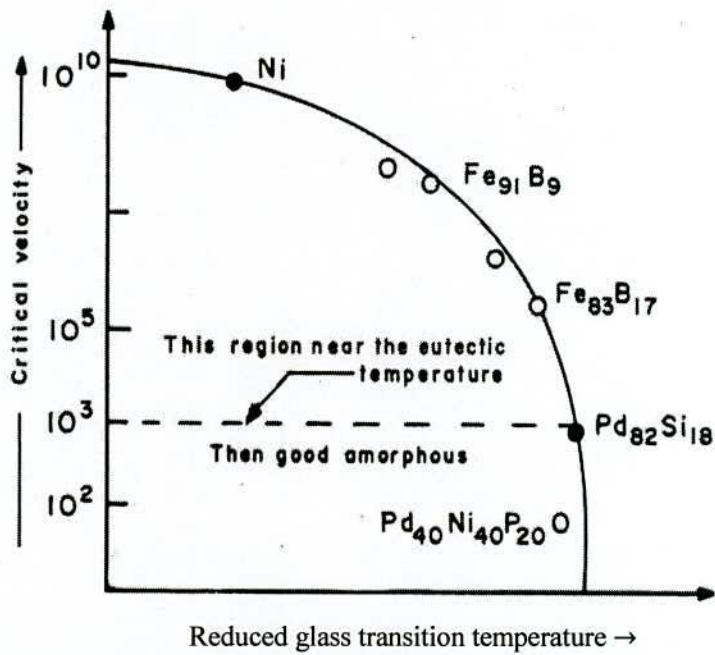


Fig. 2.6 Experimental values of critical velocity versus reduced glass transition temperature

## 2.4 Conditions Necessary for Preparing Amorphous Materials

Condition for formation of glass, in terms of viscosity and diffusion co-efficient:

- (i) For metals atomic bonding is metallic and the viscosity is lower than the diffusion co-efficient and mobility is high.
- (ii) In the case of amorphous materials viscosity is very high and the mobility and the diffusion co-efficient is low. Atomic bonds tend to be covalent-as in the case of silicate ( $SiO_2$ ).

## 2.5 Preparation Technique of Amorphous Ribbon

There are various techniques in use to produce a particular metallic alloy in an amorphous state where the atomic arrangements have no long range periodicity. Amorphous materials such as common glasses and plastics are familiar articles of use to everyone. These are usually prepared by the direct solidification from the melt since they require easily attainable cooling rates to inhibit crystallization. All of the techniques to be described result in effective cooling rates orders of magnitude faster than used for conventional silicate glasses or for casting of ingots into models. These higher cooling rates are a necessary condition for achieving the amorphous state in metallic alloys. The different experimental techniques developed to produce amorphous metallic glass can be classified into two groups.

- (i) The atomic deposition methods and
- (ii) The fast cooling of the melt

### 2.5.1 The Atomic Deposition Methods

Deposition can be described in terms of whether the added atoms is prevented from diffusing more than an atomic distance before it is fixed in position due to cooling and increased viscosity. The atomic deposition methods include condensation of a vapor on a cooled substrate by

- (a) Vacuum deposition
- (b) Sputter deposition
- (c) Electro deposition and
- (d) Chemical deposition



## 2.5.2 The Fast Cooling of the Melt

For producing an amorphous state by any of the liquid quenching devices, the alloy must be cooled through the temperature range from the melting from the melting temperature ( $T_m$ ) to the glass transition temperature ( $T_g$ ) very fast allowing no time for crystallization the factors controlling  $T_g$  and crystallization are both structural and kinetic. The structural factors are concerned with atomic arrangement, bonding and atomic size effects. These factors tend to have limited predictive value, and kinetic factors tend to be dominant. The kinetic factors as discussed by D. Turnbull [2.18] are the nucleation, crystal growth rate and diffusion rate compared to the cooling rate. The interest in this method stems from the wide variety of alloys that can be made as well as from the potential low cost of preparation. The pioneering work of P. Duwez et. al. [2.19], number of devices have been reported for obtaining the necessary high quenching rates and for producing continuous filaments. The methods using the principle of fast cooling of melt techniques are:

- (i) The gun techniques
- (ii) Single roller rapid quenching techniques
- (iii) Double roller rapid quenching techniques
- (iv) Centrifuge and rotary splat quencher techniques
- (v) Torsion catapult techniques
- (vi) Plasma-jet spray techniques
- (vii) Filamentary casting techniques
- (viii) Melt extraction techniques
- (ix) Free jet spinning techniques
- (x) The melt spinning techniques

Although the different methods used in preparing amorphous metallic ribbons are mentioned here, only the single roller rapid quenching technique, which was used to prepare the specimens for the present work, will be discussed.

### 2.5.3 Master alloy Preparation

Amorphous ribbons with the nominal composition  $\text{Fe}_x\text{Ni}_{80-x}\text{B}_{20}$  [ $x = 20, 30, 40 \text{ \& } 50$ ] were prepared in an arc furnace on a water - cooled copper hearth under an atmosphere of pure Ar. Their purity and origin of the constituent elements were Ni (99.9%), Fe (99.9%) and B (99.9%) as obtained from B. Johnson Mathy (Alfa Aesar Inc.).

The required amounts of the constituent elements were taken from pure metal bars or flakes, weighed carefully with a sensitive electronic balance and placed on the copper hearth inside the arc furnace. Before melting the furnace chamber was evacuated ( $10^{-4}$  torr), and flashed with Ar- gas. The process was repeated several times to get rid of residual air and finally the furnace chamber were kept in an Ar- atmosphere. A substantial amount of pure titanium getter, placed inside of the chamber on the side of the copper hearth was melted first in order to absorb any oxygen present in the furnace chamber. The constituent elements were then melted in the shape of buttons. The melting facilities used to prepare the samples as insulated at the centre of Materials Science, National University of Hanoi, Vietnam. The arc furnace used in the preparation of master alloy is shown in Fig. 2.7.

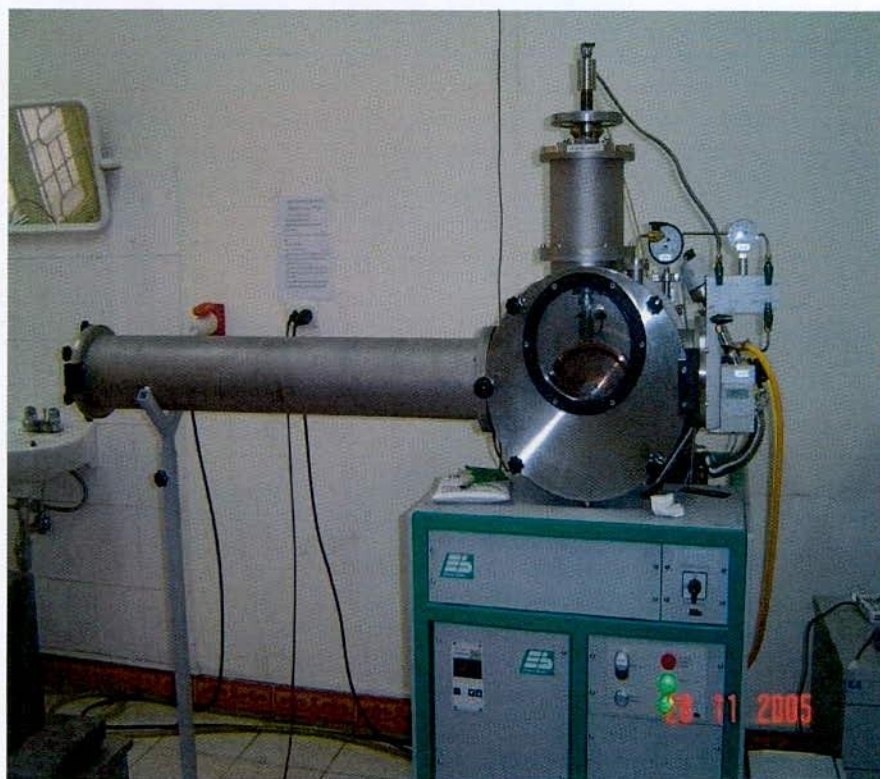


Fig. 2.7 Vacuum arc Melting Machine



## 2.5.4 Rapid Quenching Method

As shown in a schematic diagram in Fig. 2.8, the rapid quenching technique apparatus consists mainly of a copper roller, an induction heater and a nozzle. The roller was driven by a variable speed motor via a tooth belt. The angular velocity was 2000 rev/min. use of long wheel rotation enable us to vary the surface velocity in the range 20 to 30 m/s. the diameter of the copper roller was 10 cm. The use of copper for the roller material was chosen for its good conductivity and mechanical softness, which allowed cleaning and polishing to be carried out easily. For room temperature work, it showed no contamination of the ribbon from the roller material and the careful preparation of the surface was more important than the material of the roller.



Fig. 2.8 Thin layer of molten alloy intimate contact with the outer surface of metallic rotor is quenched in to amorphous



In this process one has to consider that vibration of the roller should be well below the high frequency vibration of the melt puddle to avoid any influence of it on the geometry and uniformity of the ribbon. One has to be careful and see that the ribbon does not remain in contact with the surface of the roller for a whole revolution and be hit, from the back. A bigger diameter is thus preferred for the roller. The induction heater coil is made of hollow copper tubing, which is cooled simultaneously by circulating water through its inner hole. The shape and diameter of the induction heater as also winding is to be adjusted to produce proper temperature gradient. The is to avoid, sudden cooling of the melt in its way out of the crucible and blocking the nozzle, the quartz tubing having outer diameter 20 mm which is narrowed down conically to 1mm with a hole for the nozzle 0.1 to 2 mm.

The nozzle geometry is selected to minimize the contraction in the cross-sectional area of the molten zed as it nozzle orifice. Quartz tube is suitable for repeated use in several successful runs and should be transparent to make the melting process visible. It should withstand the sudden fast changes in temperature.

## **2.6 Experimental details of the Preparation of Amorphous Ribbon**

The amorphous ribbons are prepared in a furnace in a argon atmosphere (0.2 to 0.3 atms). The Buttons prepared are about 50 grams each. Care is taken to ensure through mixing and homogeneity of the alloy composition, by turning over and re-melting each button few times. The mother alloys, which are formed in the form of buttons in a furnace by sudden cooling and is then cut in to small pieces is introduced in the quartz tube. The quartz tube is connected from the top by rubber "O" ring and metal rings to the argon cylinder through a valve and pressure gauge.

After proper cleaning of the roller surface and adjusting its speed to the desired value, as measured by stroboscope, the induction furnace is powered using high frequency generator. When the melting temperature is reached as observed through a protective spectacle, the injection pressure is applied by opening the pressure valve. To avoid the turbulence of the wind, arising from the high speed of the roller in disturbing the melt puddle, cotton pad and metallic shield are usually used just beneath the roller. To avoid oxidation of the ribbon during its formation an inert atmosphere can be created around the roller by a slow stream of helium gas. The speed of the roller, the volumetric flow rate, the orifice diameter, the

substrate orifice distance the injection angle etc, are adjusted by trial and error to get the best result in respect of the quality and the geometry of the ribbons.

### 2.6.1 Important Factors to Control the Thickness of Ribbons

- (i) Rotating speed
  - (a) Angular velocity = 2000 rev/min .and
  - (b) Surface velocity = 20m/s.
- (ii) Gap between nozzle and rotating copper drum (h) = 100 to 150  $\mu\text{m}$
- (iii) Oscillation of the rotating copper drum both static and dynamic have maximum displacement 1.5 to 5  $\mu\text{m}$
- (iv) Pressure = 0.2 to 3.0 argon atmosphere
- (v) Temperature of metals  $T_m \approx 1500^\circ\text{C}$

The temperature did not exceed  $1800^\circ\text{C}$  otherwise quartz tube would be melt.

- (vi) Stability was ensured for the drop in the surface of drum.

### 2.7 Factors Contributing to Glass Formation

There are three interrelated factors that determine glass-forming tendency. These are thermodynamic conditions that favour the liquid phase relative to the crystalline phase, the kinetic conditions that inhibit crystallization and the factors that arise due to experiential conditions. The thermodynamic factors for glass formation are liquids temperature  $T_m$  at which the alloy melts, the heat of vaporization and the free energy of all the phases that arise or could potentially arise during solidification process. Viscosity of the melt, the glass transition temperature  $T_g$  and the homogeneous nucleation rate belongs to kinetic parameters. The glass transition temperature is defined as the temperature at which the super cooled liquid takes on the rigidity of a solid or more specifically at which the viscosity approaches 15 poise.

Processing parameters are the cooling rate, the heterogeneous nucleation rate and the super cooling temperature interval. The temperature of the glass transition is slightly dependent on the cooling rate. At each cooling rate the glass will freeze in different state of internal energy. This is shown in Fig. 2.9.

At the melting point  $T_m$  the enthalpy  $H$  of a crystal includes latent heat of fusion due to long range order. In the case of rapid cooling the melt the free energy decreases since long



range order do not take place, this leaving the system at a higher energy state. Heat treatment, relaxation and stability are thus important considerations in metallic glass. The glass forming tendency also arises from as size difference between the constituent elements. It appears that appreciable size difference between the components in the glassy alloy is a necessary condition for ready glass formation.

A single parameter that expresses glass-forming tendency is the ratio of the glass transition temperature to the melting temperature defined as reduced glass transition temperature

$$\tau = \frac{T_g}{T_m} \quad (2.4)$$

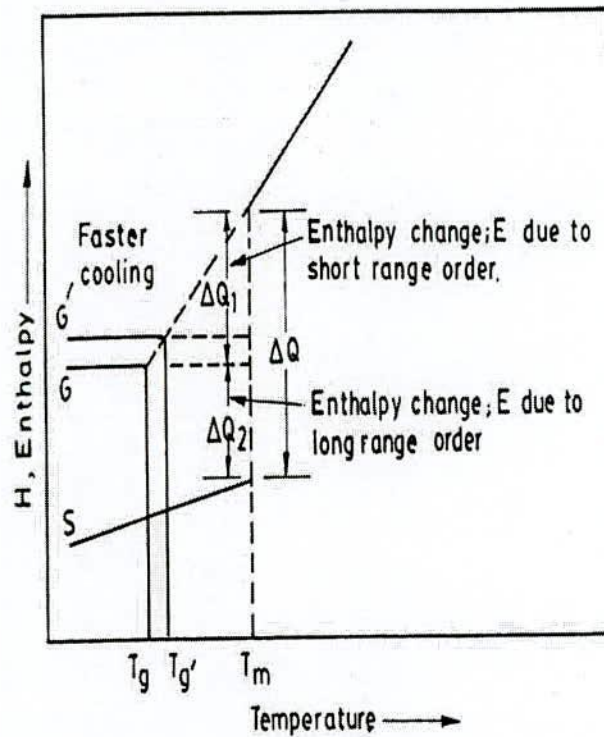


Fig. 2.9 Temperature dependence of enthalpy H, G and G' corresponds to the transition to the crystalline state

Higher values of  $\tau$  obviously favor of glass formation. For metallic glass to be formed by rapid cooling,  $\tau$  should be greater than 0.45 by H. S. Chen [2.20]. Based on alloy composition here are two major groups that rapidly form glasses. In one of these groups the metal is from Fe, Co, Ni, Pd or Pt and the metalloid is B, C, Si, Ge or P, These metallic



glasses constitute soft amorphous magnetic materials. Our working sample prepared show by Table-1.

**Table 2.1 : Thickness of Ni-based samples**

Ni-based ribbons	Thickness ( $\mu$ m)
Ni <sub>60</sub> Fe <sub>20</sub> B <sub>20</sub> .	22
Ni <sub>50</sub> Fe <sub>30</sub> B <sub>20</sub>	20
Ni <sub>40</sub> Fe <sub>40</sub> B <sub>20</sub>	23
Ni <sub>30</sub> Fe <sub>50</sub> B <sub>20</sub>	19

## 2.8 Examining the Amorphous Ribbon

The amorphousity of all the ribbons has been confirmed by X-ray diffraction using Cu-K $\alpha$  radiation. Representative ribbons were found to be amorphous as shown in Fig-2.10. The ribbons showed broad diffraction maximum and no low angle scattering. These ribbons were also ductile and those cases for which low angle scattering appear and the broad diffraction peak are subdued there is some presence of micro crystalline phase. These could be removed if the speed of the roller was increased. The thickness of an amorphous is controlled by the liner speed of roller, the gap between the nozzle and the rotating drum which was about 1.5 to 5  $\mu$ m, oscillation of the drum, both static and dynamic, pressure and temperature of the melt and the stability of the drop on the surface of the drum. The nature of the board diffraction peak as observed is shown in Fig. 2.10 for the experimental sample.

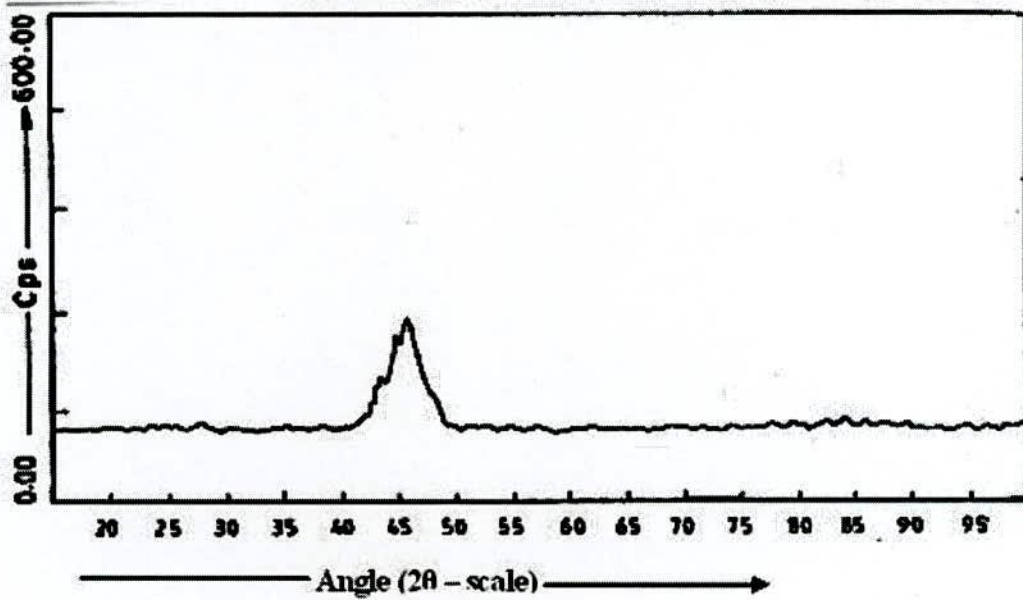


Fig. 2.10 X-ray diffraction pattern from the top surface of the amorphous ribbon with composition  $\text{Fe}_{40}\text{Ni}_{40}\text{B}_{20}$

**CHAPTER III**  
**THEORETICAL ASPECTS**



## THEORETICAL ASPECTS

### 3.1 Amorphous Alloy or Metallic Glass

In amorphous alloys, the symmetry is absent and principally each atom constitutes a structural unit. However, their higher density and the magnitude of magnetic moments and other properties being close to those of crystalline compounds suggests that the short-range order and thus also local structures are very similar to those in crystalline materials with high coordination numbers. This is due to the presence of a short range order which extends over a range of some neighbor shells of atoms up to a distance of about 1 nm. There is no long range order like in microcrystalline materials. There is a continuous transition from amorphous via 'nearly crystalline' [3.1] involving nanocrystals [3.2] to the microcrystalline structure depending on composition, preparation process and the conditions for local atomic ordering.

In Condense matter physics, an amorphous (from a Greek a, without, morph, shape, form) or non-crystalline solid is a solid that lacks the long-range order characteristic of a crystal. In part of the older literature, the term has been used synonymously with glasses. The local structure in amorphous metallic material is distinct from that of window glass. By analogy, the term 'metallic glass' usually refers to a metallic alloy rapidly quenched in order to "freeze" its structure from the liquid state.

A 'glass' refers to a molten mass that is cooled rapidly to prevent crystallization the expression 'glass' in its original sense refers to an amorphous or nanocrystalline solid formed by continuous cooling of a liquid [3.3], while a solid is define somewhat arbitrary as object having a viscosity greater than  $10^{14}$  Pas. Glasses have been found in every category of materials and of various bond types: covalent, ionic, Vander walls, hydrogen and metallic. Different types of amorphous solids include gels, thin films and nanostructured materials.

#### 3.1.1 Nature and Formation of amorphous Alloys

It is very difficult to get pure metals in the amorphous state. It is necessary to add glass forming materials to pure metals or alloy to get the amorphous state and to bring the cooling rate within a reasonable rate. Usually around 20% of glass forming materials like B,

Si, P, C etc which have atomic radii, comparatively small compared to those of metallic atoms and the glass forming atoms occupy the voids left between the bigger atoms of metals when they are closely packed. It can be showed that when there is random close packing of heard spheres, there is about 20% voids created between these atoms. The glass forming materials which have smaller atoms occupy these voids which explain the importance of the glass forming materials in the preparation of an amorphous ribbon.

The term “amorphous” defines a non crystalline body while a “glass” refers to a molten mass that is cooled rapidly to prevent crystallization. By analogy, the term “metallic glass” usually refers to a metallic alloy rapidly quenched in order to “freeze” its structure from the liquid state. The expression “glass” in its original sense refers to an amorphous or nano crystalline solid formed by continuous cooling of a liquid while a solid is defined somewhat arbitrary as object having as viscosity greater than  $10^{14}$  Pa.s [3.4]. Glass lacks three dimensional atomic periodicity beyond a few atomic distances. It is characterized by limited number of diffuse holes in X-ray, electron and neutron diffraction and no sharp diffraction contrast in high regulation electron microscopy.

Glasses are generally formed it upon cooling of a melt, crystal nucleation and/or growth are avoided. At a temperature called glass transition temperature ( $T_g$ ) the liquid freezes to a rigid solid, however without crystalline order. Thus, glasses and amorphous solids in general are structurally characterized by the absence of long range translational order. But a short range order is still present and may be similar to that found in the crystalline counterpart.

Synthesizing amorphous alloys requires rapid solidification, in order to by-pass the crystallization [3.5]. The metastable structure thus achieved nevertheless may possess a short-range order (SRO) that resembles the equilibrium crystal structure [3.6]. This indicates that the thermodynamic forces that drive crystallization in metals are extremely strong and in most cases, over powering. Thus the search for alloy systems that allows formation of amorphous structure is of keen technological importance.

Fig. 3.1 shows schematically, the time taken for a small amount of crystalline phases form in an undercooled liquid as a function of temperature. The temperature, the Temperature- Time-Transformation (TTT) diagram shows a characteristic C curve behavior. At the temperature close to melting point  $T_m$ , there is little driving force for crystallization, so



that the crystal nucleation and growth rates are small, and the crystallization onset time  $t_0$  is large. As the temperature decreases, the crystallization onset time reaches a minimum value  $t_0^*$  at a temperature  $T_n$ , and then increases again as the thermal energy becomes insufficient for atomic motion.

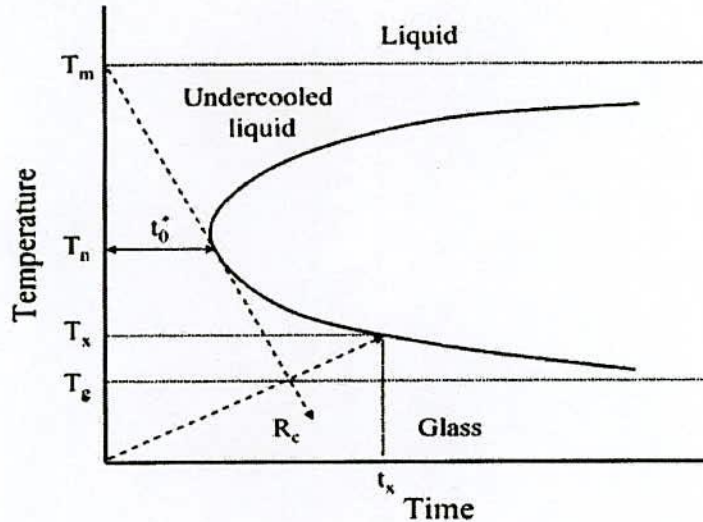


Fig. 3.1 Schematic TTT diagram for the onset of crystallization

Close to the glass transition temperature ( $T_g$ ) atomic motion is completely suppressed and the amorphous structure is frozen in, so that the crystallization onset time  $t_0$  becomes large. Therefore, critical cooling rate  $R_c$  to avoid crystallization is given below:

$$R_c = \frac{T_m - T_n}{t_0^*} \quad (3.1)$$

### 3.2 Factors Contributing to Glass Formation and Stability

There are three interrelated factors that determine glass forming tendency. There are:

- (i) Thermodynamic conditions that favor the liquid phase relative to crystalline phase.
- (ii) The kinetic conditions that inhibit crystallization and
- (iii) The process factors that arise due to the experimental condition.



The thermodynamic factors for glass formation are liquids temperature ( $T_m$ ) at which the alloy melts, the heat of vaporization and the free energy of all phases that arise or could potentially arise during solidification process. Viscosity of the melt, the glass transition temperature ( $T_g$ ) and the homogeneous nucleation rate belong the kinetic parameters. Processing parameters are the cooling rate; the heterogeneous nucleation rate and the super cooling temperature interval. The temperature of the glass transition is slightly dependent on the cooling rate. At each cooling rate, the glass will freeze in a different state of internal energy.

A single parameter that expresses glass forming tendency is the ratio of the glass transition temperature to the melting temperature defined as

$$T = \frac{T_g}{T_m} \quad (3.2)$$

which usually is mentioned as reduced glass transition temperature or reduced temperature.

Higher values of  $T$  obviously favor glass formation. For metallic glass to be formed by rapid cooling  $T$  should be greater than 0.45 as mentioned [3.7]. Based on alloy composition, there are two major groups that rapidly form glasses. In one of this groups the metal is from Fe, Co, Ni, Pd or Pt and the metalloid is B, C, Si, Ge and P. The metallic glasses constitute soft amorphous magnetic materials.

It is very difficult to get pure metals in the amorphous state. It is necessary to add glass forming materials to pure metals or alloys to get amorphous state and to bring cooling rate within a reasonable rate. Usually around 20% of glass forming metals like B, Si, P, C etc, which have atomic radii comparatively small compared to those of metallic atoms occupy the voids left between the bigger atoms of metals than they are closely packed. It can be showed that when there is random close packing of hard spheres, there is about 20% voids created between these atoms. The glass forming materials also reduces the melting point of the alloys and thereby the separation between the glass forming temperature and the crystallization temperature is reduced.

The amorphous alloy composition most favorable for glass formation is near eutectic, i.e. the composition in which the transformation from the liquid state of solid state takes place

instantaneously without passing through liquid plus solid mixed phase the deeper the eutectic, the better is the glass formation ability [3.8].

The magnitude of  $T_g$  and  $T_x$  are very different for amorphous materials and depend strongly on composition. The activation energy ranges typically energy ranges typically between 2 and 6eV [3.9]. The crystallization is associated with nucleation and growth process. Since the formation of an amorphous alloy depends on the absence of long range order; change of composition is expected to affect  $T_g$  and  $T_x$ . This is because the long range ordering of atoms depends on the free energy difference the crystalline state.

### **3.2.1 Structure and Microstructure of Amorphous and Nanocrystalline Alloys**

An amorphous solids is one in which the atomic positions do not have crystalline periodic order. The amorphous structure is postulated to be that of the frozen liquid. The local structure in amorphous metallic materials is distinct from that of window glass. A periodically spaced atom does not exist in amorphous alloys. Therefore XRD does not show any diffraction pattern. If one performs an X-ray scattering experiments on amorphous material, one does observed one or more broad peaks in the scattered intensity shown in Fig. 3.2 at angles similar to those where one or more diffraction peak could occur in a crystalline alloy of the same composition.

Scherer analysis of the breadth of the X-ray scattering peak(s), one would conclude that the 'crystallite size' was on the order of atomic dimensions. This is good argument for only short range atomic correlations being present in amorphous metals. Scattering experiments on amorphous alloys can be used to determine the so called radial distribution function that is derived from an appropriate Fourier transform of a normalized scattered intensity expressed as a function of scattering angle.

The atoms in an amorphous solid are not periodically arranged and therefore the concept of a lattice is not appropriate for describing for their positions. Thus in an amorphous solid there is not an equivalent concept to that of a lattice and a basis of region to describe atomic positions in a more probabilistic sense using the concept of a pair correlation function,  $g(r)$ . The pair correlation function is defined as the probability that two atoms in the structure are separated by a distance  $r$ . To define  $g(r)$  further begin by considering  $N$  atoms in a



volume,  $\Omega$ , Letting  $R_1, R_2, R_3, \dots, R_N$  denotes the positions of  $N$  -atoms with respect to an arbitrary origin. The distance  $r$  denotes the magnitude of the vector connecting two atoms  $i$  and  $j$ . That means,

$$r = R_i - R_j \quad (3.3)$$

Two additional atomic distribution functions related to the pair correlation function are the spatially dependent atomic density,  $\rho(r)$ , which is defined as :

$$\rho(r) = \frac{Ng(r)}{\Omega} \quad (3.4)$$

and the radial distribution function,  $RDF(r)$ , which is defined in terms of the pair correlation function as :

$$RDF(r) = 4\pi r^2 \rho(r) \quad (3.5)$$

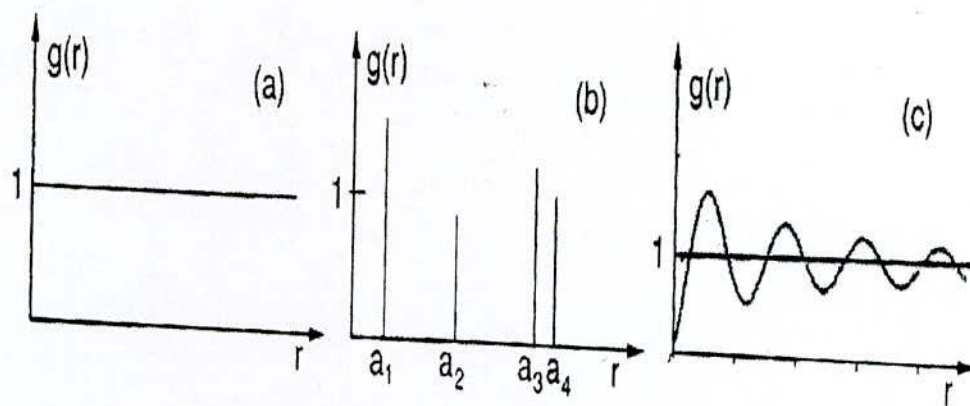


Fig. 3.2 Typical pair correlation function for (a) a completely disordered (b) a crystalline completely ordered and (c) an amorphous short-range ordered material

Fig. 3.2 illustrates schematically the distinction between the pair correlation function for a completely disordered, a crystalline completely order and an amorphous short-range ordered material. A completely disordered material, like a gas has a uniform unit probability of finding neighboring atoms at all possible distances which leads to a uniform featureless  $g(r)$ . On the other hand a crystalline solid has a set of discrete distances between atomic positions and therefore the pair correlation function in a set of discrete  $\delta$ -like functions, the amplitude which reflects the particular coordination number for nearest neighbor, next nearest



neighbor etc pairs of atoms. This is consistent with Bragg scattering (diffraction). In amorphous alloys  $g(r)$  is neither discrete nor featureless; instead broad peaks reflect the short range order in these materials.

### 3.3 Stability of the Amorphous Nanocrystalline Materials

Amorphous materials are always in a metastable state, which tend to transform into more stable crystalline phases. There are three kinds of stability of significance for amorphous magnetic alloys:

- (i) Their resistance to the initiation of crystallization
- (ii) Structural relaxation effects and
- (iii) The relaxation or re orientation of directional order.

Actually, controlled crystallization from the amorphous state seems to be the only method presently available to synthesize nanocrystalline alloys with attractive soft magnetic properties. The formation and resultant stability of amorphous alloys are important topics both theoretically and technologically. The theoretical analysis of the factors controlling the cause of formation and the stability of the resultant amorphous alloys have been extensively reviewed [3.10 -3.11]. From the thermodynamic view point [3.12-3.13], the ability of an alloy to be quenched into the glassy state is generally measured by the magnitude of the quantity

$$\Delta T_g = T_m - T_g \quad (3.6)$$

where  $T_m$  and  $T_g$  are the melting and glass transition temperature respectively. In a similar manner the stability of the glass after formation is generally measured by the magnitude of the quantity.

$$\Delta T_x = T_x - T_g \quad (3.7)$$

where  $T_x$  is the temperature for the onset of crystallization. As the temperature decreases from  $T_m$  the rate of crystallization will increase rapidly and then fall rapidly as the temperature decreases below  $T_g$ . The amorphous alloys composition most favorable for glass formation is near eutectic i.e. the composition in which the transformation from the liquid state to solid state takes place instantaneously without passing through liquid plus solid mixed phase. The deeper the eutectic the better is the glass formation ability [3.14]. There have been three approaches to relating the stability of the glass, i.e. its microstructure:

- (i) Bernal's model of randomly packed hard sphere's [3.15]. The metal atoms are assumed to form a random network of close packed hard spheres and the smaller metalloid atoms fill the holes inherent in such a structure.
- (ii) The effect of atomic sizes and inter atomic interactions [3.16], i.e. chemical bonding and suggested that it is chemical bonds which are the dominating factors in glass formation and stability.
- (iii) The third approach [3.17] is based on the role of the electron gas and showed that under certain circumstances a nearly free electron gas will produce a barrier against crystallization.

The transition to the glassy state and the crystalline state is accompanied by an exothermic heat effect giving rise to a sharp peak in temperature dependence of the heat flow. Therefore, Differential thermal analysis (DTA) is a widely used technique to study thermally induced transformations in amorphous alloys and to determine  $T_g$  and  $T_x$ . The magnitude of  $T_g$  and  $T_x$  are very different for amorphous materials and depend strongly on composition. The activation energy ranges typically between 2 to 6 eV [3.9].

### **3.3.1 Annealing Effects in Amorphous Alloy**

The amorphous structure represents a metastable state and thus any thermal treatment causes a continuous change of the atomic arrangement. Different processes can be distinguished:

- (i) Corrosion and oxidation
- (ii) Structural relaxation and
- (iii) Crystallization

The latter describes the transition to the crystalline state and this process requires an activation energy of the order of 2.5 eV. The first two processes affect the structural, magnetic and electrical properties in a specific way [3.18]. The structurally sensitive properties like the compensation temperature, the uniaxial anisotropy, the coercivity or the conductivity thus are suitable parameters to investigate the time and temperature dependence of these processes. The oxidation and structural relaxation of magnetic glasses is less important because they exhibit an even higher corrosion resistance than the corresponding crystalline alloys [3.19].



However, annealing in a magnetic field leads to strong changes in the magnetic properties [3.20].

The structural relaxation process can be described by a spectrum of activation energies according to the various atomic rearrangements possible in an amorphous material. However, that structural degradation causes only small changes in the magnetic and electronic properties as compared to the oxidation process that is associated with very low activation energy. The structural disorder of magnetic amorphous ribbon gives rise to significant changes of the mechanical, electrical, magnetic and magneto-optical properties as compared to the crystalline counterparts. Therefore, amorphous Ni-based ribbons are predominantly strong ferromagnetic, although significant differences in the magnetic properties are observed for Ni-based ribbons containing constant metalloids and other element like Fe. Annealing effect of magnetic moment variation was interpreted interims of the magnetic valence model or the environment model.

### **3.4 Initial Permeability of Amorphous Ribbons**

Amorphous Ni-Fe-B alloys are of great interest as soft magnetic materials for their static as well as dynamic applications. Fe-based magnetic alloys that have large magnetic flux density are usually used in the low frequency range, because of their inferior soft magnetic properties in the high frequency region compared to those of Fe-Ni-based amorphous ribbons. The measurement of magnetic properties as a function of frequency and its analysis by means of the complex permeability formalism has recently led to the resolution of several aspects of the magnetization process [3.13, 3.21]. The measurement of complex permeability gives us valuable information about the nature of the domain wall and their movements.

The  $\mu_i$  of the amorphous magnetic ribbons may be strongly affected by the presence of an electric current due to its heating effect, particularly in ac conditions. In dynamic measurements the eddy current loss is very important this occurs due to irreversible domain wall movements that are frequency dependent. A large number of possible mechanisms can contribute to the magnetic loss such as local variation of exchange energy, surface defects, compositional in homogeneities, anisotropy and magnetostriction [3.22-3.23], whose relative values are determined by grain size, grain orientation and thickness of the sample. Thus the magnetic characteristics are rather different annealed specimens from those of as quenched



amorphous ribbons. The present goal of most of the recent amorphous ribbons researches is to fulfill this requirement. But in this research, these techniques are applied to investigate the annealing effects of various thermal treatments on initial permeability measurement of Fe-Ni based amorphous ribbons. Before going into the complexity of initial permeability measurement, we discuss in short the theories and mechanism involved in frequency spectrum of initial permeability.

### 3.4.1 Theories of Permeability

The primary requirement is the highest possible permeability, together with low losses in the frequency range of interest. The initial permeability  $\mu_i$  is defined as the derivative of induction B with respect to the internal field H in the demagnetization state

$$\mu_i = \frac{dB}{dH}, H \rightarrow 0, B \rightarrow 0 \quad (3.8)$$

At microwave frequencies, and also in low anisotropic amorphous materials, dB and dH may be in different directions, the permeability then has a tensor character. In the case of amorphous materials containing a large number of randomly oriented magnetic atoms the permeability will be scalar, at low frequencies with

$$B = \mu_0(H + M) \quad (3.9)$$

and the susceptibility  $\chi = \frac{dM}{dH} = \frac{d}{dH} \left( \frac{1}{\mu_0} B - H \right)$

$$\chi = \left( \frac{\mu_i}{\mu_0} - 1 \right) \quad (3.10)$$

The magnetic density

$$E = \frac{1}{\mu_0} \int H \cdot dB \quad (3.11)$$

For time harmonic field  $H = H_0 \sin \omega t$ , the dissipation can be described by a phase difference  $\delta$  between H and B. In the case of permeability is namely define as the proportional its constant between the magnetic field induction B and applied intensity H,

$$B = \mu_i H \quad (3.12)$$

This definition needs modification when magnetic material is subjected to an ac magnetic field as given below.

$$H = H_o e^{i\omega t}$$

In such a field the magnetic flux(B) experience a delay with respect to H. The delay is caused due to the presence of various losses and is thus expressed as

$$B = B_o e^{i(\omega t - \delta)} \quad (3.13)$$

where  $\delta$  the phase is angle and marks the delay of B with respect to H. The permeability is then given by

$$\begin{aligned} \mu_i &= \frac{B}{H} = \frac{B_o e^{i(\omega t - \delta)}}{H_o e^{i\omega t}} \\ &= \frac{B_o e^{-i\delta}}{H_o} = \frac{B_o}{H_o} \cos \delta - i \frac{B_o}{H_o} \sin \delta \\ \mu_i &= \mu' - i\mu'' \end{aligned} \quad (3.14)$$

$$\text{Where } \mu' = \frac{B_o}{H_o} \cos \delta \text{ and } \mu'' = \frac{B_o}{H_o} \sin \delta \quad (3.15)$$

The real part  $\mu'$  of complex permeability  $\mu_i$  as expressed in equation [3.14] represents the components of B which is in phase with H, so it corresponds to the normal permeability. If there are no losses, we should have  $\mu_i = \mu'$  at very low frequency. The imaginary part  $\mu''$  corresponds to that of B, which is delayed by phase angle  $90^\circ$  from H. The presence of such a component requires a supply of energy to maintain the alternating magnetization, regardless of the origin of delay.

It is useful to introduce the loss factor or loss tangent ( $\tan \delta$ ). The ratio of  $\mu''$  to  $\mu'$  as is evident from equation [3.15], gives.

$$\frac{\mu''}{\mu'} = \frac{(B_o / H_o) \sin \delta}{(B_o / H_o) \cos \delta} = \tan \delta \quad (3.16)$$

This  $\tan \delta$  is called the loss factor or loss tangent. The Q-factor or quality factor is defined as the reciprocal of this loss factor, i.e.

$$Q = \frac{1}{\tan \delta} \quad (3.17)$$

$$\text{And the relative quality factor} = \frac{\mu_4}{\tan \delta} = \mu_4 Q \quad (3.18)$$

The behavior of  $\mu'$  and  $\mu''$  versus frequency is called the permeability spectrum. The initial permeability of a ferromagnetic substance is the combined effect of the wall permeability and rotational mechanisms.

### 3.4.2 Measurement of Initial Permeability

The real part of initial permeability is calculated by using a formula

$$\mu' = \frac{L}{L_0} \quad (3.19)$$

where L is the self inductance of the sample core and

$$L_0 = \frac{\mu_0 N^2 S}{\pi d} \quad (3.20)$$

where  $L_0$  is the inductance of the winding coil without sample core and N is the number of the turns (here N=10), S is the area of cross section as given below

$$S = \frac{m}{\pi \rho d} \quad (3.21)$$

where m = weight of the ribbon, d and  $\rho$  are the mean diameter and density of the sample as follows

$$d = \frac{d_1 + d_2}{2} \quad \text{and} \quad \rho = \frac{8M}{Nd^3} \quad (3.22)$$

For our present experiment the amorphous ribbon was wound into torrid shape. The initial permeability of this torrid shaped sample was measured by obtaining the L value provided by an inductance analyzer used for permeability measurement as value of  $L_0$  is derived by the equation given above.

### 3.4.3 Relative permeability

$$\text{Susceptibility, } \chi = \frac{dM}{dH} = \frac{d}{dH} \left( \frac{1}{\mu_0} B - H \right)$$

$$\chi = \frac{1}{\mu_0} \frac{dB}{dH} - 1$$



$$\chi = \frac{\mu}{\mu_0} \quad (3.23)$$

Relative permeability, sometimes denoted by  $\mu_r$ , is the ratio of the permeability of specific medium to the permeability of free space  $\mu_0$

$$\mu_r = \frac{\mu}{\mu_0} \quad (3.24)$$

In terms of relative permeability, the magnetic susceptibility

$$\chi_m = \mu_r - 1 \quad (3.25)$$

### 3.4.4 High Frequency Behavior and Losses

The frequency dependence of the absolute value of complex permeability and its imaginary part  $\mu''$  is expressed in terms of the relative loss factor  $\frac{\mu''}{|\mu|^2}$ . The later is directly related to the cycle losses at constant induction amplitude B

$$\frac{p}{f} = \frac{\pi B^2 \mu''}{\mu_0 |\mu|^2} \quad (3.26)$$

The favorable high frequency behavior is essentially related to

- (i) the thin ribbon gauge of  $d \approx 20 \mu m$  inherent to the production technique and
- (ii) to a relatively high electrical resistivity of typically  $\rho \approx 115 \mu\Omega - cm$  related to the high Si-content in the bcc grains [3.24] and the intergranular amorphous phase.

Both parameters are comparable to amorphous metals and yield low eddy current losses  $p_e$ , which in thin sheets at a frequency  $f$  and a induction level B are given per volume by [3.25]

$$p_e = \left( \frac{3 \sinh x - \sin x}{x \cosh x - \cos x} \right) \frac{(\pi d f B)^2}{6 \rho}$$

$$|p_e|_{x \ll 1} = \frac{(\pi d f B)^2}{6 \rho} \quad (3.27)$$

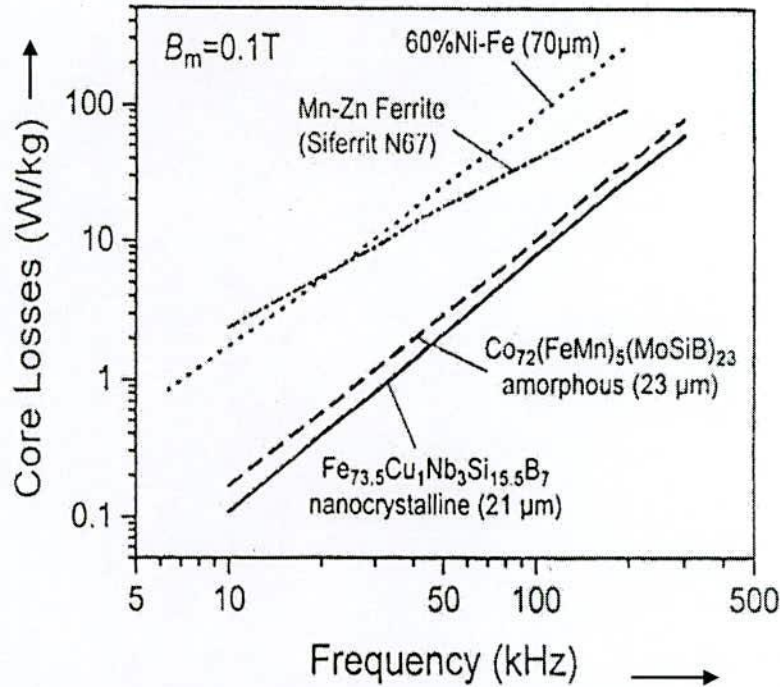


Fig. 3.3 Low core losses and Fe-based amorphous alloy at high frequency

$$\text{with } x = 2\sqrt{\frac{f}{f_w}}, \quad \text{where } f_w = \frac{4\rho}{\pi\mu_o\mu_i d^2} \quad (3.28)$$

is the limiting frequency above which the exciting magnetic field no longer fully penetrates the specimen and, accordingly, the permeability decreases as a function of the frequency.

### 3.4.5 Losses

The most important loss in ferromagnetic substance is the hysteresis loss. In the Rayleigh region where the amplitude of magnetization is very small, the loss factor due to the hysteresis loss depends on the amplitude of magnetic field. The physical origin of the hysteresis loss is eddy current or other damping phenomena associated with irreversible wall displacement or irreversible rotation magnetizing.

The hysteresis loss becomes less important in the high frequency range, because of the wall displacement which is the main origin of hysteresis, is most damped in this range and is replaced by the rotation magnetization. The next important loss for ferromagnetic metal and alloys is the eddy current loss. Since, a power loss of this type increases in proportion to the

square of the frequency in the high frequency range. Magnetic after effect also given rise to a magnetic loss for which frequency magnetization. This happens because of the insertion of a boron atom between iron atoms has a remarkable effect in changing the intensity of pseudo dipolar interaction between the iron atoms [3.26]

At intermediate and high inductions, when core losses are significant in applications, the total power losses are often expressed as the sum of a hysteresis loss and eddy current loss as

$$W = \eta B^{1.6} + eB^2 f^2 \quad (3.29)$$

When  $f$  is small, e.g. 100 Hz. At low induction  $B$  the hysteresis loss term is more nearly proportional to  $B^3 f$ . At high frequency, the losses are controlled predominately by eddy currents and are given by.

$$W_e = \frac{\pi t B^2 f^r}{(\mu \Omega)^{\frac{1}{2}}} \quad (3.30)$$

Where  $f$  varies from  $f^2$  at lower frequencies to  $f^{\frac{3}{2}}$  at higher frequencies  $t$  is the thickness  $\mu$  is the permeability and  $\Omega$  is resistivity. Loss results for both the amorphous and crystalline alloys show dependence given by

$$W \propto B^{\beta} f^{\gamma} \quad (3.31)$$

The values of the exponents  $\beta$  and  $\gamma$  vary in a given alloy after stress release, depending of the magnitude and direction of the induce anisotropy as described by F. E. Luborsky et al [3.27]. The considerable improvement losses in the result of annealing as function of frequency.

### 3.5 Magnetic Dipole Moments and Magnetization

The vast majority of soft magnetic materials have one or more of the ferromagnetic transition metal elements, Fe, Co or Ni or the rare earth metal Gd as a majority component. The magnetic dipole moments of elemental and alloy magnets are most completely understood the band theory of solids [3.28]. The band theory of solids considers the brooding of localized atomic state with discrete Eigen values into a continuum state for more if nearest



electrons over a range of energy .The theory allows for calculation of energy dispersion(i.e. energy as a function of wave vector)and orbital angular momentum specific an spin resolved energy bands and densities of state allows for the description of atom resolved magnetic dipole moments and therefore spontaneous magnetization of elemental and alloy magnetic properties are:

- (i) The production of non integral or half integral atomic dipole moments and resulting ground state magnetization in metals and alloys.
- (ii) The prediction that bandwidth and exchange splitting (energy differences between spin up and spin down bands) are intimately dependent on magnetic coordination number and atomic volume.

Table 3.1 summaries absolute zero and room temperature (RT) (where applicable) magnetization and atomic dipole moments for some important transition metal and the rare earth elemental magnets. Also shown are Curie temperature i.e. ferromagnetic ordering temperature which is not ground state properties that are directly calculated from band theory.

Table 3.1 Spontaneous and room temperature magnetizations, magnetic dipole moments and Curie temperatures for elemental ferromagnets

Element	$\mu_m$ @ 0K ( $\mu_B$ )	$\mu_s$ @ 0K	$\mu_s$ @ RT	$T_c$ (K)
Fe	2.2	1740	1707	1043
Co	1.72	1446	1400	1388
Ni	0.606	510	485	627
Gd	7.63	2060	---	292
Dy	10.2	2920	---	88

The number of spin up,  $n_+$  and spin down  $n_-$  electrons in each band can again be calculated by integrating these densities of state:

$$n_+ = \int_0^{E_F^+} g_+(E)dE \quad \text{and} \quad n_- = \int_0^{E_F^-} g_-(E)dE \quad (3.32)$$

Here the Fermi energies,  $E_F$ , are the same and the zero's of energy are different for the two spin bands and the atom resolved (i.e. Fe and Co) magnetic dipole moments can be calculated

$$\mu_m = (n_+ - n_-)\mu_B \quad (3.33)$$

Knowledge of atomic values or alloy density, then allows for the direct calculation of the alloy magnetization. Fe-Co alloys exhibit the largest magnetic inductions of any material, and also have Curie temperatures which are desirable for high temperature applications. Fe rich alloys typically have smaller inductions and lower Curie temperatures than Fe-Co alloys. Co alloys can also be soft but only if the f.c.c. phase of Co is present. Co rich alloys typically have smaller inductions and larger  $T_C$ 's.

### 3.5.1 Magnetization of the Amorphous Ribbons

The theoretical treatment of spin ordering in amorphous solids is quite complex. The topological disorders on the amorphous alloys affect the magnetic moment of the transition metal atoms, because of the change of environment of each magnetic atom. The exchange integral also varies at each point because of the varying inter atomic distance and the overlap of the electronic wave functions. The third factor determining the magnetization processes is the single ion magneto crystalline anisotropy which also changes because of the changing crystalline field. However, the magnetization of amorphous alloy is computed by introduction some drastic simplifying assumptions which are applicable in regular crystalline lattices.

The saturation magnetization of a material at a temperature of 0K is one of its basic properties. Measurements are usually expressed as average moment per magnetic atom in units of the Bohr magneton,  $\mu_B$ , or as specific saturation magnetization for its amorphous alloy,  $\sigma_s$ , in units for emu/gm. The moments of most amorphous alloys are lower than those of the pure crystalline transition metal which they contain. However, the direct effect of the structural disorder on the moments is very small. The moments are lower because of the change in the local chemical environment provided by the presence of the metalloids. The reduction is least in B-based glass and highest in P-based glass. The observed moments on TM-M glasses can approximately fitted to a formula [3.29].

$$\mu_B = \frac{\mu_{TM}C_{TM} - C_B - 2C_{Si}C - 3C_P}{C_{TM}} \quad (3.31)$$

Where  $\mu_{TM}$  is the magnetic moment of TM-M atoms, taken as 2.6, 1.6 and 0.6 respectively in Bohr magneton for Fe, Co and Ni, C's are respective concentrations. This clearly



demonstrates the change transfer from metalloid to d-band of transition metal and seems to suggest that 1, 2 or 3 electrons are transferred from each of B, Si (c, Gr) or P atom. The relative number of electrons denoted can be listed as  $-P_{13}C_7 > -Si_{15}B_{10} > -P_{16}B_6Al_3 > -P_{14}B_6 > -Si_9B_{13} > -B_{20}$  based on the relative magnitude of  $M_S$ .

### 3.5.2 Ferromagnetic ordering (Curie) Temperatures

Ferromagnetism is a collective phenomenon since individual atomic moments interact so as to promote alignment with one another. This collective interaction gives rise to the temperature dependence of the magnetization. Two models have explained the interaction between atomic moments. Mean Field Theory considers the existence of a non-local internal magnetic field, called the Weiss field, which acts to align magnetic dipole moments even in the absence of an applied field  $H_a$ . Heisenberg Exchange Theory considers a local (usually nearest neighbor) interaction between atomic moments (spins) which acts to align adjacent moments even in the absence of a field.

The basic assumption of the mean field theory is that this internal field is non-local and is directly proportional to the sample magnetization.

$$H_{INT} = \lambda_w M \quad (3.32)$$

where the constant of proportionality,  $\lambda_w$ , is called the Weiss molecular field constant.

To consider ferromagnetic response in applied field,  $H_a$ , as well as the randomizing effects of temperature, we consider the superposition of the applied and internal magnetic fields. By analogy with the problem of paramagnetic moments, the average atomic dipole moment can be expressed in terms of the Brillouin function

$$\langle \mu_m \rangle = \mu_m^{atom} B_J(\alpha') \quad (3.33)$$

where  $\alpha' = \left( \frac{\mu_0 \mu_m^{atom}}{K_B T} \right) (H + \lambda_w M)$  for a collection of classical dipole moments. The saturation magnetization

$$M_S = N_m \langle \mu_m^{atom} \rangle \quad (3.34)$$

$$\frac{M}{N_m \mu_m^{atom}} = \frac{M}{M_S} = B_J[H + \lambda_w M] \quad (3.35)$$



Under appropriate conditions, this leads to solutions for which there is a non-zero magnetization (spontaneous magnetization) even in the absence of an applied field.

For  $T > T_c$ , the ferromagnetic Curie temperature the only solution to equation (3.35) is  $M = 0$ , i.e., no spontaneous magnetization and thus paramagnetic response.

For  $T < T_c$ , we obtain solutions with a non-zero, spontaneous magnetization, the defining feature of a ferromagnet.

The Heisenberg model considers ferromagnetism and the defining spontaneous magnetization to result from nearest exchange interactions, which act to align spins in a parallel configuration, instead of a non-local, mean field. The Heisenberg model can be further generalized to account for atomic moments of different magnitude and assigns, i.e., in alloys, and for exchange interactions, which act to align nearest neighbor moments in an anti-parallel fashion, or in a non collinear relationship. Let us consider first the Heisenberg ferromagnet. Here we assume that the atomic moments (due to a spin vector  $S$ ) on nearest neighbor sites are coupled by a nearest neighbor exchange interaction that gives rise to a potential energy.

$$E_P = -J_{ex} S_i \times S_{i+1} \quad (3.36)$$

That for  $J_{ex} > 0$  favors parallel alignment of the spins. The exchange, suitably scaled, replaces the Weiss molecular field constant in the mean field theory of ferromagnetism to explain the temperature dependence of the magnetization.

Ferromagnetic exchange interactions set the scale for Curie temperatures in ferromagnetic alloys. Inter atomic exchange couplings can be calculated from first principles by considering the energy change associated with rotation of individual spins in the host material. These exchange interactions can be used within a mean field theory to estimate the Curie temperature. An empirical description of the variations of the exchange energy, with inter atomic spacing called the Bethe-Slater curve is instructive in describing the effect of alloying on ferromagnetic Curie temperatures. The interplay between electron-electron Coulomb interactions and the constraints of the Pauli Exclusion Principle determine the sign of the exchange interaction.

In transition metal solids a measure of the overlap between nearest neighbor d-orbital is given by the ratio of the atomic to the 3d ionic (or nearest neighbor) radius. In mean field theory the Curie temperature can be related to the exchange energy as follows:

$$T_c = \frac{2S(S+1)}{3K_B} \sum_{ij} T_{ij} \quad (3.37)$$

where  $S$  is the total spin angular momentum,  $K_B$  is the Boltzmann's constant and  $T_{ij}$  is the exchange interaction between atoms at the position  $r_i$  and  $r_j$ .

In first case, a unique constant exchange interaction between the magnetic atoms is assumed and the amorphous nature of the alloy is taken into account by calculating a random distribution of the local anisotropy field [3.25]. In the second approach is treating this problem of distribution of exchange integrals assumed in order to reflect the structural fluctuations in the amorphous alloy [3.30]. Both approaches predict that  $M$  vs.  $T$  curve will flat below that for the crystalline counterpart.

**CHAPTER IV**

**EXPERIMENTAL DETAILS**



## EXPERIMENTAL DETAILS

### 4.1 Thermal Treatment of the Amorphous Ribbon

With a view to study amorphous behavior by XRD and magnetic properties upon evaluation up to glass transition phase on amorphous matrix thermal treatment, i.e annealing is required to perform. For XRD, as prepared amorphous ribbon were cut into small pieces of about 2 cm lengths and for magnetic measurements such as permeability torodial core were wound for annealing treatment. A laboratory built vacuum system made by quartz tube capable of evaluating up to  $10^{-5}$  torr was used for their purpose. The samples were put into the quartz tube and evaluated ( $10^{-5}$  torr) before it had been put inside the tabular furnace heated to a present temperature and kept for the time required to complete the annealing. In this way all the isothermal annealing as a function of time were performed.

### 4.2 Annealing

Annealing in metallurgy and materials science, is heat treatment where in a material is altered, causing changes in its properties such as strength and hardness. It is a process that produces conditions by heating to above the critical temperature; maintaining a suitable temperature, and then cooling. Annealing is used to induce ductility, soften materials, relieve internal stress, refine the structure by making it homogenous and improve cold working properties.

In the causes of copper, steel, silver and brass this properties is performed by substantially heating the material (generally until glowing) for a while and allowing it to cool. Unlike ferrous metals, which must be cooled slowly to anneal, copper, silver and brass can be cooled slowly in air or quickly by quenching in water. In this fashion the metal is softened and prepared for future work such as shaping, stamping or forming.

Annealing occurs by the diffusion of atoms within a solid material, so that the material progresses towards its equilibrium state. Heat is needed to increasing the rate of diffusion by providing the energy needed to break bonds. The movement of atoms has the effect of

redistributing and destroying the dislocations in metals and (to a lesser extent) in ceramics. This attention in dislocations allows metals to deform more easily, so increases their ductility.

#### **4.2.1 Stages**

There are three stages in the annealing process, with the first being the recovery phase, which results in softening of the metal through removal of crystal defects (the primary type of which is the linear defect called a dislocation) and the internal stresses which they causes. Recovery phase covers all annealing phenomena that occur before the appearance of new strain free grains. The second phase is re crystallization, where new strain-free grains nucleate and grow to replace these deformed by internal stress. If annealing is allowed to continue once re crystallization has been completed, grain growth will occur, in which the microstructure starts to coarsen and may cause the metal to have less than satisfactory mechanical properties.

#### **4.2.2 Setup and Equipment**

Typically, large ovens are used for the annealing process. The inside of the oven is large enough to place the work piece in a position to receive maximum exposure to the circulating heated air. For high volume process annealing, gas fired conveyor furnaces are often used. For large work piece or high quantity parts, car bottom furnaces will be used in order to move the parts, in and out with ease. Once the annealing process has been successfully completed, the work pieces are sometimes left in the oven in order for the parts to have a controlled cooling process. While some work pieces are left in the oven to cool in a controlled fashion, other materials and alloys are removed from the oven. After being removed from the oven, the work pieces are often quickly cooled off in a process known as quench hardening. Some typical methods of quench hardening materials involve the use of media such as air, water, oil or salt. Quench hardening is generally applicable to some ferrous alloys, but not copper alloys.

### **4.3 Impedance Analyzer**

The Hewlett Packard 4192A LF Impedance Analyzer can measure eleven impedance parameters absolute value of impedance ( $|Z|$ ), absolute value of admittance ( $|Y|$ ), phase angle



( $\theta$ ), resistance (R), reactance (X), conductance (G), susceptance (B), inductance (L), capacitance (C), dissipation factor (D) and quality factor (Q). Measurement range of  $|Z|/R/X$  is 0.1 m $\Omega$ ; to 1.2999 M $\Omega$ ;  $|Y|/G/B$  is 1ns to 12.999s;  $\theta$  is -180.00° to +180.00°; L is 0.01 mH to 1.000 kH; C is 0.1 pF to 100.0 mF; D is 0.0001 to 19.999; Q is 0.1 to 1999.9. All have a basic accuracy of 0.1% and resolution of  $4\frac{1}{2}$  digits. Number of display digits dependence on measuring frequency and OSC level setting. We made use of the excellent experimental facilities available at the Department of Physics, Bangladesh University of Engineering & Technology (BUET), Dhaka.

The 4192A can provide measuring frequency, OSC level, and dc bias voltage equivalent to actual operating conditions. The sweep capabilities of the built-in frequency synthesizer and dc bias source permits quick and accurate measurements. The built-in frequency synthesizer can be set to measuring frequency within the range from 5 Hz to 13 MHz with 1 mHz maximum resolution. OSC level is variable from 5 mV to 1.1 V with 1 mV resolution. The internal dc bias voltage source provides  $\pm 35$  V in 10 mV increments. Measuring frequency or dc bias voltage can be automatically or manually swept in either direction. OSC level can be manually swept in either direction in 1 mV increments (5 mV for levels above 100 mV). Actual test voltage across or test signal current through the device under test is also measured. Thus the 4192A can evaluate components and circuits under a wide variety of measurements conditions.

Moreover, the 4192A's high measurement performance and capable functionality delivers a powerful tool to circuit design and development as well as materials research and development (both electronic and non electronic materials) environments:

- \* Accurate measurement over wide impedance range and wide frequency range.
- \* Powerful impedance analysis function.
- \* Ease of use and versatile PC connectivity.

**The following are application examples;**

- Impedance measurement of two terminal components such as capacitors, inductors, ferrite beads, resistors, transformers, crystal/ceramic resonators, multi-chip modules or array/network components.



### Semiconductor components

- C – R characteristic analysis of varac for diodes.
- Parasitic analysis of a diode, transistor or IC package terminal/leads.
- Amplifier input/output impedance measurement.
- Impedance evaluation of printed circuit boards, relays, switches, cables, batteries etc.

### Dielectric materials

- Permittivity and loss tangent evaluation of plastics, ceramics, printed circuit boards and other dielectric material

### Magnetic materials

- Permeability and loss tangent evaluation of ferrite, amorphous and other magnetic materials.

### Semiconductor material

Permittivity, conductivity and C – V characteristics of semiconductor materials.

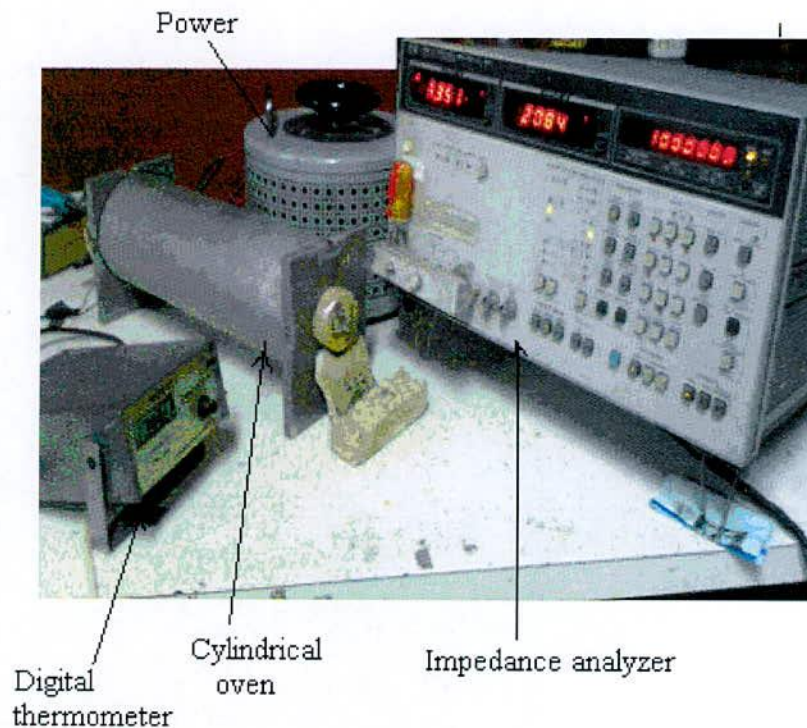


Fig. 4.1 Impedance Analyzer Model-Hewlett-Packard 4192A

### **4.3.1 Preparation of the Samples for Complex Permeability Measurement**

The amorphous ribbons were wound into toroidal cores having outer and inner diameter within 13 to 15 mm and with the ratio of outer and inner diameter always kept less than 1.2 in order to improve the homogeneity of the applied field, as also to reduce the possibility of an inhomogeneous inductance response. A low capacitance coil with 8 to 10 turns was wound around the toroids to allow the application of magnetic fields over a wide range of amplitudes. While measuring the permeability of the amorphous ribbon cores at high frequency, the high electric resistance of these materials generally precludes the trouble, some skin effect found with ribbons. However, the cross section of the amorphous ribbon core to be measured may have to be kept small in order to avoid dimensional resonance phenomena. To avoid an increase in resistance owing to skin effect, braided copper wire is used at frequencies higher than 100 kHz. The thickness of the separate wire stands being adapted in the measuring frequency of about 13MHz. the thumb rule is that, the wire thickness in microns must be smaller than the wavelength is meters.

At higher frequencies the capacitance arising from the winding gives in accurate values  $R$  and  $L_s$ . It is, therefore, necessary to kept the capacitance of the winding as low as possible. Frequency response characteristics were than investigated on these ring shaped specimens as a function of frequency.

### **4.3.2 Components of Complex Permeability Measurements**

The real ( $\mu'$ ) and imaginary ( $\mu''$ ) part of the complex permeability of the as-cast and annealed ribbons were measured as a function of frequency using the Hewlett-Packward 4192A LF Impedance Analyzer, BUET, Dhaka. From the frequency dependence of complex permeability, evolution of permeability and magnetic loss component at different stages of Ni-Fe-B amorphous ribbon as affected by thermal treatment at different temperatures was determined using toroids prepared from the ribbons wound with insulating Cu wire.

The frequency characteristics of the amorphous ribbon samples, i.e. the permeability spectra, were investigated using Impedance Analyzer model No.- 4192 ALF. The measurements were taken of inductances in the frequency range 1 KHz to 13 MHz. The

measured value of parameters obtained as a function of frequency and the real and imaginary parts of permeability and the loss factor,  $\mu'$  is calculated by using following formula.

$$L_S = L_0\mu'$$

$$\mu' = \frac{L_S}{L_0} \quad (4.1)$$

The 4192 ALF impedance analyzer directly measure the value of inductance L and loss factor (D)

$$\text{So } D = \tan\delta \quad (4.2)$$

Here, L is the inductance of the toroid and  $L_0$  is the inductance of the coil of same geometric shape in vacuum.  $L_0$  is determined by using the relation

$$L_0 = \frac{\mu_0 N^2 S}{\pi d} \quad (4.3)$$

Where  $S = \frac{m}{\rho d}$ ,  $\mu_0$  is the permeability of the vacuum, m is the mass of the sample,

N is the number of turns, S is the cross-sectional area of the toroid, d is the average diameter and  $\rho$  is the density of the material. The imaginary part of complex initial permeability can be determined by using the relation,

$$\tan \delta = \frac{\mu''}{\mu'} \quad (4.4)$$

and the relative loss factor is calculated with the relation  $\frac{\mu''}{\mu'}$  or  $\mu''/Q$

### 4.3.3 Real and Imaginary Components of Complex Permeability

Determination of permeability normally involves the measurements of the change in self-inductance of a coil in presence of the magnetic core. Methods of measurement those are commonly used are

- (i) The LCR bridge method
- (ii) Resonance circuits and
- (iii) The standing wave method



The behavior of a self-inductance can now be described as follows. If we have an ideal lossless air coil of inductance  $L$ , on insertion of magnetic core with permeability  $\mu$ , the inductance will become  $\mu L_0$ , The complex impedance  $Z$  of this coil then be expressed as

$$Z = R + iX = i\omega L_0\mu$$

$$Z = i\omega L_0(\mu' - i\mu'') \quad (4.5)$$

Where the resistive part is  $R = \omega L_0 \mu''$  (4.6)

and the reactive part is  $X = \omega L_0 \mu'$  (4.7)

The r. f permeability can be derived from the complex impedance of a coil in equation (4.5) the core has taken in the toroidal form to avoid demagnetization effects. The quantity  $L_0$  is derived geometrically as shown in equation (4.3).

#### 4.4 Curie Temperature

Curie Temperature,  $T_c$  is the most important parameter of magnetic materials. The magnetic properties and magnetic structures are effectively changed within the Curie temperature. Curie temperature provides substantial information on magnetic states of substances in respect of the strength of exchange interaction. So the determination of curie temperature accurately is of great importance. Curie temperature can be determined from the temperature dependence of permeability, temperature dependence of magnetization curve and Arott plot. Sometimes an operational procedure needs to be adopted for the determination of  $T_c$ . A slandered procedure for determination  $T_c$  in ferromagnetic materials is based on symmetry principal. A. Arott [4.1], K. P. Belov [4.2] and J. S. Kouvel [4.3] have pioneered the use of classical form of expression for magnetization and field near a ferromagnetic phase transition.

Temperature dependence of the initial permeability of the as-cast and annealed ribbons have been measured using a laboratory built furnace and Wayne Kerr 3255B inductance meter with continuous heating hate  $\approx 5^0\text{C}/\text{min}$  with very low applied ac field of  $\approx 10^{-3}\text{Oe}$ . From this measurement,  $T_c$  of the as-cast and annealed samples have been determined.

#### **4.4. Inductance Analyzer**

The 3255B precision magnetic Analyzer provides 2- terminal measurement of inductor and transformer over the frequency range 20 Hz to 500 kHz. dc resistance measurements are performed at a drive level of 100 mV. The drive level for ac measurements can be varied from 1 mV to 10 V. Automatic level control (ALC) can supply a dc bias current which is variable between 1 mA and 1 A and when used with external 3265B DC bias units, up to 125 A dc bias current is available.

The Analyzer's measurement, display and control facilities include:

- Stop frequency measurements.
- Multi- frequency measurements at a number of user defined frequencies.
- Display of actual measurement values ;
- Output of measurement-results to an Epson-compatible printer.
- Strong of components into bias according to their measured value and / or minor term (option).

All the above functions can be selected via manual front panel control or remote control via the GPIB interface for fully automated high speed testing. self calibration is performed to set calibration constants for signal processing elements in the measurement hardware and signal generator system, and to compensate for components, which drifted with time. To maintain full specified accuracy it should be run at least every three months. To measure the inductance of a component the analyzer should be powered up with the test leads or fixture connected to the foot panel BNC connectors. The analyzer should be operated in measurement mode. The component to be measured is connected to the test leads or fixture. The measurement may be performed as single short mode for single measurement or repetitive mode for continuous measurements.

#### **4.4.2 Curie Temperature determination from temperature dependence of ac permeability**

The Curie temperature which is measure of exchange interaction between the magnetic atoms is quite complicated in the case of amorphous alloys and is very much an experimental parameter. Because; theories are helpful only as a guide in rationalizing the



results obtained experimentally. So the determination of Curie temperature ( $T_c$ ) accurately is of great importance.

Our experimental set up for  $T_c$  measurement is shown in Fig. 4.2, we made use of the excellent experimental facilities available at Material Science Division (AECD). The temperature dependence of ac permeability was measured by using induction method. A laboratory built technique using an oven in which a heating wire is wound bifillerly and two identical inductions coils are wound in opposite directions such that the current induced flux in the two coils cancel each other. The whole set up is introduced in an oven. By varying temperature, ac permeability of the amorphous samples of toroidal shapes as a function of temperature was measured. When the magnetic state inside the amorphous sample changes from ferromagnetic to paramagnetic, the permeability falls sharply. From the sharp falls of specific temperature the  $T_c$  is determined. This is the basic principal used in our experimental set up.

As shown in Fig. 4.2, the circuit consists of two parts. The primary part consists of a low frequency generator, a multimeter and a resistance in series. The signal generator generates an alternating signal of frequency up to 200 kHz. A voltage drop occurs at the resistance of value 390 ohm. This voltage drop is measured by the voltmeter. The secondary part of the coil comprises of only voltmeter. The voltage induced in the secondary coil is measured by the voltmeter.

An ac current  $i$  flowing through the primary of the toroidal ring shape sample produce a magnetizing field. The dynamic field  $H$  within the primary is given by the relation

$$H = \frac{0.4N_1 \bar{I}}{d} \quad (4.8)$$

Where  $N_1$  is the total number of turns in the primary of the toroidal ring and  $d$  is given by the,  $d = \frac{d_1+d_2}{2}$ , where  $d_1$  and  $d_2$  are the inner and outer diameter of the toroidal sample respectively. Magnetic induction  $B$  calculated from the relation

$$B = \frac{E \times 10^8}{4N_2 f S} \quad (4.9)$$

where  $N_2$  is the number of turns in the secondary of the toroidal rings,  $f$  is the frequency of the balance of differential flux area of the cross section of the toroidal ring is given by  $S = dh$ ,



where  $d = \frac{d_2 - d_1}{2}$  and  $h$  is the height of the toroidal sample. Finally permeability is measured by the relation

$$\mu = \frac{B}{H}$$

$$\mu = \frac{E.d \times 10^8}{4fN_1N_2S \times 0.4i} \quad (4.10)$$

At first we wind wires in the toroidal sample to make primary and secondary coils. The number of turns in each coil is 10 and  $I$  is the current. The sample those wound in kept in a little oven with a thermocouple placed at the middle. The thermocouple measure the temperature inside the oven and also the sample. The sample is kept just in the middle part cylindrical oven so that gradient is minimized. The temperature of the oven is raised slowly. If the heating rate is very fast then temperature of the sample may not follow the temperature inside the oven and there can be misleading information on the temperature of sample. The thermocouple showing the temperature in that case will be erroneous. Due to the closed winding wire the sample may not receive the heat at once. So, a slow heating rate is used to eliminate this problem. Also heating adjustment amorphous sample ensures accuracy in the determination of  $T_c$ . The oven was kept thermally insulated from the surroundings.

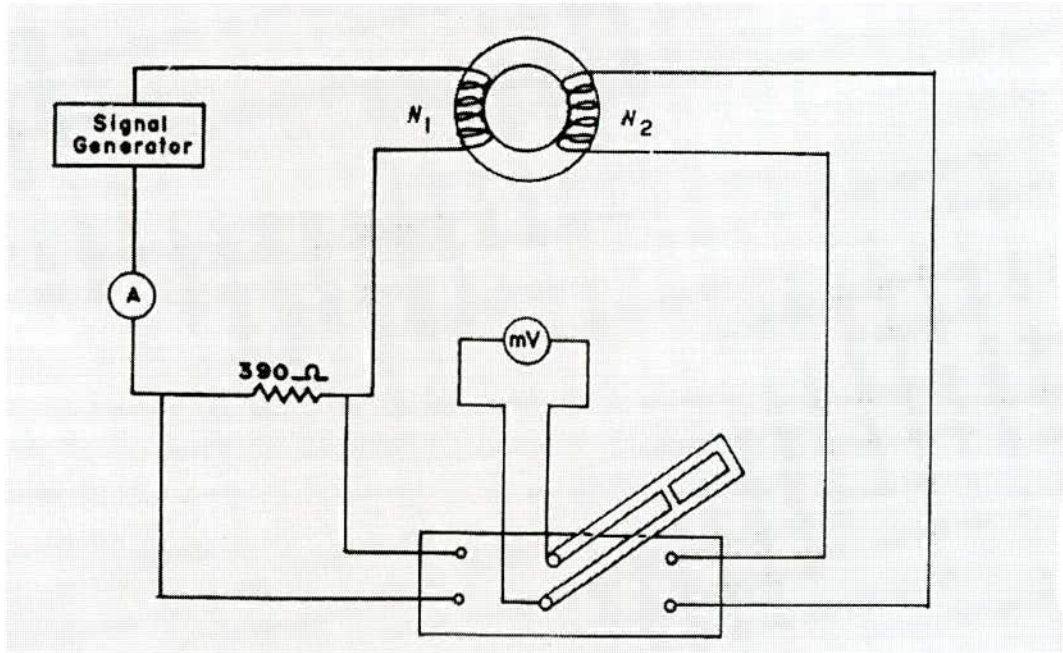


Fig. 4.2 Schematic diagram for the experimental setup for determination of Curie temperature

## **4.5 Magnetization Measurement Techniques**

In the present study magnetization has been performed using a vibrating Sample Magnetometer (VSM).

### **4.5.1 Vibration Sample Magnetometer**

A vibrating sample magnetometer (VSM) operates on Faraday's law of induction, which tells us that a changing magnetic field will produce an electric field. This electric field can be measured and can tell us information about the changing magnetic field. A VSM is used to measure the magnetic behavior of magnetic materials. VSM is a versatile and sensitive method of measuring magnetic properties developed by S. Foner [4.4 - 4.5] and is based on the flux change in a coil when the sample is vibrated near it. The VSM is designed to continuously measure the magnetic properties of materials as a function of temperature and field. In the type of magnetometer, the sample is vibrated up and down in a region surrounded by several pick-up coils. The magnetic sample is thus acting as a time changing magnetic flux, varying inside a particular region of fixed area. From Maxwell's law it is known that a time varying magnetic flux is accompanied by an electric field and the field induces a voltage in pick-up coils. This alternating voltage signal is processed by a control unit system; in order to increase the signal to noise ratio. The result is a measure of the magnetization of the sample.

### **4.5.2 The Principle of Vibration Sample Magnetometer**

The Principle of VSM is as follows:

- (i) when the sample of a magnetic material is placed in a uniform magnetic field,
- (ii) a dipole moment proportional to the product of the sample susceptibility times the applied field is induced in the sample.

If the sample is made to undergo a sinusoidal motion, an electrical signal is induced in suitably located stationary pick-up coils. This signal, which is at the vibration frequency, is proportional to the magnetic moment, vibration amplitude with vibration frequency. In order to obtain the reading of the moment only, a capacitor is made to generate another signal for comparison which varies in its moment, vibration amplitudes and vibration frequency in the



same manner as does the signal from the pick-up-coil. These two signals are applied to the two inputs of a differential amplifier, and because the differential amplifier passes only difference between the two signals, the effects of vibration amplitude and frequency changes are cancelled. Thus only the moment determines the amplitude of the signal at the output of the differential amplifier.



Fig. 4.3 Vibrating Sample Magnetometer

This signal is in turn applied to a Lock-in amplifier, where it is compared with the reference signal which is at its internal oscillator frequency and is also applied to the transducer which oscillates the sample rod. Thus the output of the Lock-in amplifier is proportional to the magnetic moment of the sample only avoiding any noise of frequency other than that of the signal. The Lock-in action yields an accuracy of 0.05% of full scale. The absolute accuracy of this system is better than 2% and reproducibility is better than 1%. Least measurable moment is  $5 \times 10^{-4}$  emu. Fig. 4.3 shows the magnet is mounted on a graduated rotating base. The standard model is modified to provide an adjustable pole gap in order that the highest possible field strength is available. The field can be varied from 0 to 20 KG, the field is measured directly.



### 4.5.3 Electronic Circuits of the VSM

The functions of the associated electronic circuits is

- i) To permit accurate calibration of the signal output obtained from the detection coils.
- ii) To produce a convenient ac output signal which is directly related to the input and which can be recorded.
- iii) To produce sufficient amplification for high sensitivity operation.

The block diagram of the electronic circuit used for the VSM consists of a mechanical vibration, a sine wave generator, an audio amplifier, a ratio transformer, a phase-shifter, a lock-in amplifier, a pick-up coil system, a reference coil system and an electromagnet as shown in Fig. 4.4.

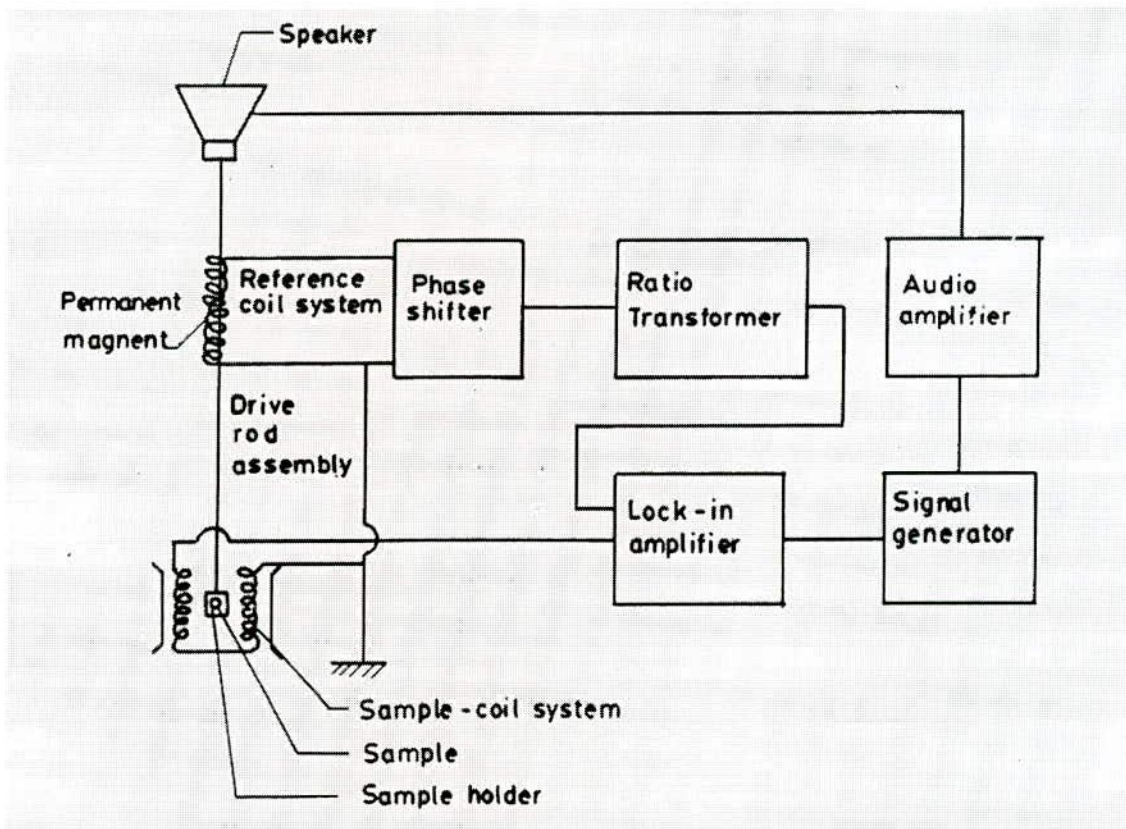


Fig. 4.4 Schematic diagram of the electronic system of the VSM

The sample magnetization by the electromagnet generates an e.m.f in pick up coils PC. The strength of this signal is proportional to the magnetization of the sample. The vibrating permanent magnet also generates an e.m.f of fixed amplitude in the surrounding reference coils. This reference signal is stepped down with the help of a ratio transformer so that its amplitude is equal to that the sample signals. The two signals are then brought in phase and put to the lock-in amplifier.

The Lock-in amplifier works as a null doctor. The ratio transformer reading is to be calibrated using spherical shape sample S of 99.99% pure nickel.

#### **4.5.3.1 Sensitivity limits**

Limits of sensitivity are determined by signal to noise ratio at the input circuit, where noise is defined as any signal not arising from the magnetic moment of the sample. The major sources of noise are the Johnson noise of the wire used for the pick-up coils, and the magnetic responses of the sample holder, which superimposes undesired signals in phase with the wanted signal. Use of a minimum mass of weakly diamagnetic material for a sample holder, carefully checked to contain no ferromagnetic impurities, is essential to minimize this coherent noise contribution. Corrections for the small magnetic contribution of the sample holder can then be made by measurements with the sample removed. This correction is much less than the equivalent case with a moving coil system.

Ore standard sample used for calibration was spherical shaped specimens of mass 0.0584gm. The different field susceptibility  $\Delta\chi \cong 5 \times 10^{-10}$  could be observed after synchronous phase detection with band width  $\cong 2 \times 10^{-2}$  cps. The other tests used were small current at 81Hz or an alternating current 81Hz passed through the coil which remained stationary.

#### **4.5.3.2 Stability Tests Differential Measurements**

With only the lock- in amplifier and the oscilloscope as a null detector, it was found that the 0.0584gm Ni- sample signal could be balanced reproducibly. Such reproducibility indicated that the long time drifts by the combined effects of vibration, amplitude changes and frequency changes a bridge sample position and other effects were negligible. Chosen synchronous phase detector added differential changes about one- tenth the size that could be recorded reproducibly.



#### **4.5.3.3 Vibration Amplitude**

The pick-to- pick vibration amplitude has been varied from less than 0.1mm up to 1.0mm in order to examine errors caused by amplitude changes. Such tests show that the measured magnetic moment varied by less than  $\pm 0.5\%$  over these of amplitude although at higher variation of amplitudes, because of the larger signals involved.

#### **4.5.3.4 Image Effects**

Image effects were also examined with a small vibrating coil carrying a dc current. The image effect was no greater than  $\pm 1\%$  for fields up to 5KG produced in an air gap 3.6cm. Undoubtedly, there is an image induced in the magnet poles. It appears however, that when the sample is vibrated, the effective image vibration is reduced by eddy current shielding.

#### **4.5.3.5 Vibration Frequency**

The Vibration frequency is not critical. High frequency operation is limited by the driving mechanism and capacitive shunting in the detection coils. Frequencies of 100Hz or less permit the use of inexpensive components and minimize eddy current shielding by the vacuum chamber. The measurements are completely independent of eddy currents in the surrounding parts, if measurements and calibration are made at the same temperature. The thickness of conducting parts has been minimized, so that the temperature dependence of penetration depth is less than 1%.

#### **4.5.3.6 Vibration problems**

Mechanical coupling between the Vibration system and the fixed detection coils must be avoided. Although the coils are arranged for minimum sensitivity to external vibration, a noticeable background signal is obtained when the vacuum chamber contacts the detection coils. Such mechanical effects are difficult to eliminate electronically, because the spurious background signal has the same frequency as the sample signal and maintains a constant phase differences with respect to the sample signal. Usually the magnetometer and detection coils are both supported by the magnetic coupling. So that, some mechanical coupling may be noticed at highest sensitivity.



**CHAPTER V**

**RESULTS AND DISCUSSION**

## RESULTS AND DISCUSSION

### 5.1 Dynamic Magnetic Properties of Fe-Ni Based Amorphous Ribbons

Dynamic magnetic properties of as-cast Fe-Ni-B system with composition  $\text{Fe}_x\text{Ni}_{80-x}\text{B}_{20}$  [ $x=20, 30, 40$  and  $50$ ] have been determined using LF impedance analyzer (LF impedance analyzer, 4192A, Range 5kHz to 13 MHz, Agilent Technologies, Japan limited, Japan). Permeability measurements were performed on toroidal samples at frequency of 1 kHz to 13 MHz and an applied ac driving field ( $\approx 0.11$  A/m) low enough to ensure the measurements of initial permeability. The measurement has been done both in the as-cast and different annealing condition. In order to avoid the experimental error due to fluctuation in ribbon thickness and thermal treatments, just one piece of each ribbon has been measured at room temperature and subsequent annealing temperature at constant annealing time of one hour. The as-quenched amorphous magnetic ribbons were wound into toroidal cores having outer and inner diameters within 12 to 15 mm and the ratio of the outer and inner diameter always kept less than 1.2 in order to improve the homogeneity of the applied field as well as to reduce the possibility of an inhomogeneous inductance response. The specimen was then annealed at temperatures less than Curie temperature ( $T_C$ ) with an interval of about  $50^\circ\text{C}$ . The sample under investigation is annealed in a quartz tube in air without any applied field using a furnace.

A low capacitance coil with 8 to 10 turns was wound around the toroids to allow the application of magnetic fields over a wide range of amplitudes. At room temperature the frequency and field dependence of the complex permeability  $\mu = \mu' - i\mu''$  and the core loss of the as-quenched and annealed samples were measured. The compositional dependence of initial permeability is determined for different values of  $x$  and their frequency dependence of complex magnetic characteristics, like real and imaginary parts of initial permeability; loss factor and relative quality factor are analyzed. In order to correlate the microstructural features with soft magnetic properties of the Fe-Ni-B ribbon alloys under study initial permeability of the toroidal shaped samples annealed at different temperatures are measured at room temperature with an applied ac field of 0.11 A/m.

### 5.1.1 Initial permeability of as-cast Fe-Ni-B Amorphous Ribbons

Frequency measurements were performed with an impedance analyzer in the frequency 1 kHz at room temperature and with various applied field. The initial permeability of the ribbons with composition  $\text{Fe}_x\text{Ni}_{80-x}\text{B}_{20}$  calculated from low ac magnetic field dependence of permeability in the limit of frequency 1 kHz and various magnetic fields is shown in Fig. 5.1. The initial permeability ( $\mu_i$ ) of the amorphous ribbons, which is extrapolated to zero frequency and for vanishing magnetic field, is estimated. Since permeability cannot be measured without applying some field, the initial permeability for the vanishing field is estimated by extrapolation of the initial permeability of the amorphous ribbons at very low frequency in dynamic measurements.

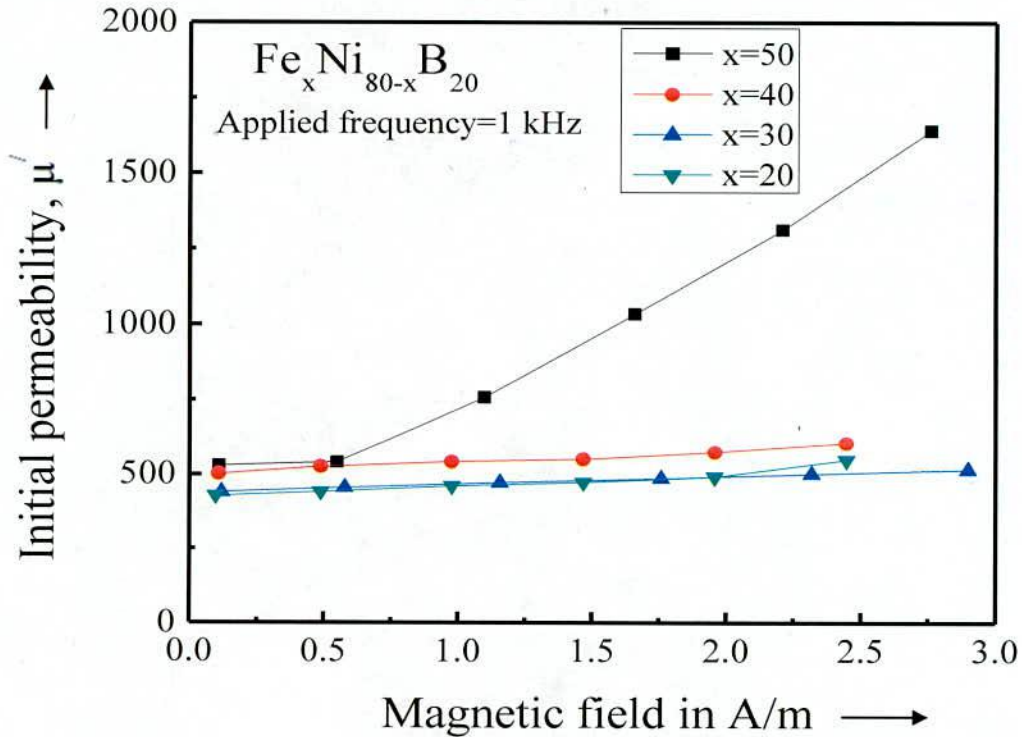


Fig. 5.1 Permeability versus ac magnetic field of amorphous ribbon with composition  $\text{Fe}_x\text{Ni}_{80-x}\text{B}_{20}$

It is assumed that the limit of low frequency corresponds to static field. The results are shown in Table 5.1. Initial permeability is controlled by the irreversible part of the domain wall motion. The preparation technique determines the defects and the associated energy



barriers to domain wall motion. Fig. 5.2 shows that  $\mu_i$  of Fe-Ni-B amorphous system increases almost monotonously with the replacement of Fe.

Table 5.1: The initial permeability in the vanishing field region of the amorphous ribbon with composition  $\text{Fe}_x\text{Ni}_{80-x}\text{B}_{20}$

$\text{Fe}_x\text{Ni}_{80-x}\text{B}_{20}$	X=20	X=30	X=40	X=50
$\mu'$	431	443	503	529

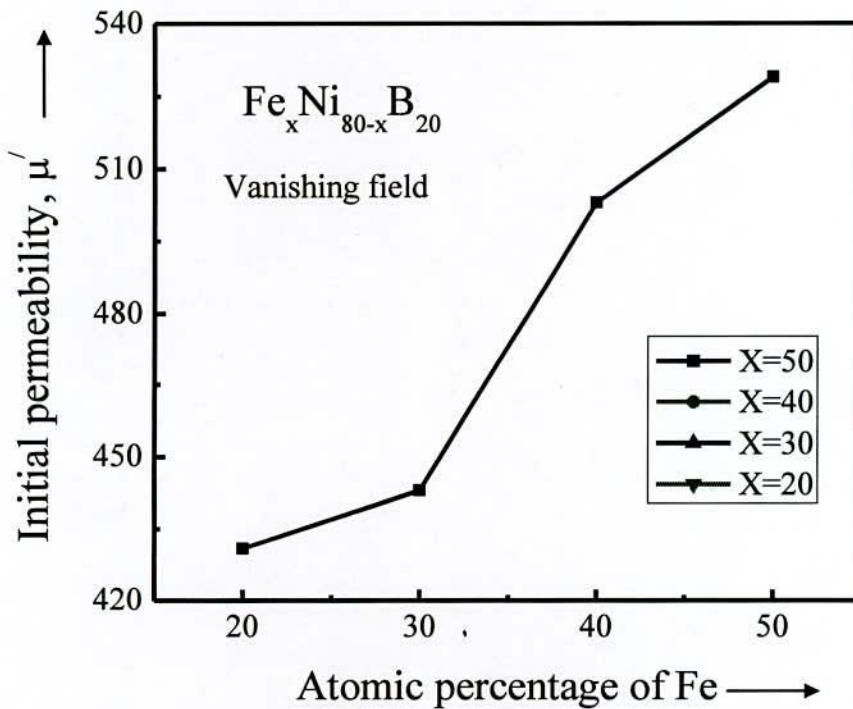
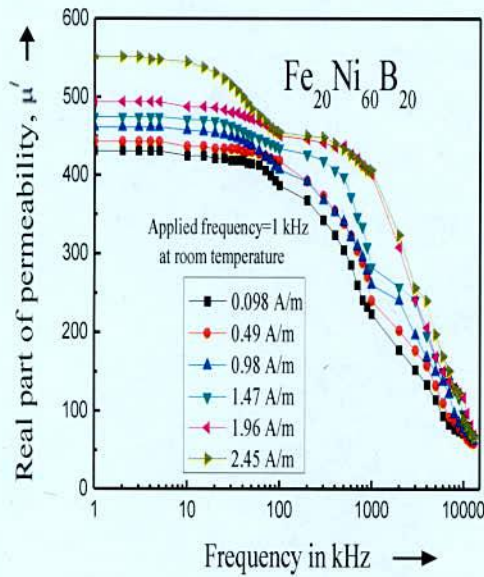


Fig.5.2 Variation of Initial permeability with the change in the Fe-content in  $\text{Fe}_x\text{Ni}_{80-x}\text{B}_{20}$  at  $H = 0.11\text{A/m}$

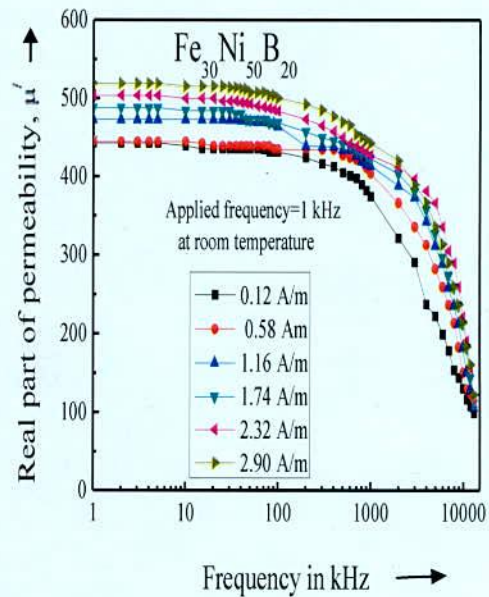
The permeability spectra for the amorphous magnetic ribbon of composition  $\text{Fe}_x\text{Ni}_{80-x}\text{B}_{20}$  at different applied field are shown in Fig. 5.3 (a, b, c, d). From the Fig. 5.1 it is shown that the initial permeability in the vanishing field region for all the ribbons except the one with composition  $\text{Fe}_{50}\text{Ni}_{30}\text{B}_{20}$  remains almost constant with slight variation of the field. The ribbon of composition  $\text{Fe}_{50}\text{Ni}_{30}\text{B}_{20}$  shows a large increase in the permeability with field

even in the low field region which is quite interesting and is rather complicated. It is difficult to explain the values of these parameters quantitatively, because of the various contributing factors.

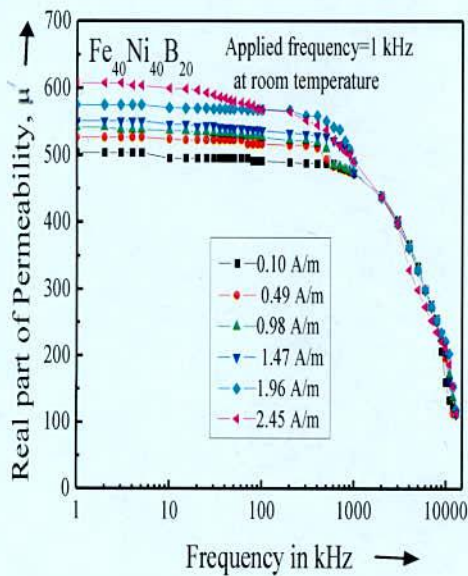
For the applied magnetic field lower than or equal to the value of the propagation field,  $\sim 0.5$  A/m, the real part of the complex permeability is independent of the applied field as shown in Fig. 5.1. The real part of the complex permeability is dependent on the applied field and shows dispersion are frequency dependent as shown in Fig. 5.3(a) and Fig. 5.3(b). But the real part of the complex permeability is independent of the applied field and shows dispersion at  $\sim 10^5$  Hz are shown in Fig. 5.3(c) and Fig. 5.3(d). For low field the permeability shows frequency independence. As the field is increased with increasing permeability, the low field behavior corresponds to the reversible bowing of domain walls pinned to inhomogeneities of the sample [5.1]. The dispersion of the reversible part has a relaxation character for low field initial permeability. The hysteresis dispersion is a complex process that can be represented by Warburg-type impedance [5.2].



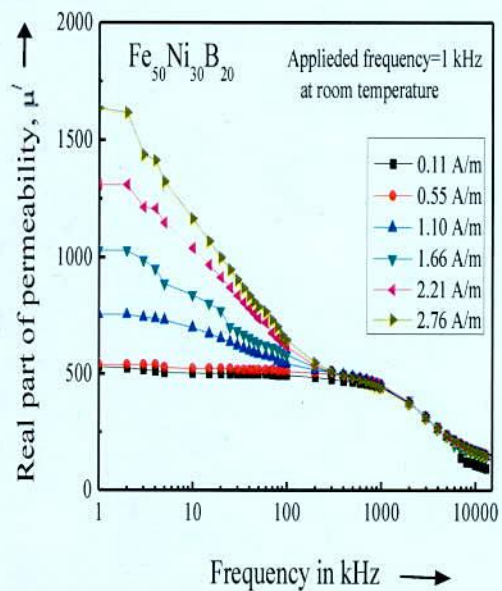
(a)



(b)



(c)



(d)

Fig.5.3 Frequency dependence of the real part of initial permeability of amorphous ribbon for different field with composition  $Fe_xNi_{80-x}B_{20}$  at constant annealing time 1 hour (a)  $x=20$ , (b)  $x=30$ , (c)  $x=40$  & (d)  $x=50$



### 5.1.2 Complex Permeability of the Fe-Ni-B Amorphous Ribbons

The compositional dependence of initial permeability of amorphous ribbons with composition  $\text{Fe}_x\text{Ni}_{80-x}\text{B}_{20}$  were determined for different values of  $x$  and their frequency dependence of complex magnetic characteristics, like real and imaginary parts of initial permeability, loss factor and relative quality factor are analyzed. The measurements were performed at room temperature using an ac fields with a very low constant values of  $H = 0.11$  A/m and a frequency from 1kHz to 13MHz. From the real part and the imaginary part of the complex permeability, the quality factor as a function of frequency has been calculated for different compositions. The frequency dependence of the real part of complex permeability is shown in Fig. 5.4. The flat region up to the frequency 3MHz indicates that except the ribbon with composition  $\text{Fe}_{20}\text{Ni}_{60}\text{B}_{20}$  all the other three samples of composition  $\text{Fe}_{50}\text{Ni}_{30}\text{B}_{20}$ ,  $\text{Fe}_{40}\text{Ni}_{40}\text{B}_{20}$  and  $\text{Fe}_{30}\text{Ni}_{50}\text{B}_{20}$  are very suitable, as core materials at low fields. However, the maximum frequency ranges for which the permeability is maintained constant in order of  $10^3$  Hz to  $10^4$  Hz.

The imaginary part of the complex permeability for different composition over the frequency range 1kHz to 13 kHz are shown in Fig -5.5. The imaginary part of the complex permeability ( $\mu''$ ) is equal to the initial real part of complex permeability ( $\mu'$ ) multiply the loss factor ( $\tan\delta$ ). The origin of the loss factors can be attributed to various domain effects [5.3], which include non uniform and non repetitive domain wall motion, domain wall bowing, localized variation of flux density, and nucleation and annihilation of domain walls. The principal cause of eddy current loss in amorphous ribbon is attributed to non sinusoidal and repetitive motion of domain walls.

At low frequency the loss is controlled by hysteresis and eddy current losses and at high frequency the flux penetration becomes low and loss is controlled mainly by interaction between the grains. As a result grain size, grain orientation and specimen thickness become important factors. The precipitation of very small percent of particles improves the high frequency losses and permeability [5.4]. The Nickel content has important effect in this case. Except the ribbon with composition  $\text{Fe}_{20}\text{Ni}_{60}\text{B}_{20}$  the other three materials having composition  $\text{Fe}_{30}\text{Ni}_{50}\text{B}_{20}$ ,  $\text{Fe}_{40}\text{Ni}_{40}\text{B}_{20}$  and  $\text{Fe}_{50}\text{Ni}_{30}\text{B}_{20}$  are almost identical in their performances and have low loss factors in frequencies up to 2 MHz.

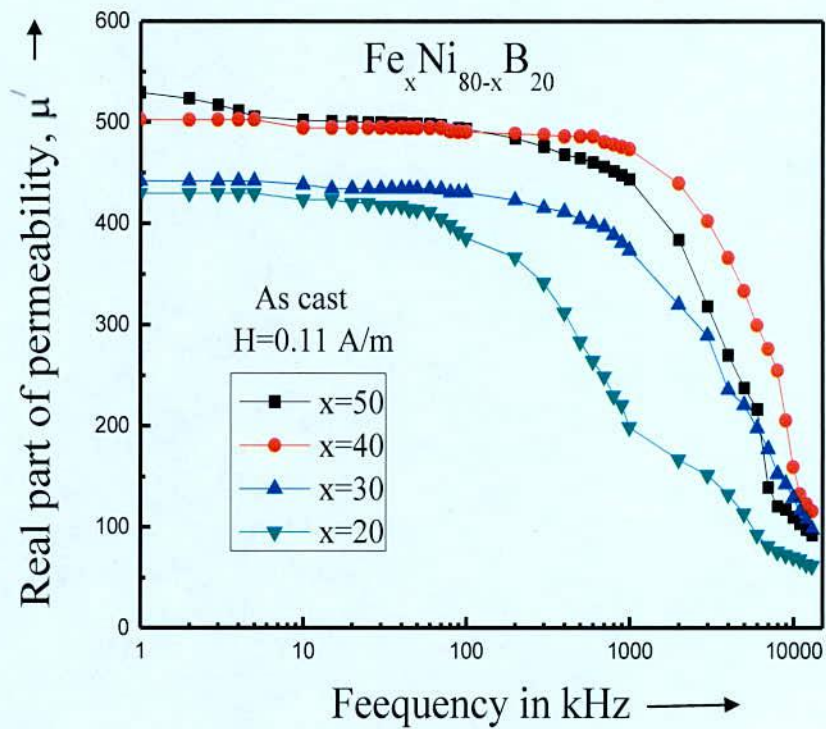


Fig. 5.4 Frequency dependence of the real part of complex permeability of amorphous ribbons with composition  $\text{Fe}_x \text{Ni}_{80-x} \text{B}_{20}$

The frequency dependence of the relative quality factors is shown in Fig. 5.6. The relative quality factor is controlled by the real part of complex permeability and quite high values in the range 15 kHz to 1 MHz for all three ribbons having composition  $\text{Fe}_{30} \text{Ni}_{50} \text{B}_{20}$ ,  $\text{Fe}_{40} \text{Ni}_{40} \text{B}_{20}$  and  $\text{Fe}_{50} \text{Ni}_{30} \text{B}_{20}$  and quite naturally these samples have low loss factors as mentioned before. The other sample having composition  $\text{Fe}_{20} \text{Ni}_{60} \text{B}_{20}$  have high loss factor and relatively low quality factor.

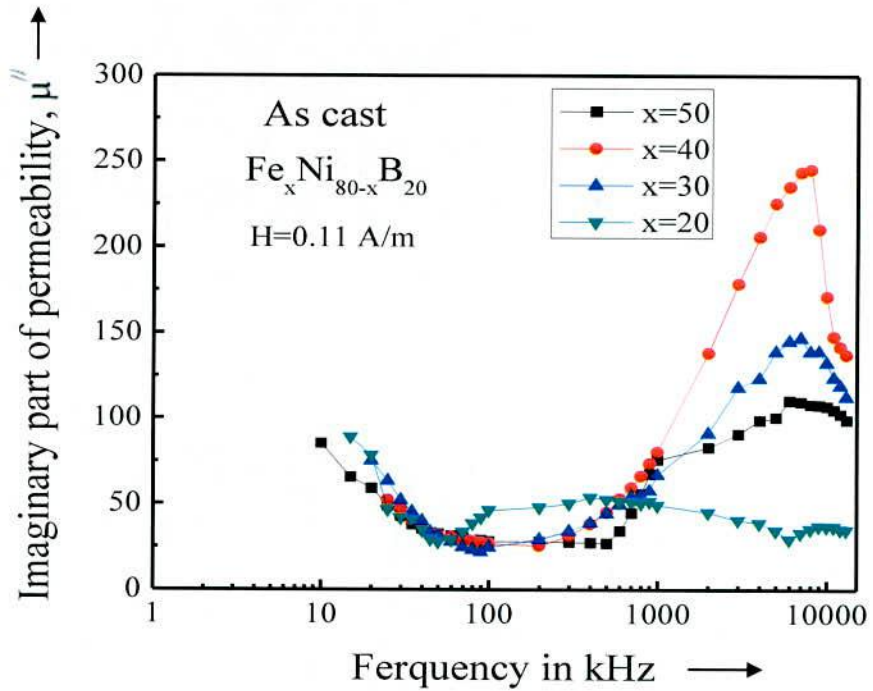


Fig. 5.5 Frequency dependence of the imaginary part of permeability of amorphous ribbons with compositions  $\text{Fe}_x\text{Ni}_{80-x}\text{B}_{20}$

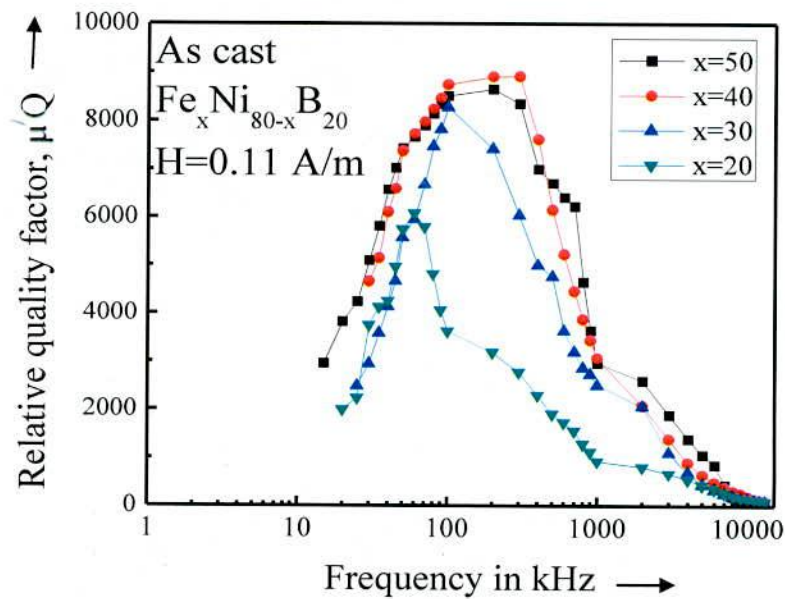


Fig. 5.6 Frequency dependence of relative quality factor of amorphous ribbons with compositions  $\text{Fe}_x\text{Ni}_{80-x}\text{B}_{20}$



### 5.1.3 Frequency Dependence of the Real part of the Complex Permeability Fe-Ni-B Amorphous Ribbons with Different Annealing Temperatures

The annealing effect on complex permeability of Fe-Ni-B amorphous ribbons with composition  $Fe_xNi_{80-x}B_{20}$  [ $x=20, 30, 40$  &  $50$ ] has been measured as a function of frequency in the range 1 kHz to 13 MHz. The measurements have been done both on the as-cast and annealed ribbons. The annealing temperature was varied from 25 to 450°C with constant annealing time 1 hour. Fig-5.7 to Fig-5.10 show frequency dependence of the real part of initial permeability for different annealing temperature at constant annealing time 1 hour.

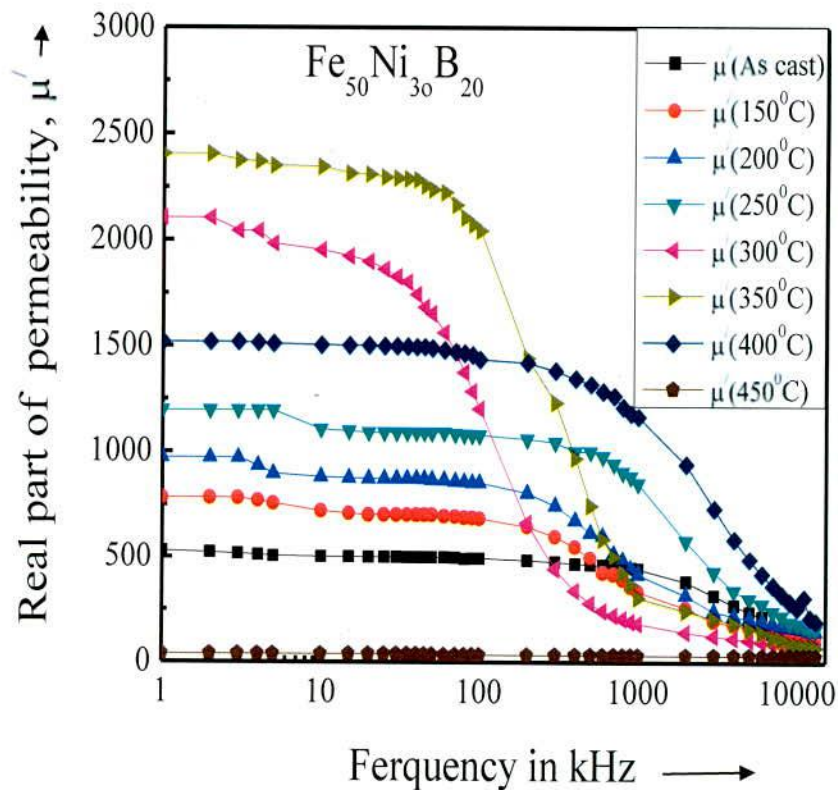


Fig. 5.7 Frequency dependence of the real part of permeability of amorphous ribbon for different annealing temperature with composition  $Fe_{50}Ni_{30}B_{20}$  at constant 1 hr annealing time

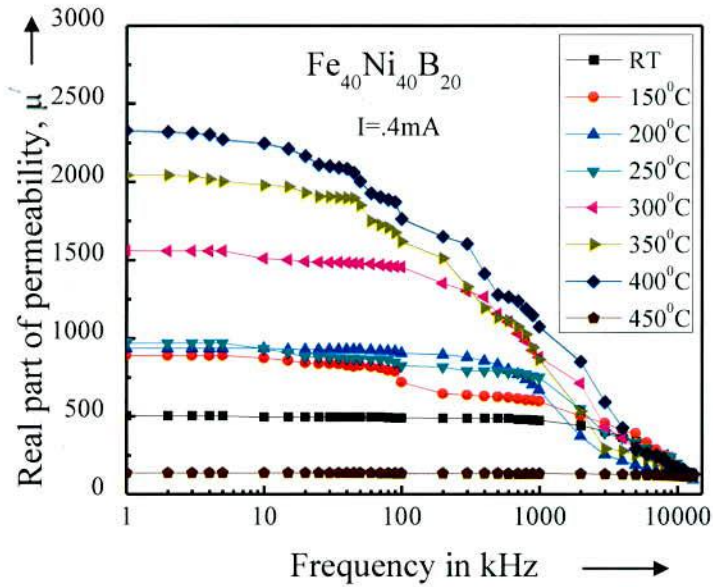


Fig. 5.8 Frequency dependence of the real part of permeability of amorphous ribbon for different annealing temperature with composition  $\text{Fe}_{40}\text{Ni}_{40}\text{B}_{20}$  at constant 1hr annealing time

For samples annealed for 1 hour it is observed that there is consistent increase in the initial permeability value with increasing annealing temperature. At very low field a significant increase in the real part of the complex permeability of the annealed samples is observed with respect to the as-cast samples up to the annealing temperature  $350^{\circ}\text{C}$  for  $\text{Fe}_{50}\text{Ni}_{30}\text{B}_{20}$  as shown in Fig. 5.7,  $400^{\circ}\text{C}$  for  $\text{Fe}_{40}\text{Ni}_{40}\text{B}_{20}$ , as shown in Fig. 5.8,  $300^{\circ}\text{C}$  for  $\text{Fe}_{30}\text{Ni}_{50}\text{B}_{20}$  as shown in Fig. 5.9,  $250^{\circ}\text{C}$  for  $\text{Fe}_{20}\text{Ni}_{60}\text{B}_{20}$  as shown in Fig. 5.10, and after these annealing temperature the permeability values decrease sharply. It can be observed that the real part of the initial complex permeability enhancement with annealing temperature is more effective at constant short time annealing time.

These studies of annealed samples on permeability provide information regarding the thermal stability of these materials as a transformer core when used at an elevated temperature. From these results are evident that annealing temperature and annealing time are both important parameter in controlling the frequency response of permeability of samples. The best choice of these parameters depends on the desired characteristics of the materials in respect of permeability value and its frequency dependence.

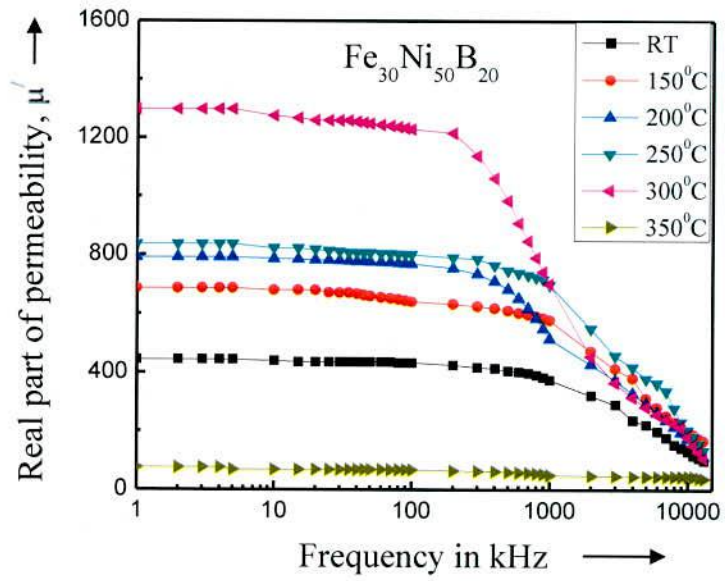


Fig.5.9 Frequency dependence of the real part of permeability of amorphous ribbon for different annealing temperature with composition  $\text{Fe}_{30}\text{Ni}_{50}\text{B}_{20}$  at constant 1 hr annealing time

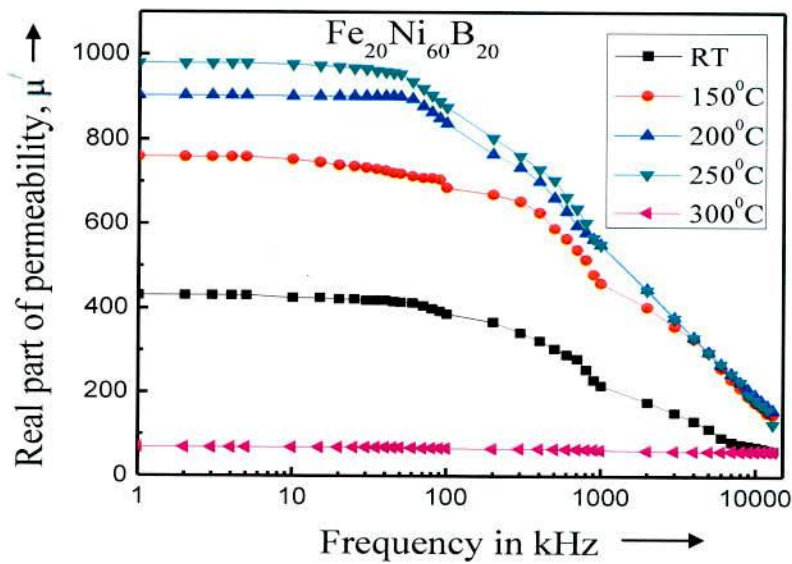


Fig.5.10 Frequency dependence of the real part of permeability of amorphous ribbon for different annealing temperature with composition  $\text{Fe}_{20}\text{Ni}_{60}\text{B}_{20}$  at constant 1 hr annealing time.



For the present work the main interest is the measurements of permeability and therefore the applied field was kept constant and small in its value 0.11 A/m. The initial permeability of all sample as affected by annealing at different temperature with constant 1 hour annealing time in each case, is measured at low frequency (1 kHz) and at very low field ( $H=0.11$  A/m)

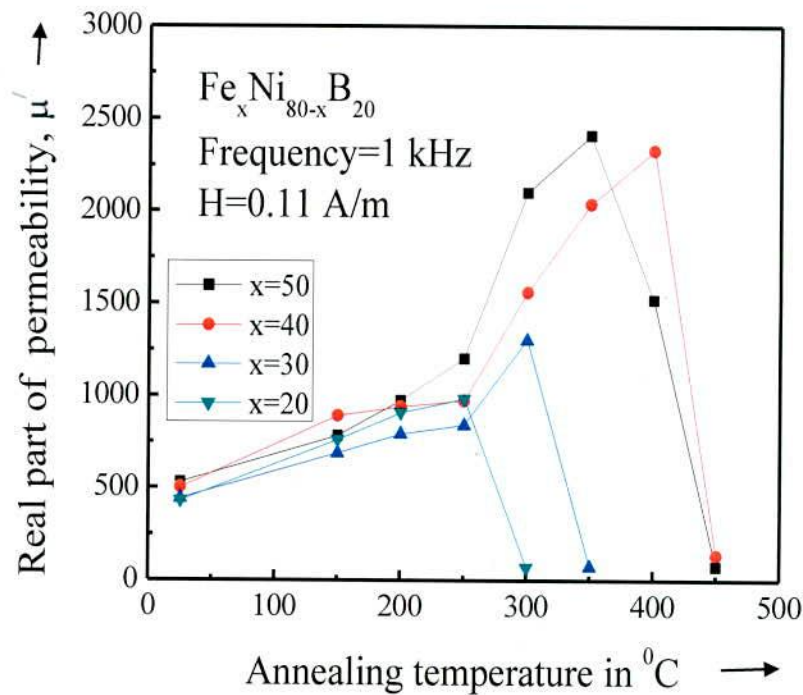


Fig.5.11 Real part of permeability versus annealing temperature of amorphous ribbons with composition  $Fe_xNi_{80-x}B_{20}$  at applied frequency 1 kHz and applied low field 0.11A/m

Fig. 5.11 shows the effect of annealing temperature on the initial permeability on amorphous ribbons with composition  $Fe_xNi_{80-x}B_{20}$  at constant 1 hr annealing time. The real part of permeability of the specimen increases monotonously but nonlinearly as function of annealing temperature up to 350 for  $Fe_{50}Ni_{30}B_{20}$ , 250 for  $Fe_{20}Ni_{60}B_{20}$ , after decrease sharply. The fall of the initial permeability indicates that the nuclei of the panel centers grow due this thermal treatment. Below this temperature, however, the stress induced reversible defects centers removed due to the annealing giving rise to an increase in permeability. In the Fe-based amorphous alloy reported by M. A. Asgar et. al. [5.5] the initial permeability increases with annealing temperature and attains the maximum value just before  $T_C$  which is explained

in terms of Hopkinson effect as desired by Kersten and Angew [5.6]. The kinetics of the stress relieving process depends somewhat on the previous thermal history of the sample [5.6]. The values of the initial permeability at different annealing temperatures for the composition  $Fe_xNi_{80-x}B_{20}$  are summarized in Table 5.2 for 1 kHz, Table 5.3 for 100 kHz and Table 5.4 for 1MHz.

Table 5.2: The real part of permeability of the amorphous magnetic ribbon  $Fe_xNi_{80-x}B_{20}$  at different annealing temperature at a constant low field of  $H=0.11$  A/m and constant 1 hr annealing time for 1kHz

Sample	At room temperature	150 <sup>0</sup> C	200 <sup>0</sup> C	250 <sup>0</sup> C	300 <sup>0</sup> C	350 <sup>0</sup> C	400 <sup>0</sup> C	450 <sup>0</sup> C
$Fe_{50}Ni_{30}B_{20}$	529	782	973	1200	2100	2400	1520	75
$Fe_{40}Ni_{40}B_{20}$	503	892	941	973	1560	2040	2330	137
$Fe_{30}Ni_{50}B_{20}$	443	688	791	840	1300	76	.....	.....
$Fe_{20}Ni_{60}B_{20}$	431	760	906	982	70	.....	.....	.....

Table 5.3 The real part of permeability of the amorphous magnetic ribbon  $Fe_xNi_{80-x}B_{20}$  at different annealing temperature at a constant low field of  $H=0.11$  A/m and constant 1 hr annealing time for 100kHz

Sample	At room temperature	150 <sup>0</sup> C	200 <sup>0</sup> C	250 <sup>0</sup> C	300 <sup>0</sup> C	350 <sup>0</sup> C	400 <sup>0</sup> C	450 <sup>0</sup> C
$Fe_{50}Ni_{30}B_{20}$	493	686	856	1080	1200	2040	1440	32
$Fe_{40}Ni_{40}B_{20}$	491	722	910	827	1460	1620	1690	134
$Fe_{30}Ni_{50}B_{20}$	432	642	772	804	1230	67	.....	.....
$Fe_{20}Ni_{60}B_{20}$	387	697	830	883	68	.....	.....	.....

Table 5.4 The real part of permeability of the amorphous magnetic ribbon  $Fe_xNi_{80-x}B_{20}$  at different annealing temperature at a constant low field of  $H=0.11$  A/m and constant 1 hr annealing time for 1MHz

Sample	At room temperature	150 <sup>0</sup> C	200 <sup>0</sup> C	250 <sup>0</sup> C	300 <sup>0</sup> C	350 <sup>0</sup> C	400 <sup>0</sup> C	450 <sup>0</sup> C
$Fe_{50}Ni_{30}B_{20}$	109	138	171	188	83	82	260	30
$Fe_{40}Ni_{40}B_{20}$	160	176	122	203	168	170	168	118
$Fe_{30}Ni_{50}B_{20}$	130	200	177	207	183	46	.....	.....
$Fe_{20}Ni_{60}B_{20}$	71	179	196	195	61	.....	.....	.....

In general, the value of initial permeability ( $\mu_i$ ) increases with the annealing temperature which is different for different samples and then decreases with further increase of the annealing temperature. The initial increases is explained as due to the removal of pinning centers and the final decreases  $\mu_i$  is explained as due to the nucleation of crystallites and their growth. One is the removal of local defects in homogeneity and stresses that hinders the moment of domains by pinning effects and the other is the other is the growth of the nucleation centers of crystallites that also hinders the movement of domain walls. Since effect of annealing is to remove the pinning centers of the first kinds and to enhance the growth of the pinning centers of the second kind, the result of annealing depends on the composition of the amorphous ribbons and the condition of preparation of the as-cast samples. Our results of the annealing on Ni-Fe-B samples, which show a increase of  $\mu_i$  with annealing temperatures are explained as due to the growth of the nucleation centers of the crystallites formed during the preparation. For annealing temperatures which are above or near the Curie temperature, the absence of domain wall leads to a random distribution of the short range order configuration and hence, to a significant decrease in domain wall pinning.



### 5.1.4 Frequency Dependence of Imaginary Part of the Complex Permeability of Fe-Ni-B Amorphous Ribbons with Different Annealing Temperature

The imaginary part of the complex permeability ( $\mu''$ ) at constant annealing time one hour with different annealing temperature over the frequency range 1 kHz to 13 MHz are shown in Fig. 5.12 to Fig. 5.15. These results are quite complimentary to the result for the real part of the complex permeability for all samples. The complex permeability for all samples at low frequencies has relative high value and corresponds to high loss factor and low quality factor as shown in all figures. The origin of the loss factor can be attributed to various domain effects [5.7], which include non-uniform and non-repetitive domain wall motion, domain wall bowing, localized variation of flux densities, and nucleation and annihilation of domain walls.

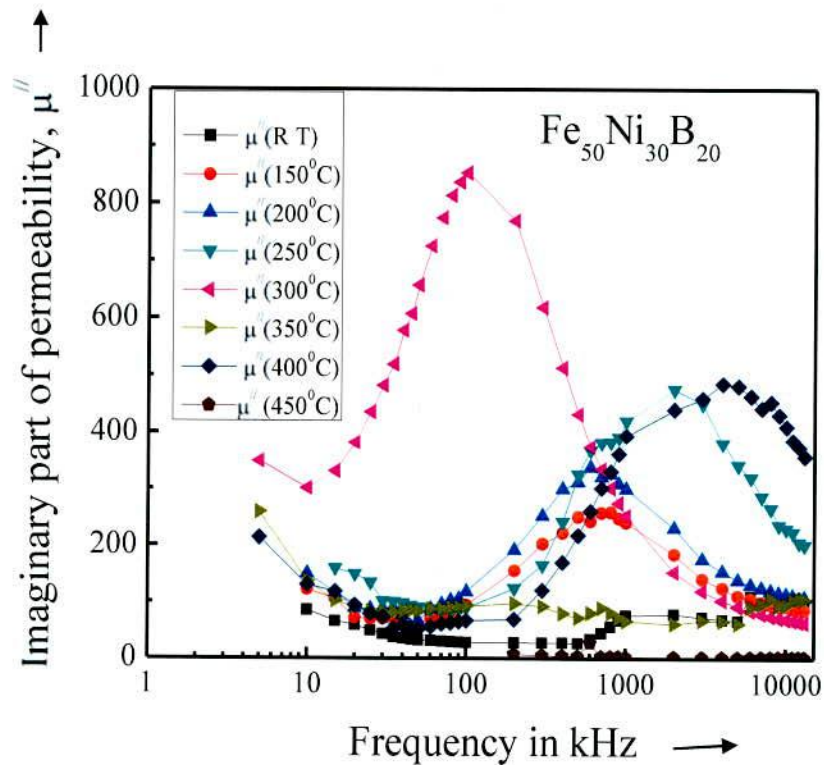


Fig. 5.12 Frequency dependence of the imaginary part of permeability of amorphous ribbons for different annealing temperature with composition  $\text{Fe}_{50}\text{Ni}_{30}\text{B}_{20}$  at constant 1 hr annealing time

Magnetic relaxation process may become important in technical application since they give rise to magnetic losses and magnetic instability. With respect to the influence of annealing on the magnetic relaxation phenomenon there is some doubt, whether there exists a unique annealing procedure, which simultaneously increases both initial permeability and dynamic losses. The frequency dependence of  $\mu''$  of the samples annealed at different temperatures can be attributed to the growth and distribution of the crystallites. The  $\mu''$  increases for the annealed samples indicating higher annealing temperature that causes further growth of crystallites and their stability. These are explained as due to the stabilization of the crystallites.

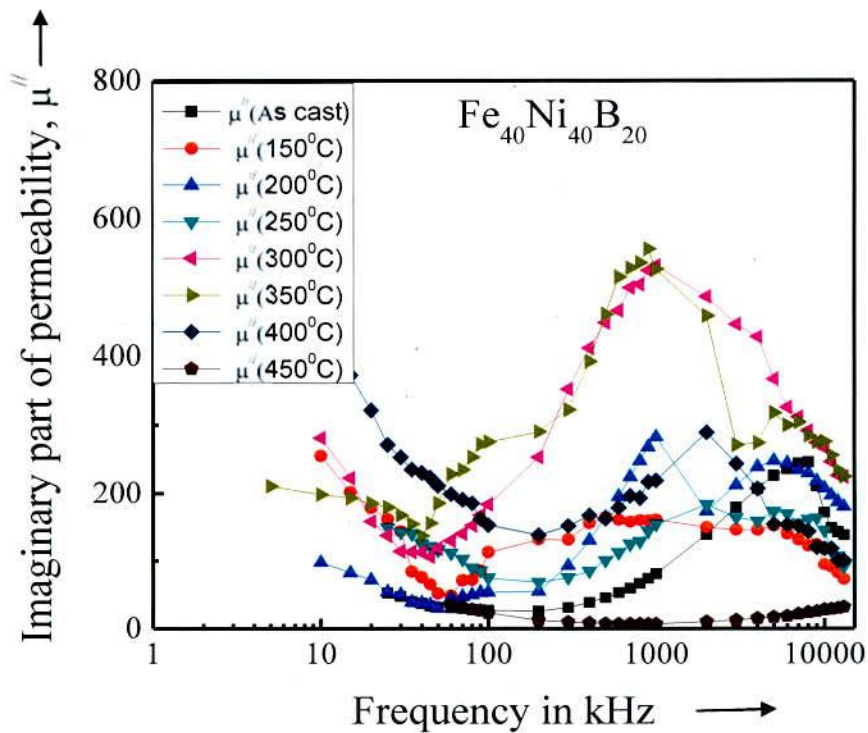


Fig.5.13 Frequency dependence of the imaginary part of permeability of amorphous ribbons for different annealing temperature with composition  $\text{Fe}_{40}\text{Ni}_{40}\text{B}_{20}$  at constant 1hr annealing time

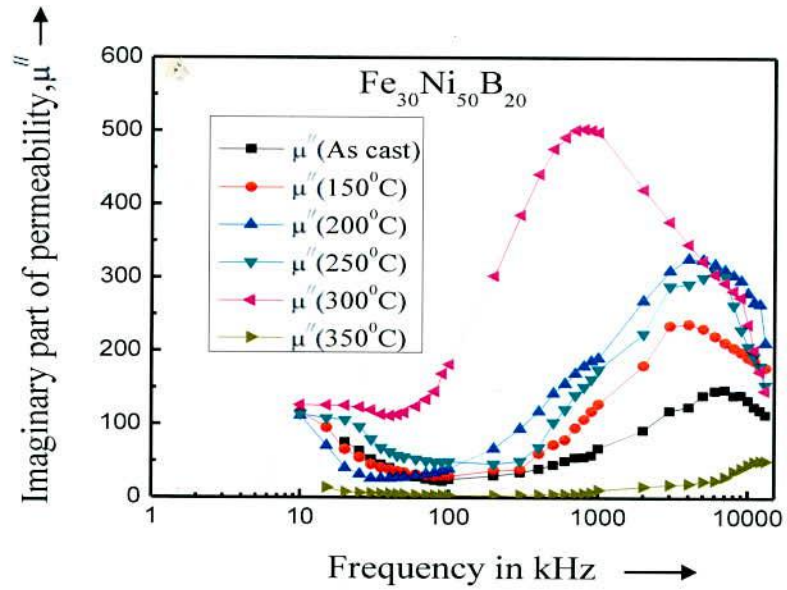


Fig.5.14 Frequency dependence of the imaginary part of the initial permeability of amorphous ribbons for different annealing temperature with composition  $\text{Fe}_{30}\text{Ni}_{50}\text{B}_{20}$  at constant 1 hr. annealing time

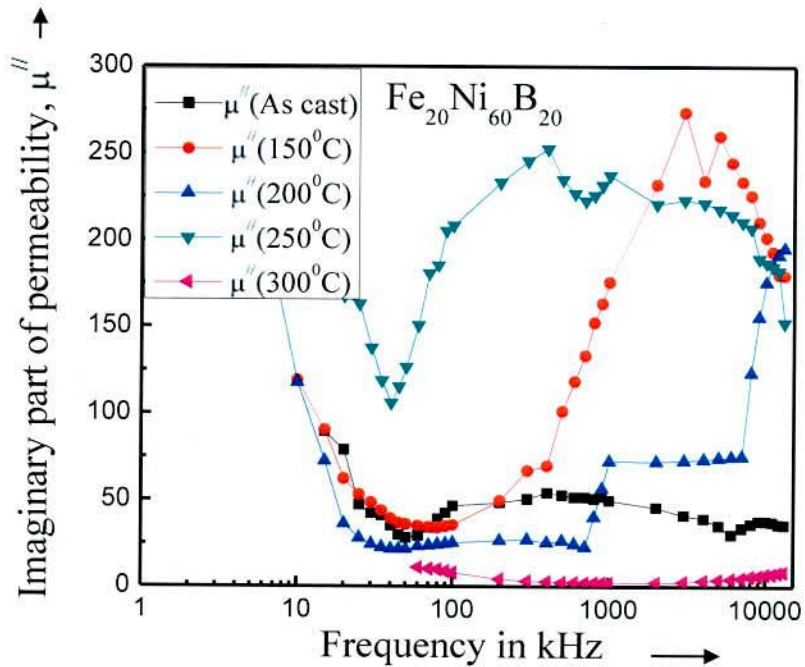


Fig.5.15 Frequency dependence of the imaginary part of the permeability of amorphous ribbons for different annealing temperature with composition  $\text{Fe}_{20}\text{Ni}_{60}\text{B}_{20}$  at constant 1 hr annealing time



### 5.1.5 Relative Quality Factor of Fe-Ni-B Amorphous Ribbons with Different Annealing Temperatures

Loss factor ( $\tan\delta$ ) and relative quality factor ( $\mu'Q$ ) are important parameters for the soft magnetic materials from the application point of relative quality factors are preconditions for achievement of good soft magnetic properties in amorphous ribbons. The loss factor is given by the ratio of real and imaginary parts of the complex permeability i.e  $\tan \delta = \frac{\mu''}{\mu'}$ . The loss factor arises due to eddy current loss as well as for the phase lag of the spin reorientation with respect to external field. Since the net  $\tan\delta$  found for this amorphous magnetic ribbons is quite complex, it is difficult to separate out the contribution from the eddy current loss and the phase lag of the spins with respect to the fields. The loss factor in general is found to be high for the entire sample at low frequency as well as for high frequency. Loss factor ( $\tan\delta$ ) is directly measured by the LF impedance analyzer.

The frequency dependence of  $\frac{\mu'}{\tan \delta}$  or  $\mu'Q$  at constant annealing time 1 hour with different annealing temperatures with composition  $Fe_xNi_{80-x}B_{20}$  [ $x = 20, 30, 40$  &  $50$ ] are shown in Fig. 5.16 to Fig. 5.19.  $\mu'Q$  as controlled by the real part of the complex permeability, have very high values in the range 10 kHz to 300 kHz for the ribbon having composition  $Fe_{50}Ni_{30}B_{20}$  annealed at  $200^\circ C$  shown in Fig. 5.16, 30 kHz to 500 kHz for the ribbon having composition  $Fe_{40}Ni_{40}B_{20}$  annealed at  $400^\circ C$  shown in Fig. 5.17, 40kHz to 100kHz for the ribbon having composition  $Fe_{30}Ni_{50}B_{20}$  annealed at  $200^\circ C$  and 20kHz to 200kHz for the ribbon having composition  $Fe_{20}Ni_{60}B_{20}$  annealed at  $200^\circ C$ .

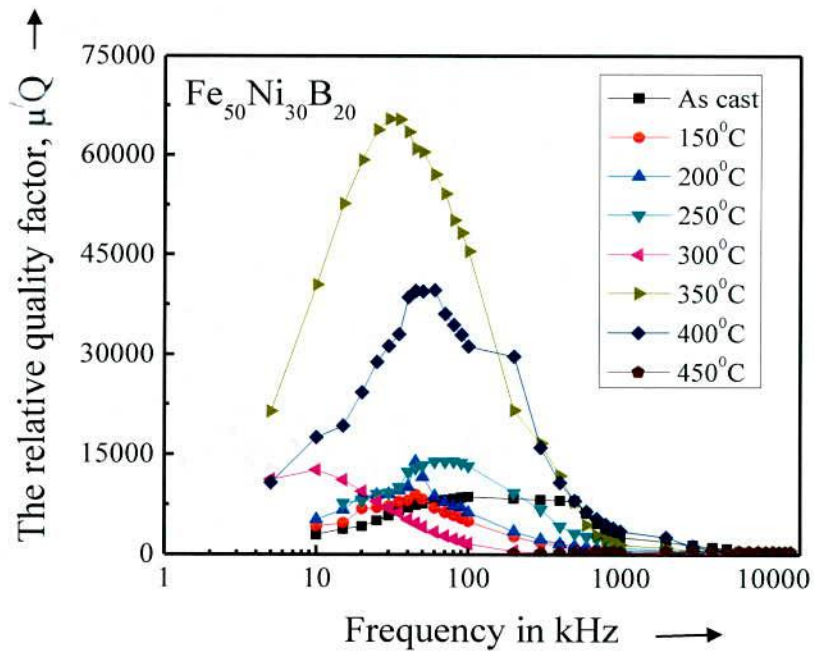


Fig. 5.16 Frequency dependence of the relative quality factor of  $\text{Fe}_{50}\text{Ni}_{30}\text{B}_{20}$  amorphous ribbon for different temperature at constant annealing time 1 hr ( $H = 0.11$  A/m)

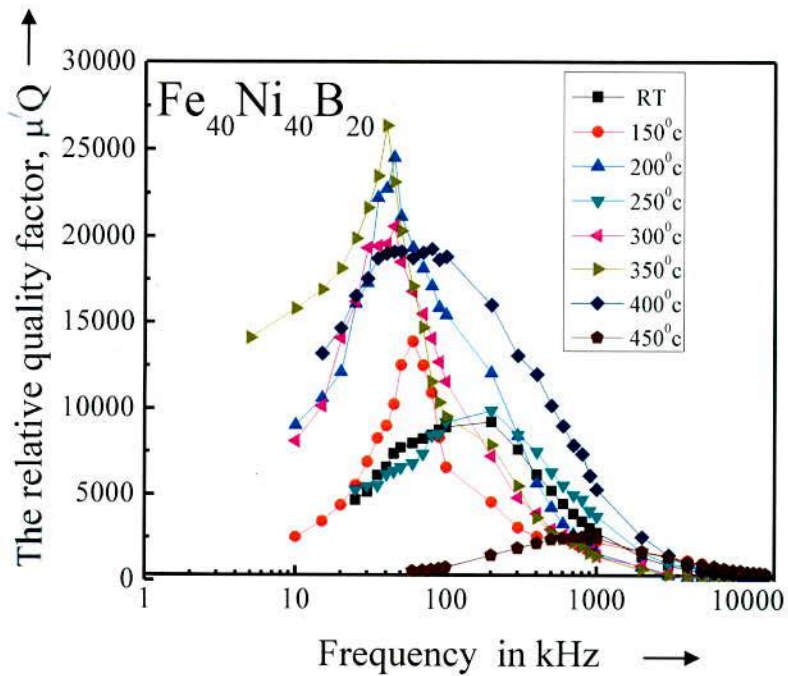


Fig. 5.17 Frequency dependence of the relative quality factor of  $\text{Fe}_{40}\text{Ni}_{40}\text{B}_{20}$  amorphous ribbon for different annealing temperature at constant annealing time 1 hr ( $H = 0.11$  A/m)

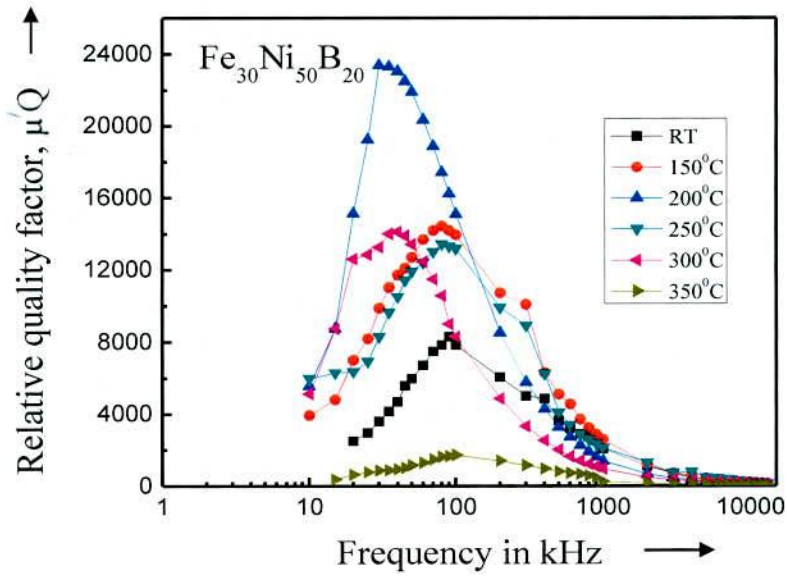


Fig. 5.18 Frequency dependence of the relative quality factor of  $\text{Fe}_{30}\text{Ni}_{50}\text{B}_{20}$  amorphous ribbon for different annealing temperature at constant annealing time 1 hr ( $H = 0.11$  A/m)

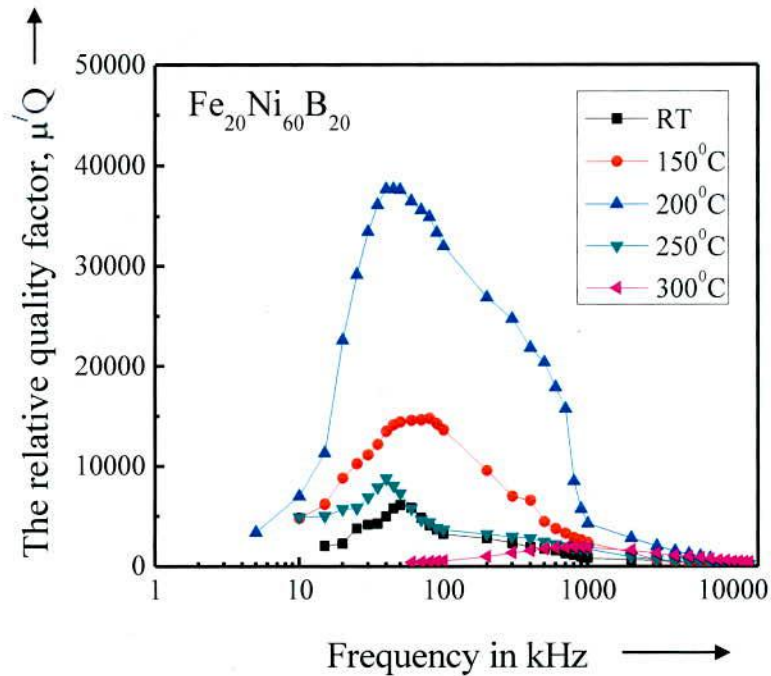


Fig. 5.19 Frequency dependence of the relative quality factor of  $\text{Fe}_{20}\text{Ni}_{60}\text{B}_{20}$  amorphous ribbon for different annealing temperature at constant annealing time 1 hr ( $H = 0.11$  A/m)



This gives a choice of annealing temperature on the operating frequency of the specimen. Thus the frequency range for application area might be chosen. It is well known that optimal annealing amorphous ribbons display minimum loss and very high relative quality factor,  $\mu/Q$  of the order of  $3.4 \times 10^4$  to  $6.4 \times 10^4$  for  $\text{Fe}_{50}\text{Ni}_{30}\text{B}_{20}$ , order of  $1.7 \times 10^4$  to  $2.6 \times 10^4$  for  $\text{Fe}_{40}\text{Ni}_{40}\text{B}_{20}$ , order of  $1.1 \times 10^4$  to  $2.2 \times 10^4$  for  $\text{Fe}_{30}\text{Ni}_{50}\text{B}_{20}$  and order of  $1.1 \times 10^4$  to  $3.6 \times 10^4$  for  $\text{Fe}_{20}\text{Ni}_{60}\text{B}_{20}$ . The optimal annealing temperature is determined through successive annealing of the alloys from  $200^\circ\text{C}$  to  $400^\circ\text{C}$  for  $\text{Fe}_{50}\text{Ni}_{30}\text{B}_{20}$  (Fig.-5.16),  $200^\circ\text{C}$  to  $400^\circ\text{C}$  for  $\text{Fe}_{40}\text{Ni}_{40}\text{B}_{20}$  (Fig. 5.17),  $200^\circ\text{C}$  to  $300^\circ\text{C}$  for  $\text{Fe}_{30}\text{Ni}_{50}\text{B}_{20}$  (Fig. 5.18) and  $150^\circ\text{C}$  to  $200^\circ\text{C}$  for  $\text{Fe}_{20}\text{Ni}_{60}\text{B}_{20}$  (Fig. 5.19). The values of the relative quality for  $\text{Fe}_{50}\text{Ni}_{30}\text{B}_{20}$  after  $400^\circ\text{C}$ ,  $\text{Fe}_{40}\text{Ni}_{40}\text{B}_{20}$  after  $400^\circ\text{C}$ ,  $\text{Fe}_{30}\text{Ni}_{50}\text{B}_{20}$  after  $300^\circ\text{C}$  and  $\text{Fe}_{20}\text{Ni}_{60}\text{B}_{20}$  after  $200^\circ\text{C}$  are very low and almost steady for the whole range of frequency.

High relative quality factor and low loss factor of the ribbons indicate that this can be useful as a soft magnetic material. The loss factor in general is found to be high for all sample at low frequency as well as for high frequency. The increase of the loss factor with annealing temperature indicates that longer annealing time causes further growth of crystallites and their stability. The loss factor arises due to the eddy current loss as well as for the phase lag of the spin orientation with respect to the external field. At low frequencies magnetic losses are controlled by hysteresis caused by irreversible magnetization process and at high frequency, the flux penetration becomes low and loss is mainly controlled by interaction between the grains as well as eddy current.

The relative quality factor curve initially rises with respect to increasing frequency and after reaching a peak value, it decreases. The peak value for each curve represents the best soft magnetic behavior for the corresponding annealing temperature. Beyond the peak value, the quality factor is found to decrease which may be attributed to increase of loss components. This gives a choice of optimal annealing temperature for annealing soft magnetic properties. The highest value of best quality factor is found for the sample  $\text{Fe}_{50}\text{Ni}_{30}\text{B}_{20}$  annealed at  $200^\circ\text{C}$ , sample  $\text{Fe}_{40}\text{Ni}_{40}\text{B}_{20}$  annealed at  $400^\circ\text{C}$ , sample  $\text{Fe}_{30}\text{Ni}_{50}\text{B}_{20}$  annealed at  $200^\circ\text{C}$  and sample  $\text{Fe}_{20}\text{Ni}_{60}\text{B}_{20}$  annealed at  $200^\circ\text{C}$ . Which also indicates the best heat treatment temperature and to obtain the highest value of quality factor. Since these amorphous ribbons are conducting the net loss factor given by  $\tan\delta$  is quite complex. It is difficult to separate out the contribution

from the eddy current loss and the phase of the spins with respect to the field. For all the ribbons minimum losses well as maximum quality factors occurs around 70 kHz.

## 5.2 Curie Temperature Measurements of Amorphous Fe-Ni-B Ribbons

The  $T_c$  is a basic parameter in the study of magnetic phase transitions in ferromagnetic alloys. It is well known that  $T_c$  of an alloy in the crystalline and the amorphous states differ, and in spite of chemical and structural disorder an amorphous ferromagnetic, most often, demonstrate a well defined ferromagnetic ordering, temperature  $T_c$  which has been confirmed by magnetization versus temperature curves, Mossbauer effects and specific heat measurement [5.7]. It is demonstrated that  $T_c$  determined for the magnetization versus temperature curve do not provide unambiguous results due to structural disorder and chemical disorder. The accurate determination of the  $T_c$  of the amorphous materials is quite difficult, because one has to have adequate knowledge of the relaxation processes that generally take place during the measurement of the  $T_c$  the heating rate should be adjusted in such a way that, no crystallization can virtually take place. It is shown that for temperature below  $100^{\circ}\text{C}$  no noticeable effects in glassy materials are produced [5.8].

Amorphous Fe-Ni-B ribbons having composition  $\text{Fe}_x\text{Ni}_{80-x}\text{B}_{20}$  [ $x = 20, 30, 40 \text{ \& } 50$ ] have been chosen for the determination of  $T_c$ , using  $\mu'$  vs.  $T$  curves. The  $T_c$  corresponds to temperature at which the sharp fall of permeability occurs. Temperature dependence of permeability of the samples subjected to a heating rate  $10^{\circ}\text{C}/\text{min}$  and the constant frequency of 10 kHz has been used for measuring  $T_c$  as shown in Fig-5.20. The numerical values of  $T_c$ 's for all the samples are shown in Table 5.5

Table 5.5: Curie temperature of Fe-Ni-B ribbons for as cast condition

$\text{Fe}_x\text{Ni}_{80-x}\text{B}_{20}$	X=50	X=40	X=30	X=20
$T_c$ ( $^{\circ}\text{C}$ )	446	410	333	260



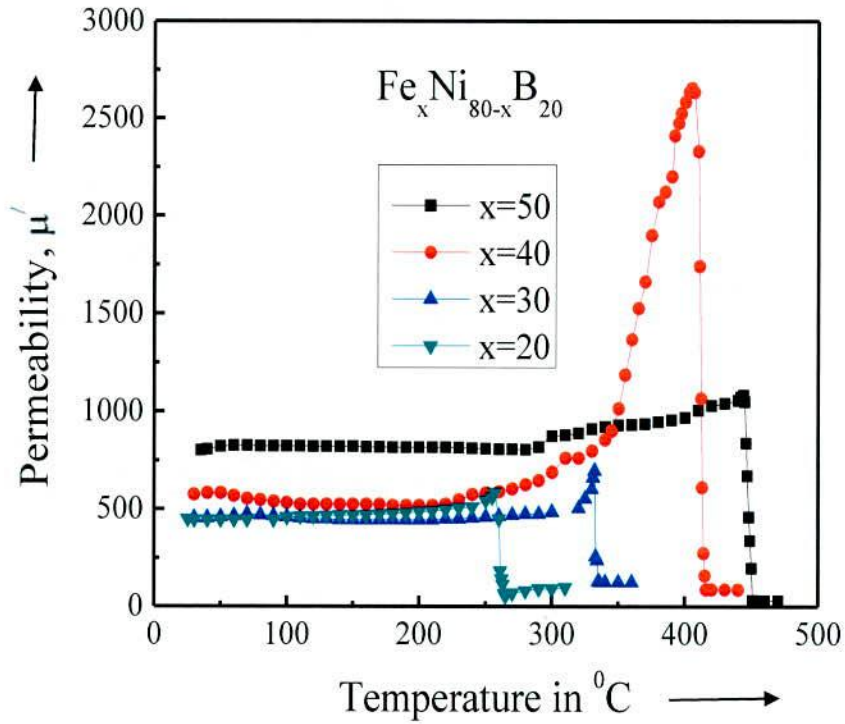


Fig. 5.20  $T_c$  determination from temperature dependence of real part of complex initial permeability of amorphous ribbons with composition  $Fe_x Ni_{80-x} B_{20}$  at constant frequency 10kHz and heating rate  $10^0 C/min$

Curie temperature has been estimated from the  $\mu'$  vs  $T$  curves, where the  $T_c$  corresponds to temperature at which  $\frac{dM}{dt}$  attains a maximum value. It is interesting to note the sharp fall of permeability at the  $T_c$  enables us to determine  $T_c$  unambiguously. From the experiences during the course of this work it is found out that the heating rate should be above  $5^0 C/min$  to determine  $T_c$  of an amorphous sample in this system. It is also noticed that a higher  $T_c$  and a lower heating rate fails to determine  $T_c$ . Because the longer time initiate nucleation of crystallites which hampers the determination of  $T_c$  of the perfect amorphous state. The sharp fall of the permeability at  $T_c$  indicates that the material is quite homogeneous from the point of view of amorphousity increases with temperature and attains the maximum value just before  $T_c$  for sample  $Fe_{40}Ni_{40}B_{20}$ , which is considered to be due to Hopkinson effect [5.9]. This can be determined by the temperature dependence of the intrinsic anisotropy of the material.



Although the chemical disorder appears to be largely responsible for reduction of  $T_c$  in amorphous ribbons, the effect of non-crystalline is also significant. The dependence of  $T_c$  on the composition and the nature of the metalloids is not very systematic. Fig-5.21 shows the dependence of  $T_c$  on the Ni-content. It is noticed that  $T_c$  decreases monotonically with increasing Ni Content. Addition of Ni to replace Fe, with fixed concentration of boron, decreases  $T_c$  rather slowly for low concentration, but the higher concentration of Ni,  $T_c$  falls sharply. It is explained as arising from the weakening of the exchange interaction between the magnetic atoms due to the replacement of Fe atom by Ni atoms.

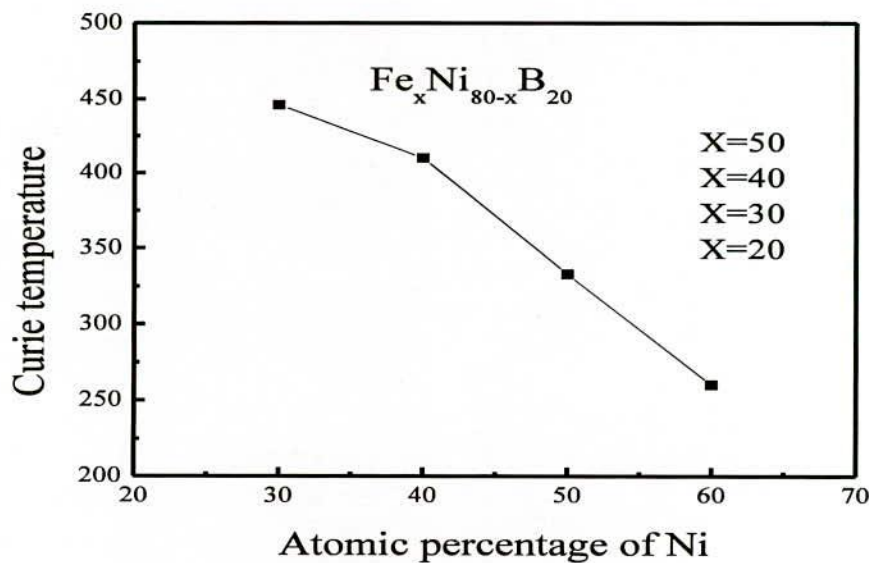


Fig.5.21 Variation of Curie temperature due to change in the Ni-content in  $Fe_xNi_{80-x}B_{20}$  amorphous ribbons

### 5.2.1 Annealing Temperature Effects on Curie Temperature Measurements of Fe-Ni-B Amorphous Ribbons

In Fig. 5.22 to Fig. 5.25, shows the real part of Complex Initial Permeability ( $\mu'$ ) has presented as a function of temperature at a fixed frequency of 10 kHz and different annealing temperature. The curve reveals strong dependence of initial permeability on annealing temperature. For samples annealed from 150°C to 400°C as shown in Fig. 5.22 (sample  $Fe_{50}Ni_{30}B_{20}$ ), 150°C to 350°C as shown in Fig. 5.23 (sample  $Fe_{40}Ni_{40}B_{20}$ ), 150°C to 300°C as

shown in Fig. 5.24 (sample  $\text{Fe}_{30}\text{Ni}_{50}\text{B}_{20}$ ) and  $150^\circ\text{C}$  to  $250^\circ\text{C}$  as shown in Fig. 5.25 (sample  $\text{Fe}_{20}\text{Ni}_{60}\text{B}_{20}$ ). All the samples permeability passes through a maximum just before a sharp fall to near zero with the manifestation of Hopkinson effect characterizing the Ferro - paramagnetic transition which is compatible with reported results [5.10]. Practically the accurate determination of  $T_c$  of amorphous material is really difficult due to irreversible component of the structural relaxation like long range internal stress, topological and chemical short range order.

The structural relaxation without destroying the amorphous state may influence  $T_c$ . Therefore during the measurement of  $T_c$  the heating rate has been adjusted in such a way that no substantial relaxation takes place. The numerical values of  $T_c$ 's for the annealed samples are shown in Table 5.6.  $T_c$  of the amorphous matrix decreases significantly when annealed at and above crystallization temperature. The probable reason of decreasing the  $T_c$  of the amorphous phase when annealed at above the crystallization temperature is that amorphous matrix is depleted with Fe and the relative amount of Ni in the amorphous matrix increase, which weakens the exchange interaction resulting in a decreases of  $T_c$  of the amorphous matrix.

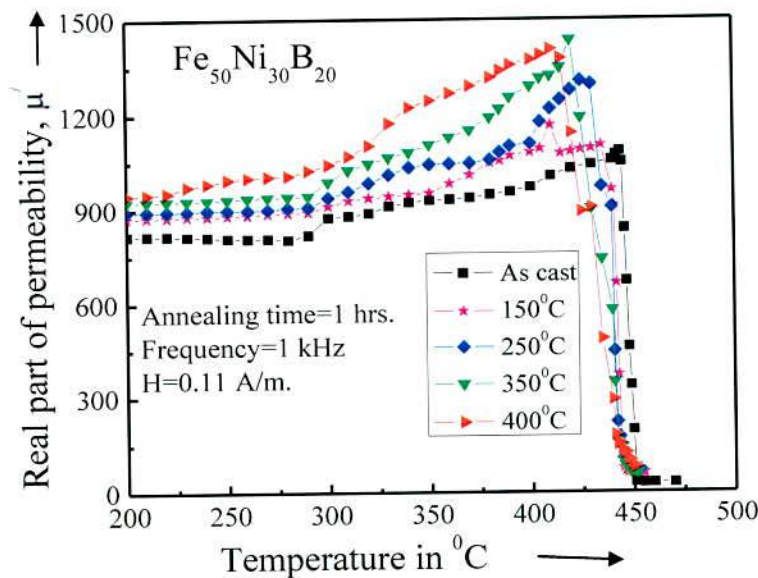


Fig.5.22 Temperature dependence real part of complex initial permeability of  $\text{Fe}_{50}\text{Ni}_{30}\text{B}_{20}$  ribbon at different annealing temperature for constant annealing time 1 hr

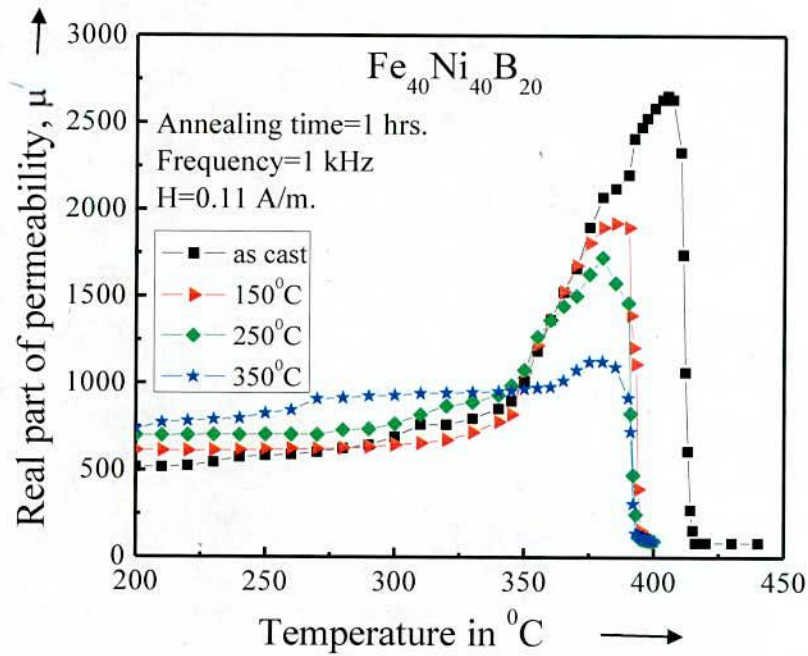


Fig.5.23 Temperature dependence real part of complex initial permeability of  $\text{Fe}_{40}\text{Ni}_{40}\text{B}_{20}$  ribbon at different annealing temperature for constant annealing time 1 hr

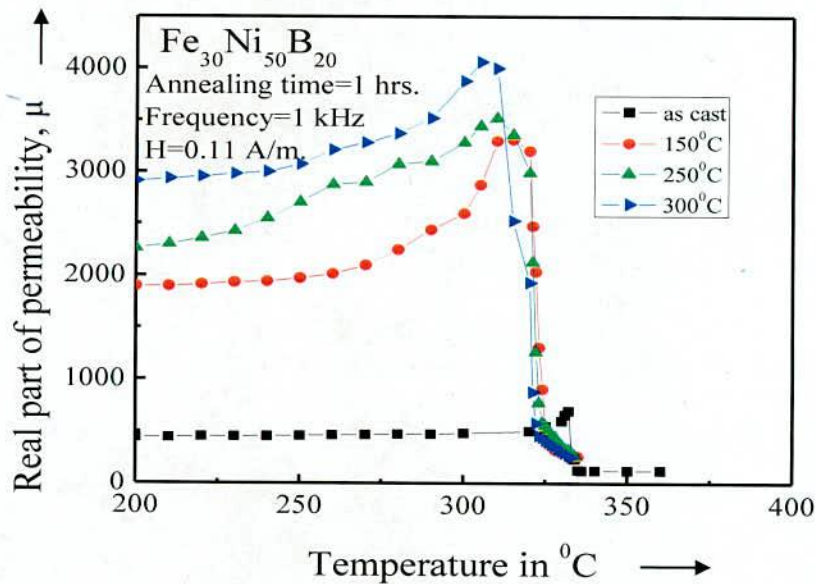


Fig.5.24 Temperature dependence real part of complex initial permeability of  $\text{Fe}_{30}\text{Ni}_{50}\text{B}_{20}$  ribbon at different annealing temperature for constant annealing time 1 hr



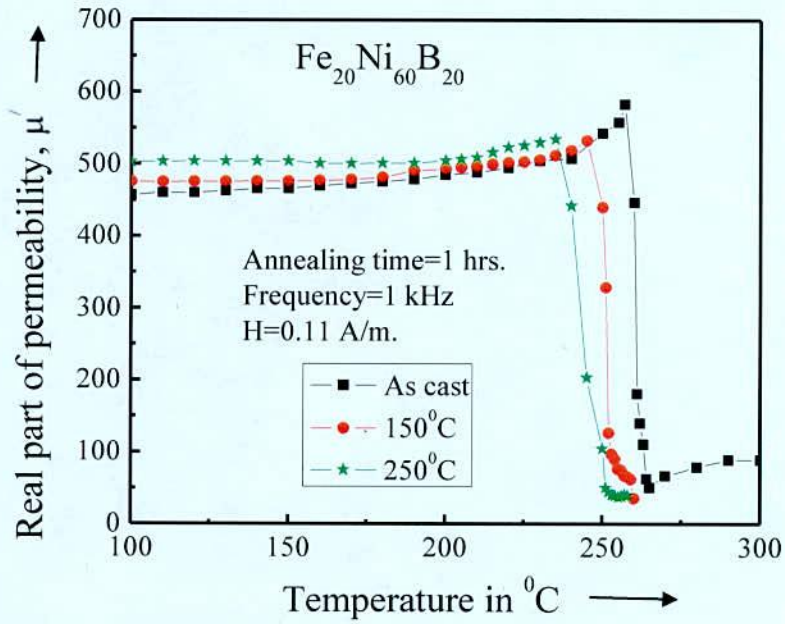


Fig.5.25 Temperature dependence real part of complex initial permeability of  $\text{Fe}_{20}\text{Ni}_{60}\text{B}_{20}$  ribbon at different annealing temperature for constant annealing time 1 hr

Table 5.6: Curie temperature of  $\text{Fe}_x\text{Ni}_{80-x}\text{B}_{20}$  amorphous ribbons for as cast and different annealing temperature at constant 1 hr annealing time

Sample	Annealing temperature, in $^{\circ}\text{C}$	Curie temperature, $T_c$ in $^{\circ}\text{C}$
$\text{Fe}_{50}\text{Ni}_{30}\text{B}_{20}$	As cast	446
	150	435
	250	430
	350	425
	400	420
$\text{Fe}_{40}\text{Ni}_{40}\text{B}_{20}$	As cast	410
	150	393
	250	390
	350	390
$\text{Fe}_{30}\text{Ni}_{50}\text{B}_{20}$	As cast	333
	150	320
	250	315
	300	310
$\text{Fe}_{20}\text{Ni}_{60}\text{B}_{20}$	As cast	260
	150	251
	250	240

### 5.3 Specific Magnetization Measurements of Fe-Ni-B Amorphous Ribbons

The specific magnetization of Fe-Ni-B amorphous ribbons with composition  $Fe_xNi_{80-x}B_{20}$  [ $x = 20, 30, 40 \text{ \& } 50$ ] in the as-cast condition was measured using a vibrating sample magnetometer (VSM). In this type of magnetometer the sample is vibrated up and down in a reason surrounded by several pick up coils. The magnetic sample is thus acting as a time changing magnetic flux, varying inside a particular region of fixed area. The magnetometer was calibrated using a high purity of Ni disk considering the saturation magnetization of Ni = 54.75 emu/g at room temperature. The ribbon sample were cut into small shapes, weighed and glued to a standard sample holder.

The specific saturation magnetization ( $\sigma_s$ ) have been calculated using formula

$$\sigma_s = \frac{kk'}{m} \text{ emu/g}$$

where  $K =$  VSM calibration constant,  $m =$  weight of the sample and  $k' =$ Decade transformer reading.

The specific saturation magnetization process as a function field is shown in Fig. 5.26. The specific saturation magnetization process for this ribbons have lower values for increasing replacement of Fe by Ni .It is observed that while the ribbon with composition  $Fe_{50}Ni_{30}B_{20}$  reaches its saturation value around 3.4kG, the ribbon with composition  $Fe_{40}Ni_{40}B_{20}$  requires 3.2kG, for the composition  $Ni_{50}Fe_{30}B_{20}$  2.8kG and for the composition  $Fe_{20}Ni_{60}B_{20}$  2.4kG. The specific saturation magnetizations ( $\sigma_s$ ) for different samples are calculated as shown in Table 5.7

Table 5.7: specific magnetization of  $Fe_xNi_{80-x}B_{20}$  at room temperature

$Fe_xNi_{80-x}B_{20}$	$x=50$	$x=40$	$x=30$	$x=20$
$\sigma_s$ in emu/g	124	119	89	77

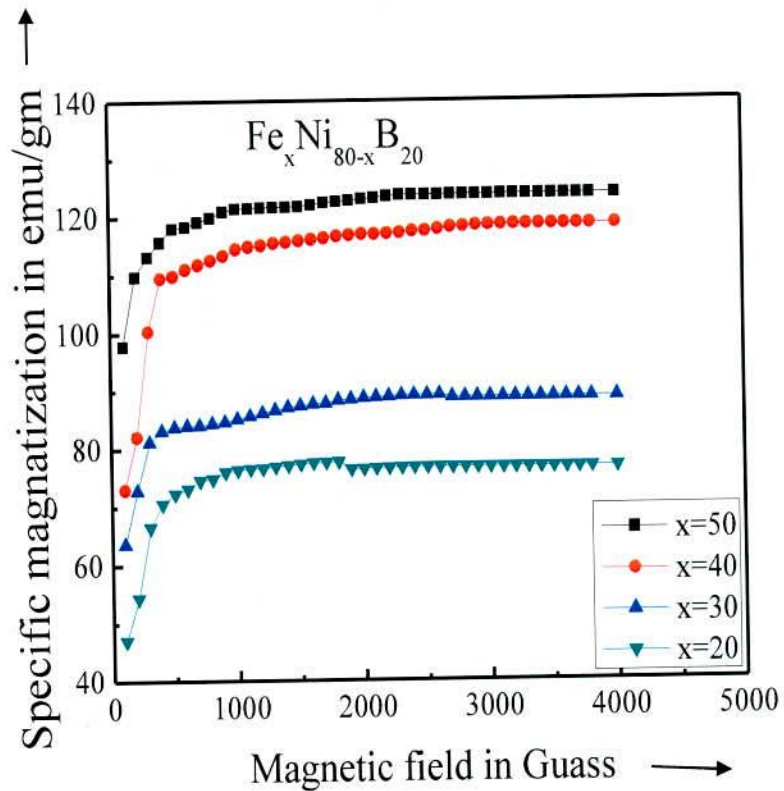


Fig.5.26 Specific magnetization versus magnetic field of amorphous ribbons with composition  $\text{Fe}_x\text{Ni}_{80-x}\text{B}_{20}$

The  $\sigma_s$  decreases with increasing replacement of Fe by Ni as shown in Fig. 5.27. For Fe-Ni-B amorphous ribbon with fixed metalloid B, this is a reduction in moment of Fe-Ni series with increasing Ni content in place of Fe. A simple approach is to replace a randomly local field at the moment site Fe by Ni. The data agree qualitatively with the rigid band model using the sample moments  $0.6 \mu_B$  for Ni and  $2.1 \mu_B$  for Fe. The result indicating that the average moment of the transition metal alloy decreases with the replacement of Fe with Ni. However, the rigid band model is not strictly followed.



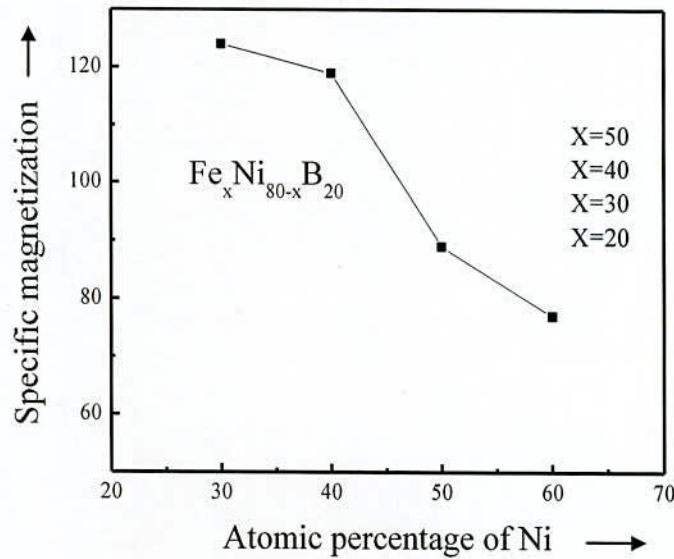


Fig.5.27 Variation of Specific magnetization due to change in the Ni- content in  $Fe_xNi_{80-x}B_{20}$  amorphous ribbons

### 5.3.1 Effect of Annealing Temperature on Specific Magnetization of Fe-Ni-B Amorphous Ribbons at Room Temperature

The present work mainly aimed at studying the magnetization process of  $Fe_xNi_{80-x}B_{20}$  [ $x = 20, 30, 40$  &  $50$ ] amorphous ribbons as affected by varying annealing temperature at constant 1 hour annealing time. This provides information about the nature of residual strain in as prepared melt spun ribbons and their effects on domain wall pinning. This study also provides important technical information about the possibility of using this ribbon at elevating annealing temperature and the optimum operating points of these ribbons, when they are used as soft magnetic materials under varying fields. The detailed quantitative analysis of the situation is, therefore, very complex and present understanding of the problem of magnetization process as affected by these defects is not yet clear.

The magnetization of the amorphous ribbons of composition  $Fe_xNi_{80-x}B_x$  [ $x = 20, 30, 40$  &  $50$ ] alloy annealed for constant 1 hour annealing time at varying temperature  $200^{\circ}C$  to  $400^{\circ}C$  for  $Fe_{50}Ni_{30}B_{20}$  &  $Fe_{40}Ni_{40}B_{20}$ ,  $200^{\circ}C$  to  $350^{\circ}C$  for  $Fe_{30}Ni_{50}B_{20}$  and  $200^{\circ}C$  to  $250^{\circ}C$  for  $Fe_{20}Ni_{60}B_{20}$ . Fig. 5.28 to Fig. 5.31 shows the field dependence of specific magnetization for

annealed Ni Fe B amorphous ribbon and there by treated sample measured by VSM. An increase of  $\sigma_s$  for the annealed samples compared with as cast samples due to the irreversible structural relaxation, cleaning the degree of chemical disorder of the amorphous state [5.11] and enhanced volume fraction of Fe - Ni alloy are exchanged coupled. The saturation magnetizations are shown in Table 5.8.

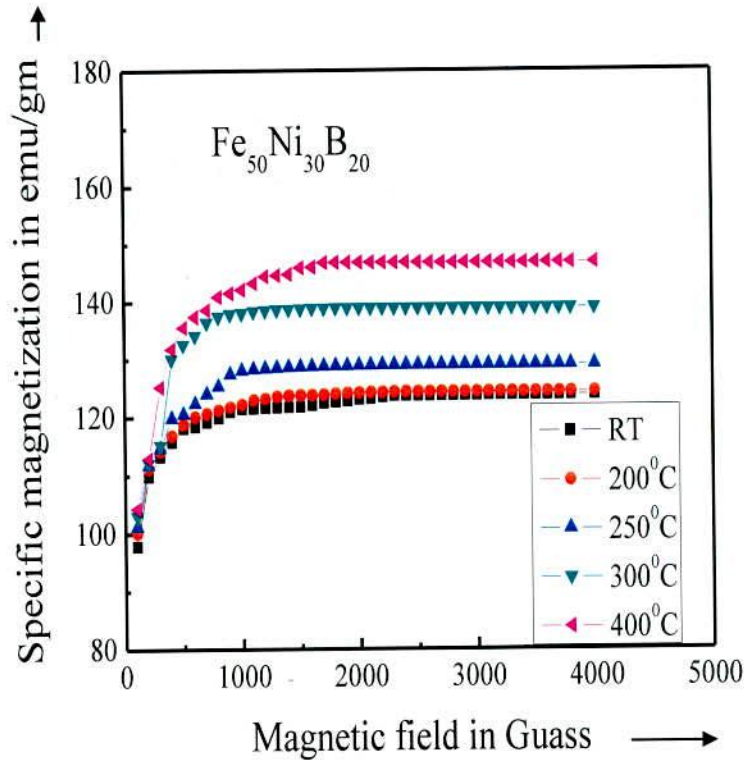


Fig.5.28 Specific Magnetization versus magnetic field of Fe<sub>50</sub>Ni<sub>30</sub>B<sub>20</sub> ribbon at different annealing temperature for constant annealing time 1 hr.

The present results are interpreted in terms of conventional domain theory of ferromagnetism, where it is postulated that the effect of annealing temperature is to partially remove the pinning centers of the domain wall and thereby improving the magnetic softness of this ribbon. It is observed that saturation magnetization increases slightly with increasing annealing temperature but has much larger effect on the domain wall movements, which is reflected in the easiness of magnetization of the annealed samples as seen in the Fig. 5.28 to Fig. 5.31. This explained due to the relaxation of defects in the as- cast ribbons. Since domain walls are pinned at the defect centers, the annealing process thermally relaxes the sample to

lower energy states distinguish reversible and irreversible types of relaxation due to annealing temperature. Thus reversibility of magnetization is not possible in these causes by reversing the external field. The reversible relaxation on the other hand means micro structural atomic arrangement within the domain wall potential in a way that allows the reversal of the magnetic domain wall movements through reversing of the direction of the magnetic field. The present work will be confined to the latter situation only.

Table 5.8 Saturation magnetization of  $\text{Fe}_x\text{Ni}_{80-x}\text{B}_{20}$  amorphous ribbons for as cast and different annealing temperature for 1 hr

Sample	Annealing temperature in $^{\circ}\text{C}$	Saturation magnetization in emu/g
$\text{Fe}_{50}\text{Ni}_{30}\text{B}_{20}$	As cast	124
	200	125
	250	129
	300	139
	400	147
$\text{Fe}_{40}\text{Ni}_{40}\text{B}_{20}$	As cast	119
	200	119
	250	120
	300	132
	400	136
$\text{Fe}_{30}\text{Ni}_{50}\text{B}_{20}$	As cast	89
	200	91
	250	93
	300	95
	350	97
$\text{Fe}_{20}\text{Ni}_{60}\text{B}_{20}$	As cast	77
	200	81
	250	82



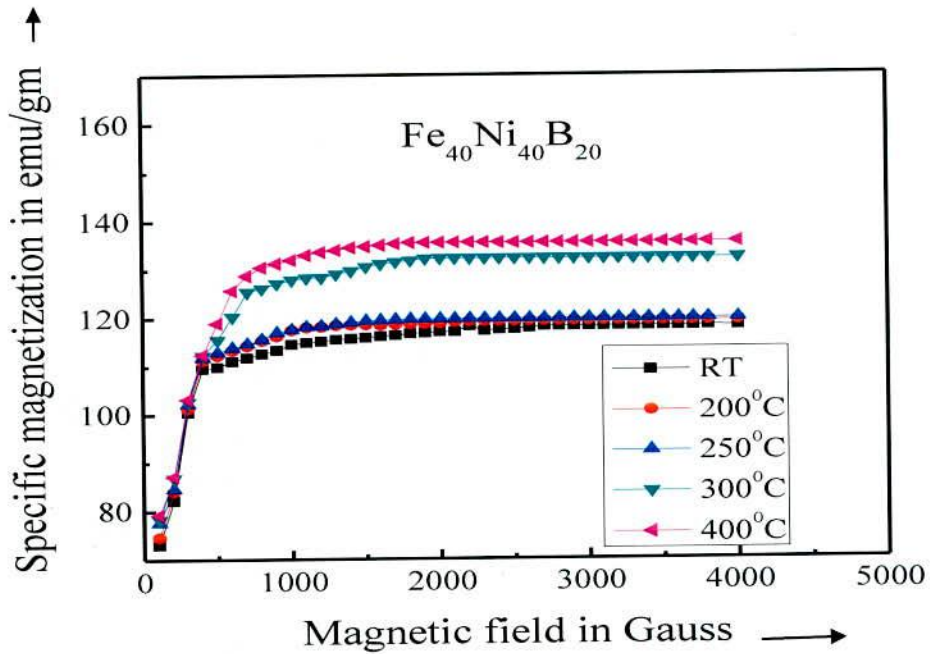


Fig.5.29 Specific Magnetization versus magnetic field of Fe<sub>40</sub>Ni<sub>40</sub>B<sub>20</sub> ribbons at different annealing temperature for constant annealing time 1 hr.

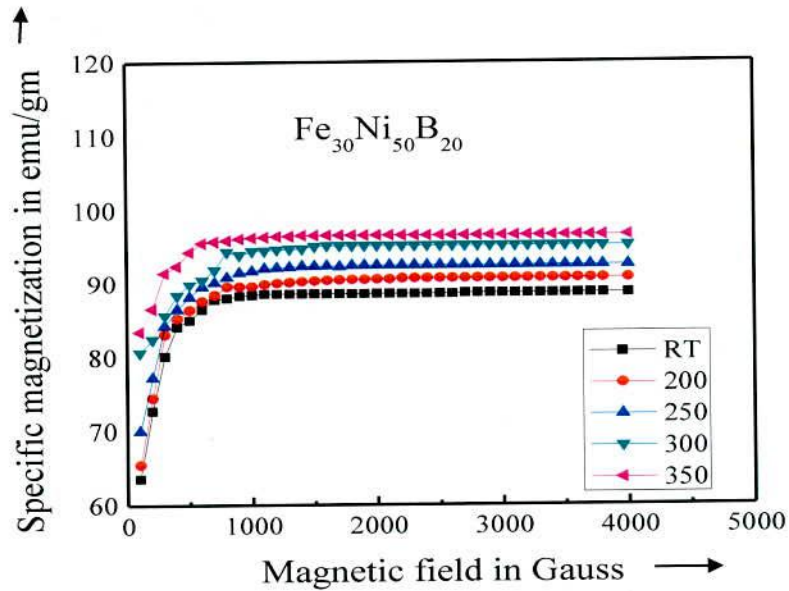


Fig.5.30 Specific Magnetization versus magnetic field of Fe<sub>30</sub>Ni<sub>50</sub>B<sub>20</sub> ribbons at different annealing temperature for constant annealing time 1 hr

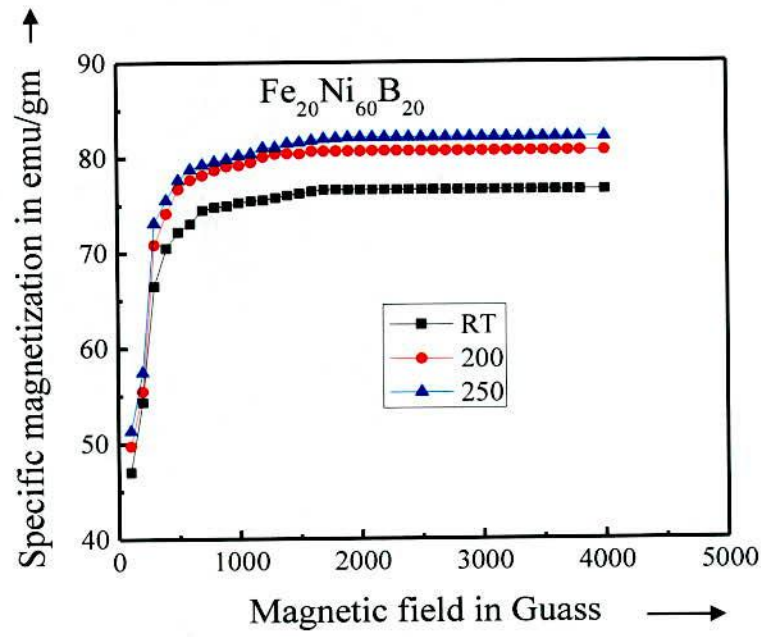


Fig.5.31 Specific Magnetization versus magnetic field of  $Fe_{20}Ni_{60}B_{20}$  ribbon at different annealing temperature for constant annealing time 1 hr

**CHAPTER VI**

**CONCLUSIONS**



## CONCLUSIONS

### 6.1 Conclusions

The effect on annealing on the soft magnetic properties like initial permeability, Curie temperature and saturation magnetization of melt spun  $\text{Fe}_x\text{Ni}_{80-x}\text{B}_{20}$  amorphous alloys has been studied. These ribbons were produced by melt spinning technique with 19 - 23 $\mu\text{m}$  thickness.

A comparison between the behavior of the initial permeability and other magnetic properties for Ni-Fe-B amorphous ribbon and the corresponding ribbon alloy, which depends on annealing at various temperatures at constant annealing time. The general composition of  $\text{Fe}_x\text{Ni}_{80-x}\text{B}_{20}$  [ $x = 20, 30, 40 \text{ \& } 50$ ] is very interesting in respect of the dependence of initial permeability and relative quality factor on the atomic percentage of Fe. The presence of Fe controls the average magnetic moment and the net magnetization of these amorphous samples. This gives an opportunity to tailor the magnetic characteristics of these ribbon alloy systems by controlling the composition of the ribbon alloy in respect of the Fe-atoms present. In this case initial permeability of Fe-Ni-B system increases with increasing Fe-content. The initial permeability increases with increasing annealing temperature and then it decreases with further increase of annealing temperature. The increase of initial permeability with increasing annealing temperature most probably due to the removal of defects and inhomogeneity, but with further increase of annealing temperature the initial permeability decreases due to nucleation of crystallites and their growth.

Fe-Ni-B amorphous magnetic ribbon shows interesting magnetic properties as soft magnetic material. These ribbons can be very useful as a core material in the as-quenched condition and at elevated annealing temperature. In the annealing temperature region i.e. 350 $^{\circ}\text{C}$  for  $\text{Fe}_{50}\text{Ni}_{30}\text{B}_{20}$ , 400 $^{\circ}\text{C}$  for  $\text{Fe}_{40}\text{Ni}_{40}\text{B}_{20}$ , 300 $^{\circ}\text{C}$  for  $\text{Fe}_{30}\text{Ni}_{50}\text{B}_{20}$  and 250 $^{\circ}\text{C}$  for  $\text{Fe}_{20}\text{Ni}_{60}\text{B}_{20}$  sample. In as cast ribbon permeability is reasonably higher and remains constant over large frequency range up to 100 kHz except  $\text{Fe}_{40}\text{Ni}_{40}\text{B}_{20}$ . Magnetic relaxation process may become important in technical application since they rise the magnetic losses and magnetic instability with rising annealing temperature. There exists a situation for this ribbon

where annealing at higher temperature simultaneously decrease the initial permeability and increases the dynamic losses. Actual under ac condition the number of domain wall increases and more deeply pinned walls begin to move as the frequency is increased. These effects contribute to an increase of the real part of the permeability but at the same time the imaginary component is also influenced, particularly due to eddy current effects. The advantage realizes higher saturation induction and better thermal stability with soft magnetic properties at application annealed samples.

For technological uses of amorphous materials at elevated temperature and for magnetic stability it is important to look for compositions that give higher value of Curie temperature ( $T_c$ ). This Fe-Ni-B amorphous ribbons  $T_c$  decreases monotonically with increasing Ni-content. The highest value of  $T_c$  corresponds to the composition  $Fe_{50}Ni_{30}B_{20}$ .  $T_c$  of interfacial amorphous phase has been found to decrease with increasing annealing temperature.

The saturation magnetization for these ribbons has higher values with increasing replacement of Ni by Fe. For all the ribbon alloy systems saturation specific magnetization depends on the atomic magnetic moments of the constituent 3d transition moment. The effect of the glass forming materials is explained as due to transfer of p- electron to the 3d band. However a quantitative agreement is not found on the basis of rigid band model. This shows that amorphous systems cannot be treated in the same way as crystalline materials in respect of band structure. Amorphous ribbons although have enormous potential, they are in metastable states, and magnetic softness of these materials depend on the annealing process. The effect of annealing of specific magnetization curve, it is observed that the saturation behavior responds very sensitively to a small change in increased saturation magnetization ( $\sigma_s$ ) of those samples at constant annealing time. The annealing temperatures are selected to partially remove the pinning centers of the domain walls and thereby improving the magnetic softness of these ribbons. Since the complex process involves the energy distributions from various aspects such as induced magnetic anisotropy, magnetostriction demagnetizing factors etc, quantitative, analysis o the effect of annealing temperature on magnetization process is not possible at the present state of knowledge.

## **6.2 Suggestions for further work**

Further work with finer variation of composition can be useful in dealing out the effect of glass forming material on magnetic characteristics low temperature measurements of magnetization is needed for actual theoretical understanding. Another important study that can be taken up is the measurement of magnetostriction as a function of composition and annealed temperature to confirm the suggestions regarding at the origin of increasing initial permeability. Certain important parameters like induced anisotropy and magnetostriction need to studied in detail for their variation with the preparation techniques, composition, annealing temperature and annealing time.



## **REFERENCES**

## REFERENCES

### CHAPTER-I

- [1.1] F. E. Luborsky; "Amorphous Ferromagnetism", Ferromagnetic materials, Vol.1; Edited by F. P. Wohlfurth; North Holland Publishing Company; P451, 1980
- [1.2] G. A. Petrakovskii; "Amorphous magnetic materials", Institute of Physics, Siberian Branch academy of Science of the USSR Kragnoyarsky USP. Fiz. Nauk; 134, 305 - 331, June1981
- [1.3] F. E. Luborsky and J. L. Walter; "Stability of amorphous metallic alloys"; J. Appl. Phys.; Vol. 47, 3648, 1976
- [1.4] Recep Sahingoz, Mustafa Erol, Mike R. J. Gibbs; "Observation of changing of magnetic Properties and Microstructure of Metallic Glass  $Fe_{78}Si_9B_{13}$  with annealing"; J. Magn. Magn. Mat. 271, 74 – 78, 2004
- [1.5] A. L. Gubanov; FIZ. Tver. Tel.2, 502, 1960
- [1.6] A. Brenner, D. E Couch and E. K. Williams; J. Ros. Nat. Bureau Standards, 44, 109, 1950
- [1.7] P. R. Duwez, H. Willens and W. Klemml Jr.; J. Appl. Phys. 31, 1136, 1960
- [1.8] R. Lorentz, J. Hafisar; "Non collinear magnetic structures in amorphous iron and iron based alloys"; J. Magn. Magn. Mat.; 139, 209 – 227; 1995
- [1.9] W. Grimm, B. Metzger and A. Haberf; "Optimized domain patterns in metallic glasses prepared by magnetic field heat treatment and/or surface crystallization"; J. Magn. Magn. Mat.; 41, 171 – 174; 1984
- [1.10] A. K. M. Zakaria, M. A. Asgar, S. S. Sikder and F. U. Ahmed; "The effect of annealing temperature on the complex permeability of Iron – Bron - Silicon Amorphous Ribbons"; Nuclear Science and Application; Vol.6; No.1 & 2; December1997
- [1.11] A. K. M. Zakaria, S. S. Sikder and M. A. Asgar; "Study of the complex permeability of amorphous magnetic ribbon  $Fe_{82}Si_8B_{10}$  and their dependence on thermal annealing and frequency"; Jahangirnagar University, Journal of Science; Vol. 24; pp/141 – 150; 2001

- [1.12] S. S. Sikder, M. A. Asgar, M. A. Hakim and M. A. Mazid; "The effect of annealing in the magnetization process of Iron - Bron Ribbons"; Journal Academy of Science; Vol. 20; No.2, 237 – 245; 1995
- [1.13] S. S. Yoon, S. D. Kwon, Jong Ho Kim, C. G. Kim; "Determination of magnetization rotation and domain wall motion components in reversible complex susceptibility spectra of Co-based amorphous ribbons with various annealing temperature"; J. Magn Magn Mat.; 242 – 245, 261 -264, 2002
- [1.14] S. S. Sikder and M. A. Asgar; "The kinetics of atomic and magnetic ordering of Co-based amorphous ribbons as affected by Iron substitution"; Thermo Chimica Acta 326, 119 – 126; 1999
- [1.15] A. K. M. Zakaria, M. A. Asgar, S. S. Sikder and F. U. Ahmed; "The effect of annealing temperature on the complex permeability of Iron - Aluminum – Bron - Silicon Amorphous Ribbons"; Nuclear Science and Application; Vol.6; No.1,2; p.47 – 55, December 1997
- [1.16] Z. H. Khan, S. S. Sikder, M. A. Asgar and A. H. Bhuiyan; "Effect of annealing temperature on the complex initial permeability of  $Co_{80-x}Fe_xB_{10}Si_{10}$  amorphous ribbons"; Bangladesh Journal of Physics, 3, 15 – 22, 2007
- [1.17] Md. Sultan Mahmud, M. A. Asgar, S. S. Sikder and A. K. M. Zakaria; " Effect of annealing temperature on ac initial permeability of Nanocrystalline amorphous ribbons with composition  $Fe_{74}Cu_{1.5}Nb_{2.5}Si_{12}B_{10}$ "; Nuclear Science and Applications; Vol. 13, No. 1 ,2, P 27 - 34, December 2004
- [1.18] E. Amano, R. Velenzuela, J. T. S. Irvine and A. R. West; J. Appl. Phys. 67, 5589 (1990)
- [1.19] J. T. S. Irvine, E. Amano and R. Velenzuela; Mater. Sci. Eng. A133, 140, 1991
- [1.20] K. M. Polivanov; Izv. Akad. Nauk. SSSR (Ser.Fiz) 16, 449, 1952
- [1.21] R. H. Pry and C. P. Bean; J. Appl. Phys. 17, 451, 1966
- [1.22] J. E. L. Bishop; Brit. J. Appl. Phys. 29, 532, 1958
- [1.23] G. Ban, L. Szentmiklosi, P. Arato and M. Juhasz; J. Magn. Magn. Mater. 41, 382 - 384, 1984
- [1.24] G. Ban, P. Arato and L. Szentmiklosi; J. Magn. Magn. Mater.; 37, 309, 1983



- [1.25] G. Buttino, Aeecchetti, M. Poppi and G. Zini; IEEE Trans. Magn. MAG – 18, 1400, 1982
- [1.26] S. D. Washko, M. L. Oshorn and W. G. Verrarragharan; J. Appl. Phys., 52, 1899, 1980
- [1.27] B. T. Cong; J. Magn. Magn. Mater. 117, 126, 1992
- [1.28] T. K. Miyaki, K. Yamanchi, S. Arakawa, Y. Yoshizawa and S. Nakajima; Bulletin Japan, Inst. Metals. 26, 299, 1987
- [1.29] O. Komoto, H. Hujishima, S. Sumiya, H. Itomasa and T. Ojima; Bulletin Japan, Inst. Metals. 27, 293, 1988
- [1.30] H. Fujimori, M. kikuchi, Y. Obi and T. Masumoto; Sci. Rep. RITO, A-26,36, 1976
- [1.31] S. S. Sikder; M. Phil Thesis; Department of Physics, BUET, Dhaka, July 1988
- [1.32] M. A. Asgar and S. S. Sikder; "Influence of glass forming material on atomic and magnetic ordering of Fe – based metallic glass"; Indian J. Phys. 73A (4) 493 - 502 1999
- [1.33] Z. H. Khan; M. Phil Thesis; Department of Physics; KUET, Khulna, May 2005
- [1.34] S. S. Sikder, M. A. Asgar and M. A. Hakim; "Temperature dependence on a.c. Initial permeability of amorphous ribbons with composition  $\text{Co}_{80-x}\text{Fe}_x\text{B}_{10}\text{Si}_{10}$  [x=0, 2, 4, 6 & 8]"; Indian J. Phy. 73A (5); 639 – 646, 1999
- [1.35] G. Lehmann, G. Dietzmann and M. Schacfer; Hermsderfer Techn. Mitt. 80, 2563, 1991
- [1.36] M. Schaefer and G. Dietzmann; J. Magn. Magn. Mater. 133, 303 – 305, 1994
- [1.37] Zhang Yan Zhang; J. Magn. Magn. Mater.; 68, 145 – 150, 1987
- [1.38] Y. Z. Zhang; Scienta Sinica; Series A30, 317 (in English), 1987
- [1.39] K. Ohta and T. Matsuyama; J. Magn. Magn. Mater. 19, 165, 1980
- [1.40] T. Mizoguchi et. al.; Proc. 4<sup>th</sup> Int. Conf. on Rapidly Quenched Metals, Sendai; p- 1195, 1981
- [1.41] T. Jagielinski, T. Walecki; Phys. Stat. Sol. (a) 60, k31, 1980
- [1.42] R. Alben, J. I. Bundnick and G. S. Cargill III; in metallic glasses (eds. H. S. Leamy and J. J. Gilman ) (American Society for Metals. Park. Ohio Ch12, 1977
- [1.43] W. Felsch; Z. Angew. Phys. 29, 218, 1970
- [1.44] Y. Shimada and H. Kojima; J. Appl. Phys. 47 4156, 1976

- [1.45] J. G. Wright; IEEE Trans. Magnetics, MAG-12, 95, 1976
- [1.46] J. J. Becker, F. E. Luborsky and J. L. Walter; IEEE Trans. Magnetics MAG - 13, 988, 1977
- [1.47] J. S. Kouvel; in Magnetism and Metallurgy (eds. A. E. Berkowitz and E. Kneller) (Academic Press, New York) p.523 – 575, 1969
- [1.48] H. Fujimeri, H. Morita, Y. Obi and S. Ohta; in Amorphous Magnetism- II (eds. R. A. Levy and R. Hasegawa ) (Plenum Press, New York) p.393, 1977
- [1.49] J. Durand and M. Yung; in Amorphous Magnetism- II (eds. R. A. Levy and R. Hasegawa ) (Plenum Press, New York) p.275, 1977
- [1.50] J. Horvat, E. Babic and Z .Morohnic; J. Magn. Magn. Mater. 86, LI-L-6, 1990
- [1.51] J. Horvat, Z. Morohnic and E. Bubic; J. Magn. Magn.Mater. 82, 5, 1989
- [1.52] J. W. Cable; J. Appl. Phys., Vol. 49, No.3, 1527,1978
- [1.53] E. Figueroa, L. Lundgren, O. Beckman and S. M. Bhagat; Solid State Commun, Vol. 20, 961, 1976
- [1.54] R. Malmhall, G. BackStrom, S. M. Bhagat and K. V. Rao; J. Phys. F. Met, Phys., Vol.9, No.2, 317, 1979

## CHAPTER- II

- [2.1] P. Duwez; J. Am. Inst. Metall. Eng.; 191: 765, 1951
- [2.2] P. Duwez, R. H. Willens and W. Kelment; J. Appl. Phys.; 31:1136, 1960
- [2.3] P. Duwez; Trans. Am. SOC Met.; 60 : 607, 1967
- [2.4] P. Duwez; Ann. Rev. Mat. Sci.; 6 : 83, 1976
- [2.5] S. Mader, A. S Nowick; Appl. Phys. Lett.; 7 : 57, 1965
- [2.6] W. Klement Jr., R. H. Willens and P. Duwez, Nature, 187, 809, 1960
- [2.7] A. I. Gubanov; Fiz. Tver. Tel. 2502, 1960
- [2.8] R. Pond Jr. and R. Maddin; Trans. Met. SOC, ALME 245, 2475, 1969
- [2.9] C. C Tsuei and P. Duwez; J. Appl. Phys.; 37: 435, 1960
- [2.10] T. Mizoguchi; IBM Research Report, RC 6054, 1976
- [2.11] R. Alben, J. I. Budnick, G. S. Cargill; III, Metallic glasses (American SOC .for metals. p-304, 1978
- [2.12] E. M. Gyorgy; ibid, p-275



- [2.13] G. S. Cargill:III; Solid State Physics, Vol. 30, Ed. Ehrenreich et. al., Academic Press, New York; p-257, 1975
- [2.14] T. Masumoto, S. Ohnuma, K. Shirakawa, M. A Nose and K. Kaboyshi; Int. Conf on liquid and Amorphous Metals. Grenoble France, 1980
- [2.15] G. S. Cargill:III; Solid State Physics , Vol 30, 227, 1975 a
- [2.16] M. A. Asgar; Mechanical Engineering Research Bulletin (BUET).P.1, Vol 1, 1984
- [2.17] R. Alben, J. I. Budnick and G. S. Cargill III; in Metallic glasses (eds. H. S. Leamy and J. J Gilman ) (American Society for Metals Metals Park, Ohio ) Ch.12, 1977
- [2.18] D. Turnbull; Contemp.Phy.10,473, 1969
- [2.19] P. Duwez, R. H. Willens and W. Kelment Jr.; J. Appl. Phys. 31, 1136, 1960
- [2.20] H. S. Chen; Rep. Prog. Phys. 43, 23, 1980

### CHAPTER-III

- [3.1] R. C. O' Handly; Phys. Rev. B18, 930. 1978a
- [3.2] Z. G. Li and D. J. Smith; Appl. Phys. Lett. 55, 919, 1989
- [3.3] W. Heisenberg; Z. Phys. 619, 1928
- [3.4] D. Turnbull; "Under what condition can a glass be formed?" Contemp. Phys. 10 473-488, 1969
- [3.5] W. L. Johnson; "Thermodynamic and kinetic aspects of the crystal to glass transformation in metallic materials"; Progress in Materials Science; 30, 81 – 134, 1986
- [3.6] D. Louca, K. Ahn, V. Ponnambalam and S. J. Poon; "Local order in amorphous Fe-alloys"; Mat. Res. SOC. Proc. 754, pp. CC7.7.1 – CC7.7.6, 2003
- [3.7] R. Harris, M. Plischke and M. J. Zuckerman; "New model for amorphous magnetism"; Phys. Rev. Lett. 31, 160 – 162, 1973
- [3.8] M. Cohen and D. Turnbull; "Composition Requirments for Glass Formation in Metallic and Ionic Systems"; Nature, 189, 131 – 132, 1961
- [3.9] A. E. Berkowitz, J. L. Walter and K. F. Wall; "Magnetic properties of amorphous particles produced by Spark Erosion"; Phys. Rev. Lett. 46, 1484, 1981
- [3.10] H. Jones; Rep. Prog. Phys., 36, 1425, 1973



- [3.11] D. Turnbull; J. dc Physique, 35, C4-1, 1974
- [3.12] S. Takayama; J. Materials Sci., 11, 164, 1976
- [3.13] J. T. S. Irvine, E. Amano, A. Huanosta, R. Valenzuela, A. R. West; "Solid State should Peak at  $T_c$ "; Ionic , 40/41, 220, 1990
- [3.14] M. H. Cohen and D. Turnbull; Nature, 189, 131, 1961
- [3.15] G. Gargill III; J. Appl. Phys. 41, 2248, 1970
- [3.16] H. S. Chen; Acta Meta. 22, 1505, 1974
- [3.17] S. R. Nagel and J. Taue; "Nearly- Free- Electron approach to the theory of Metallic Glass Alloys"; Phys. Rev. Lett., 35, 380, 1975
- [3.18] T. Egami; J. Magn. Magn. Mat.; 7, 143, 1984
- [3.19] Y. Waseda and K. T. Aust; J. Mater. Sci. 16, 2337, 1981
- [3.20] F. E. Luborsky; J. Magn. Magn. Mar.; 7, 143, 1978
- [3.21] E. Amano, R. Valenzuela, J. T. S. Irvine and A. R. West; J. Appl. Phys. 67, 5589, 1990
- [3.22] R. M. Jones; IEEE Trans. Magn. MAG-18, 1559, 1982
- [3.23] M. R. J. Gibbs; Proc. Conf. Metallic Glasses Science and Technology, Budapest; Vol.2C hargitai, J. Bakonyi and T. Kemeny (Kultura, Budapest) p.37, 1980
- [3.24] R. Harries, M. Pliseke, M. J. Zuckorman; New Model for Amorphous Magnetism" Phys. Rev. Lett.; 31, 160, 1973
- [3.25] R. Bozroth; "Ferromagnetism"; D. Van-Nostrand, Princeton N. J., 76, 1951
- [3.26] L. Nill; J. Phys. Radi., 13, 249, 1952
- [3.27] F. E. Luborsky; Materials Sci. Eng., 28, 139, 1977a
- [3.28] J. S. Kouvel; "Magnetism and Metallurgy"; eds. A. Berkowitz and E. Kneller (Academic Press, New York) Vol.2, p.523, 1961
- [3.29] K. Yamaguchi and T. Mizaguchi; J. Phys. SOC. Japan, 39, 541, 1975
- [3.30] K. Handrich; "Conditions for the Existence of Amorphous Ferromagnets"; phys. Stat. SOL.(b) 53, k17, 1972

#### CHAPTER-IV

- [4.1] A. Arott; "Criterion for Ferromagnetism for observations of Magnetic Isotherms"; Phys. Rev. 108, 1394, 1957

- [4.2] K. P. Belov; Magnetic Transition, Consultants Bureau (New York), 1961
- [4.3] J. S. Kouvel and M. E. Fisher; "Detailed Magnetic Behavior of Nickel near its Curie Point"; Phys. Rev. 136, A1626, 1964
- [4.4] M. A. Mazid and M. A. Chowdhury; "Design and construction of Forner Type Vibrating Sample Magnetometer"; AECD/ MMD/ I, June, 1986 (Bangladesh)
- [4.5] Simon Forner; "Versatile and Sensitive Vibrating Sample Magnetometer"; Rev. Sci. Instr. 30, 160, 1959

## CHAPTER-V

- [5.1] E. Amano, R. Valenzuela, J. T. S. Irvine and A. R. West; J. Appl. Phys., 67, 5589, 1990
- [5.2] J. T. S. Irvine, E. Amano and R. Valenzuela; Mater. Sci. Eng., A 133, 140, 1991
- [5.3] W. A. PHILLIPS; J. Low. Temp. Phys., 7, 351, 1972
- [5.4] D. Nathusingh and C. H. Smith; J. Proc. Conf. on Power Conversion 7, Paper B2 San Diego, 1980
- [5.5] M. A. Asgar and S. S. Sikder; Indian J. Phys. 73A(4), 493 – 502, 1999
- [5.6] M. Kersten and Z. Angew; Physics, 7, 313 (1956); 8, 382, 496, 1956
- [5.7] J. G. Wright; IEEE Trans. Magnetics MAG-12:95, 1976
- [5.8] F. E. Luborsky, J. J. Becker and R. O. Mc Cary; IEE Trans. Mag. Mag. 1644, 1975
- [5.9] M. Kersten and Z. Angew; Physics, 7; 313; 8: 382.496, 1956
- [5.10] Siba Pada Mondal; "Study of Nanocrystalline formation in FINEMET Metallic Glasses and their Magnetic Properties". M. Phil Thesis; November, KUET, P- 94-100, 2008
- [5.11] A. Lovas, L. F. Kiss, L. Balong; "Saturation magnetization and amorphous Curie point charges during the early stage of amorphous nanocrystalline transformation of a FINEMET type alloy"; J. Mag. Mag. Mater. 215-216, 463, 2000

## CONFERENCE PAPER

- [1] **N. C. Mollick**, S. K. Shil, S. S. Sikder and A. H. Bhuiyan; “Effect of Field and Annealing Temperature on Complex Permeability of Amorphous Ribbon with Composition  $\text{Fe}_{40}\text{Ni}_{40}\text{B}_{20}$ ”; International Conference on Physics for Energy and Environment, Atomic Energy Centre, 06 – 08 March, 2014
- [2] **N. C. Mollick**, S. K. Shil, S. S. Sikder and A. H. Bhuiyan; “Effect of Annealing Temperature on Complex Initial Permeability of Amorphous Ribbon with Composition  $\text{Fe}_{50}\text{Ni}_{30}\text{B}_{20}$ ”; National Conference on Physics for Sustainable Development; KUET, Khulna, 15 February 2014